

# PERFORMANCE ESTIMATION OF DC MOTOR DRIVE IN ELECTRIC TRACTION

## A DISSERTATION

*Submitted in partial fulfilment of the  
requirements for the award of the degree  
of*

**MASTER OF TECHNOLOGY**

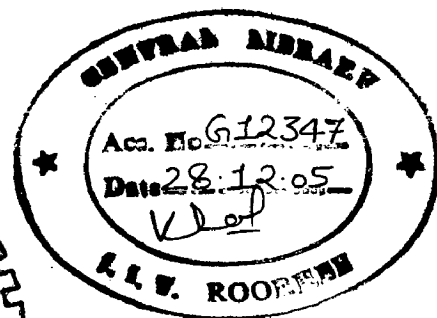
*in*

**ELECTRICAL ENGINEERING**

**(With Specialization in Power Apparatus and Electric Drives)**

*By*

**ALOK NAYAL**



**DEPARTMENT OF ELECTRICAL ENGINEERING  
INDIAN INSTITUTE OF TECHNOLOGY ROORKEE  
ROORKEE-247 667 (INDIA)**

**JUNE, 2005**

## CANDIDATE'S DECLARATION


---

I hereby declare that the work, which is being presented in the dissertation entitled "PERFORMANCE ESTIMATION OF DC MOTOR DRIVE IN ELECTRIC TRACTION" towards partial fulfillment of the requirement for the award of degree of Master of Technology in Electrical Engineering with specialization in Power Apparatus and Electric Drives, submitted to the Department of Electrical Engineering, Indian Institute of Technology, Roorkee, is an authentic record of my own work carried out from July 2004 to June 2005, under the guidance of Dr. S.P. Gupta, Prof and Dr. S.P Singh, Associate Prof., Department of Electrical Engineering, IIT Roorkee.

I have not submitted the matter embodied in this dissertation for the award of any other degree or diploma.

Date: 27.06.2005

Place: Roorkee

  
(ALOK NAYAL)


---

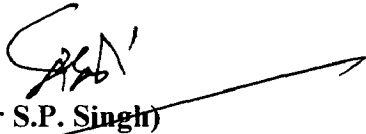
## CERTIFICATE

This is to certify that the above statement made by the candidate is correct to the best of my knowledge.

Date: 27.06.2005

Place: Roorkee

  
(Dr S.P. Gupta)  
Prof, Deptt of Electrical Engg,  
IIT Roorkee,  
Roorkee- 247667, INDIA

  
(Dr S.P. Singh)  
Associate Prof, Deptt of Electrical Engg,  
IIT Roorkee,  
Roorkee- 247667, INDIA

## ACKNOWLEDGEMENTS

I wish to express my deep sense of gratitude to Dr. S.P Gupta, Prof, Department of Electrical Engineering and Dr S.P Singh, Associate Prof, Department of Electrical Engineering, IIT Roorkee for their unfailing inspiration, whole-hearted co-operation and painstaking supervision for this thesis work. Their encouragement and incisive comments have proved to be the backbone for successful completion of this dissertation.

I am very grateful to Dr H.O. Gupta, Head of the Department of Electrical Engineering for providing all the necessary facilities and administrative supports.

I also appreciate and thank staff of P.C Laboratory, Department of Electrical Engineering, for providing invaluable assistance.

I would like to express my heartfelt gratitude towards my family members who gave me much needed encouragement during this dissertation.

Finally I would like to thank all my friends who have helped me in some way or the other way in preparing this thesis work.

**Date-27.06.2005**

**Place: Roorkee**



**(Alok Nayal)**

## ABSTRACT

A majority of railway traction drives in use today still utilize DC motors. The most appreciated DC motor for traction purpose is DC series motor because of its inherent high starting torque capacity. In early days most of the dc motor traction drives used inefficient resistance control to control the speed of the motor. However, with time, these drives were replaced with much efficient thyristor based drives which enabled the use of high power AC supply in Electric Traction. With closed loop DC drive, it became possible to control acceleration of the motor by controlling the motor torque. This was done by controlling the voltage from a low value at start to the high value at high speed.

However, a high acceleration of the DC motor alone does not guarantee a high acceleration of the train which also depends upon the wheel-rail interaction. Thus the rotation of the wheel (a consequence of motor speed) may not completely result in translational motion of the train. When this happens, the wheel starts slipping on the track. This results in wearing of the wheel and also unnecessary wastage of precious electrical energy without yielding any acceleration to the train.

In this work a DC motor drive for traction purpose has been simulated with effective wheel slip control strategies. A converter based DC motor drive has been used for this analysis. As a first step towards this objective, a DC series motor, its characteristics and its behavior when fed from converter, both in open loop and closed loop has been studied. After developing a sufficient understanding of the behavior of a closed loop DC drive, a traction load model was developed. This model was then integrated with the motor drive to form a DC motor drive which yields an effective wheel slip control. The performance estimation of the drive for various mechanical conditions viz. flat track, inclined track and variable track conditions has been made.

# CONTENTS

Page No.

<b>Acknowledgement</b>	ii
<b>Abstract</b>	iii
<b>List of figures</b>	vi
<b>Chapter 1 Introduction</b>	1
1.1 Electric Traction	1
1.1.1 Historical Background and General Features	1
1.1.1.1 Electrical Drive System	2
1.1.1.2 Mechanical Load System	3
1.2 Literature review	4
1.3 Objectives of the Present work	6
1.4 Approach adopted for mathematical modeling	6
1.5 Outline of the present work.	6
<b>Chapter 2 Modeling of Converter fed DC Series motor Drive</b>	7
2.1 DC Series Motor and its characteristics.	7
2.2 Speed control of DC motor	10
2.2.1 Armature Voltage Control	11
2.2.2 Field Flux Control	11
2.3 Open loop speed control of DC Series motor using half controlled converter	12
2.3.1 Theory	12
2.3.2 Simulation with MATLAB	13
2.3.2.1 DC Series motor	14
2.3.2.2 Single phase half controlled Converter	14
2.3.2.3 Firing Circuit Logic	16
2.3.3 Results	18
2.4 Closed loop Control of DC Series motor	21
2.4.1 Theory	21
2.4.2 Implementation of the closed loop control of DC Series motor	22
2.4.2.1 Motoring mode	24
2.4.2.2 Braking mode	24
2.4.2.3 Results	30
2.4.3 Two stage sequence control of half controlled converters	34

2.4.4 Implementation of two stage sequence control of half controlled converters	36
2.4.4.1 Results	38
<b>Chapter 3 Mechanics of Traction load</b>	<b>40</b>
3.1 Motion of locomotive	40
3.2 Coefficient of Adhesion	41
3.3 Nature of Traction Load	43
3.4 Dynamic Mechanical model	43
3.4.1 Wheel dynamics	43
3.4.2 Train dynamics	44
3.5 MATLAB Implementation of Mechanical load	45
<b>Chapter 4 Electrical Traction Drive with wheel slip control</b>	<b>47</b>
4.1 Wheel Slip Control	47
4.2 Slip Control to the reference value.	48
4.2.1 Theory	48
4.2.2 Implementation with MATLAB	49
4.2.3 Results	52
4.3 Gradient Control Scheme	67
4.3.1 Theory	67
4.3.2 Implementation with MATLAB	68
4.3.3 Results	70
<b>Chapter 5 Conclusions and Scope for Further Work</b>	<b>89</b>
5.1 Summary	89
5.2 Recommendations for further work	90
<b>References</b>	<b>91</b>
<b>Appendix A Specifications of DC motor.</b>	<b>93</b>
<b>Appendix B Programs</b>	<b>94</b>

## LIST OF FIGURES

2.1	Torque-Speed characteristic of DC series motor.	9
2.2	Simulated and Theoretical Torque-Speed Characteristic of DC series motor	10
2.3	Schematic layout of converter fed DC series motor	12
2.4	Output voltage of converter	12
2.5	Torque-Speed Curves of converter fed dc series motor at different firing angles	13
2.6	SIMULINK implementation of open loop control of half controlled converter fed DC series motor.	14
2.7	SIMULINK block for Single Phase Half Controlled Converter	15
2.8	SIMULINK block implementing firing circuit logic	17
2.9	Generation of firing pulses	17
2.10	Performance of DC series motor when fed from converter with $\alpha=0^0$	18
2.11	Efficiency of DC series motor when fed from converter with $\alpha=0^0$	18
2.12	Voltage applied to the DC series motor	19
2.13	Performance of DC series motor when from converter with $\alpha=60^0$	19
2.14	Efficiency of DC series motor when fed from converter with $\alpha=60^0$	20
2.15	Voltage applied to the DC series motor	20
2.16	Simulated Torque-Speed Curves of converter fed DC series motor at different firing angles	20
2.17	Schematic layout of closed loop dc drive with inner current loop and outer speed loop	21
2.18	SIMULINK implementation of closed loop DC drive with braking capability.	23
2.19	Braking with field reversal	24
2.20	Braking with field connected to separate dc source	25
2.21	A SIMULINK block diagram representation of PI Controller	26
2.22	Sample response of current controller	27
2.23	Current response for a improper gain of current controller	28
2.24	Current response for proper gain of current controller	28
2.25	Speed response for a improper gain of speed controller	29
2.26	Speed response for a proper gain of speed controller	29
2.27	Performance of DC Series motor under closed loop control	30
2.28	Voltage applied to the motor	30
2.29	Variation of Power factor on the source side	31
2.30	Active and Reactive Power drawn by the motor from the supply	31
2.31	Performance of drive when toggled from motoring to braking and back to motoring mode	32
2.32	Voltage applied to the motor	33
2.33	Variation of Power factor on the source side	33
2.34	Active and Reactive Power drawn by the motor from the supply	34
2.35	Two half controlled converters connected in series for two stage control	34
2.36	Variation of reactive power with DC output voltage	35

2.37	SIMULINK implementation of Two half controlled converters connected in series	36
2.38	SIMULINK implementation of closed loop scheme employing sequence control of two stage half controlled converter.	37
2.39	Performance of closed loop drive when fed from two stage sequence controlled half controlled converters	38
2.40	Spread out view of armature and supply voltage	38
2.41	Variation of Power factor on the source side	39
2.42	Active and Reactive Power drawn by the motor from the supply	39
3.1	Forces acting on the wheel and the surface of the rail	41
3.2	Coefficient of adhesion vs. wheel slip ratio for various track conditions	42
3.3	Variation of coefficient of adhesion with velocity of the train	42
3.4	Control block diagram representation of wheel dynamics	44
3.5	Block diagram for entire mechanical system	45
3.6	SIMULINK block diagram of mechanical load	46
4.1	Image of desired slip control	48
4.2	Block diagram of slip ratio control to the reference value	49
4.3	SIMULINK implementation of closed loop traction drive with slip control to reference value	51
4.4	$\mu$ - $\lambda$ characteristic for the track	52
4.5	Armature current and Torque developed by the motor as the slip ratio is being controlled to the commanded value while the train builds up to the desired value of speed on a flat track	53
4.6	Variation of Coefficient of adhesion with time	54
4.7	Variation of force of adhesion with time	54
4.8	Variation of Tractive effort with time	55
4.9	Torque developed by the motor and load torque on the drive	55
4.10	Variation of Power factor on the source side	56
4.11	Active and Reactive Power drawn by the motor from the supply	56
4.12	Armature current and Torque developed by the motor as the slip ratio is being controlled to the commanded value while the train builds up to the desired value of speed on an inclined track	57
4.13	Variation of coefficient of adhesion with time	58
4.14	Variation of force of adhesion with time	58
4.15	Variation of Tractive effort with time	59
4.16	Variation of Power factor on the source side	59
4.17	Active and Reactive Power drawn by the motor from the supply	60
4.18	The $\mu$ - $\lambda$ curves for two tracks used in the simulation	61
4.19	Movement of train on the tracks	61
4.20	Armature current and Torque developed by the motor as the slip ratio is being controlled to the commanded value while the train builds up to the desired value of speed on a changing track	62
4.21	Variation of slip ratio with time	62
4.22	Variation of wheel speed and train speed with time	63
4.23	Variation of coefficient of adhesion with time	63



4.24	Variation of force of adhesion with time	64
4.25	Variation of Tractive effort with time	64
4.26	Variation of Power factor on the source side	65
4.27	Active and Reactive Power drawn by the motor from the supply	65
4.28	The $\mu$ - $\lambda$ curves for two tracks showing a possible shift into unstable zone	66
4.29	The $\mu$ - $\lambda$ curve showing stable and unstable regions and gradient at operating point	67
4.30	Block diagram of gradient control Scheme	68
4.31	SIMULINK implementation of closed loop traction drive employing gradient control	69
4.32	SIMULINK implementation of gradient detector	70
4.33	$\mu$ - $\lambda$ characteristic for the track	70
4.34	Armature current and Torque developed by the motor as the slip ratio is being controlled through gradient control while the train builds up to the desired value of speed on a flat track	71
4.35	Variation of slip ratio with time	72
4.36	Variation of coefficient of adhesion with time	72
4.37	Variation of force of adhesion with time	73
4.38	Variation of Tractive effort with time	73
4.39	Torque developed by the motor and load torque on the drive	74
4.40	Variation of Power factor on the source side	74
4.41	Active and Reactive Power drawn by the motor from the supply	75
4.42	Armature current and Torque developed by the motor as the slip ratio is being controlled through gradient control while the train builds up to the desired value of speed on an inclined track	76
4.43	Variation of slip ratio with time	77
4.44	Variation of coefficient of adhesion with time	77
4.45	Variation of force of adhesion with time	78
4.46	Variation of Tractive effort with time	78
4.47	Torque developed by the motor and load torque on the drive	79
4.48	Variation of Power factor on the source side	79
4.49	Active and Reactive Power drawn by the motor from the supply	80
4.50	$\mu$ - $\lambda$ curves	81
4.51	Movement of train on the tracks	81
4.52	Armature current and Torque developed by the motor as the slip ratio is being controlled through gradient control while the train builds up to the desired value of speed on a changing track	82
4.53	Locus of the $\mu$ - $\lambda$ curve followed by the train	83
4.54	Magnified view of $\mu$ - $\lambda$ locus followed by the train	84
4.55	Variation of wheel speed and train speed with time	84
4.56	Variation of slip ratio with time	85
4.57	Variation of coefficient of adhesion with time	85
4.58	Variation of force of adhesion with time	86
4.59	Variation of Tractive effort with time	86
4.60	Torque developed by the motor and load torque on the drive	87

4.61	Variation of Power factor on the source side	87
4.62	Active and Reactive Power drawn by the motor from the supply	88

## Introduction

---

### 1.1 Electric Traction

#### 1.1.1 Historical Background and General Features.

Electric Traction commenced with experiments on battery propulsion in Davenport, MA in 1837 and Davidson, Scotland in 1838. The first practical vehicles involving power supply drawn along a traction line were Werner von Siemens' demonstration of a small DC locomotive in Berlin in 1879 [11]. The first electric train in India ran between Bombay's Victoria Terminus and Kurla along the Harbour Line of CR, on February 3, 1925, a distance of 9.5 miles [21]. The electrification on 1500V dc was extended to the suburban services around Madras also by 1931[7]. In 1957, the Railway Board took a decision to introduce 25 KV, 50 Hz ac system. Also in 1958, Indian railways went for extensive mainline dieselization. Diesel electric system employs a self contained motive power unit using a diesel engine which drives a DC generator. This generator supplies electric power to the traction motors which are geared to the driving motors [7]. A converter fed drive (AC to DC or DC to DC) does with the need to use the generator system in traction drives. The converter converts 50 Hz supply and feeds it to the motor.

An electric traction is a combination of electric drive system and complex mechanics of Traction load. Thus a study of electric traction is not only involves study of electrical system but also a comprehensive understanding of mechanical system which governs the torque produced by the motor to achieve desired results. Thus it becomes extremely important to study the performance of electric drive and nature of Traction mechanics and adaptability of electric drive in response to any change in behavior of traction load. Thus, a complete electric traction may be divided into two subsystems

- Electric drive system
- Mechanical load system.

### **1.1.1.1 Electric Drive System**

This system deals with electric drive system that is used in traction application. A traction drive may use either an ac or a dc motor. Both these motors have their own advantages and disadvantages which dictate their use for the purpose.

#### ***DC motor in traction drive***

DC motor is widely used for traction purpose because of their easy speed control. DC series motor has been conventionally used as traction motor. It has high starting torque and capability for high torque overloads. The torque-speed characteristic of series motor is also suitable for better sharing of loads between motor [2].

With the availability of semiconductor converters, separately excited motor is sometimes used as traction motor. With independent control of armature and field, the speed torque characteristic of separately excited motor can be shaped to satisfy the traction requirement in optimum manner. Further, due to low speed regulation of its torque speed characteristic, the coefficient of adhesion has higher value (to be discussed later) [2].

However all DC motor suffer with a major drawback of presence of commutator and brushes which require frequent maintenance. This has prompted the use of ac machines for traction purposes. DC motors, however, are still widely used for traction purposes because of easy speed control.

#### ***AC motor in traction drive***

Due to availability of reliable variable frequency semiconductor inverters, squirrel cage induction motors and synchronous motors are now being used. Squirrel cage induction motor has the advantage of being rugged, thus requiring less maintenance, have lower cost, weight and volume, have higher efficiency, and ability to work satisfactorily in with sharp voltage fluctuations. However the control of the drive is comparatively complex.

Both these motors are employed in semiconductor converter (inverter) controlled drives.

#### ***Semiconductor based Converter controlled fed-traction drives***

Semiconductor based converter controlled drives are now widely used in both AC and DC traction. The semiconductor converter controlled drives have several advantages over the other primitive control schemes. Some of them are as follows.

- High efficiency.

- Low maintenance requirement.
- Better adhesion to the track due to step less control
- Higher acceleration due to better adhesion.
- Longer life.
- Flexible control, which makes it amenable to microcomputer/microprocessor/PLC control, leading to efficient performance.

The preferred configuration for the converter fed drive uses single semi controlled bridge converter. The semi controlled bridge converter has the following advantages over fully controlled converter for traction applications.

- Cost effective - this is due to less number of thyristors.
- Yields better power factor.
- Produces lower armature current harmonics (hence reduces motor torque ripple).

However the basic semi controlled bridge cannot regenerate power. This is not usually a significant disadvantage because regenerative operation is of little use on long distance railways [10].

#### **1.1.1.2 Mechanical Load System**

The mechanical system deals with the mechanics of traction including the dynamics of wheel-rail interaction which contributes significantly to the overall traction load seen by the motor. This includes slip-spin effects of the wheel on the track. These effects are governed by the complex interaction between motor, its controller and wheel-rail adhesion characteristics. This link is tenuous however, since adhesion is not an infinite force. Therefore at some point the limit of adhesion is exceeded and an imbalance of forces would occur in favour of motor torque. The maximum adhesion limit is then a fundamental limitation on the performance of the locomotive [10]. Thus a model of mechanical load could be developed which would include the wheel-rail interaction. This could then be used to determine the effects of various conditions of this interaction on the electrical drive system.

## 1.2 Literature Review

As discussed electric traction is a complex interaction of electric drive and the wheel-rail dynamics. Therefore study of both electric drive and traction mechanics provide important areas of study. Various researchers have focused on different aspects of electric traction. This section is an attempt to present a brief review of the available literature. There are number of interesting tasks that have been taken up earlier and in this review they have been broadly classified into categories as per their pertinence to the field.

- *DC Traction motor*

A number of research papers have been published to simulate and evaluate the performance of DC traction motor. W. Oghanna et al. [16] presents a two dimensional saturation model of DC traction motor including saturation of main poles and interlopes. For this two look up tables have been employed. One is  $E_m(i_f)$ , armature open circuit voltage against the field current when the motor is run as generator at rated speed. The other is  $E_{ac}(i_f)$ , the armature open circuit voltage against the interpole current when the motor is driven as generator at the rated speed, with all the brushes moved by 90° (electrical) from their original positions. Besides, the saturation caused by field currents, an algorithm is developed to account for the field weakening caused by the armature reaction. Using all these, a Simulink model for the DC traction motor has been developed. The model also presents the effect of saturation on all inductance parameters. S.L. Ho et al. [17] presents a thorough thermal analysis on DC Traction motors. The focal point of the study is to examine the feasibility of taking away the field shunt (current shunt across the field) at the beginning of the starting period. In this study a finite element method has been developed to simulate the temperature profile at different parts inside the traction motor. The simulation results have been verified by conducting a test on a light rail vehicle. G.Reyne et al. [18] introduces a finite element modeling for the assessment of electromagnetic force developed in the motor. It also studies the electromagnetic vibrations caused by these forces as the local densities of these forces is the only significant cause of such vibrations. It also introduces various modeling tools towards achievement of these aims.

- ***Electric Traction Drive***

The study of electric drive offers a number of challenges some of which have been discussed in the research papers discussed below. S. Burdett et al. [13] suggests a number of methods for improving power factor for traction drives. Some of the suggested methods are use two stage control of series connected half controlled converter, use on board second and higher order filters and using pulse converters. The efficiency of traction drive under operating conditions is generally poor. Parviz Famaouri, [14] suggests a design of high efficiency traction drive employing DC series motor under accelerating conditions. The suggested drive minimizes the armature and field winding copper loss. M.W Winterling et al. [15] study the behavior of the traction drive under fault conditions. The two kind of faults considered are (a) loss of speed probe (b) short circuit of electric motor.

- ***Wheel-rail interaction and slip control***

The behavior of electric drive in response to wheel-rail interaction is a forms a very important subject of study. This includes the challenge of comprehension of the dynamics of wheel-rail interaction. Steven Senini et al. [10] proposed a simplified dynamic model which provides a useful insight at this problem. A simulation of entire locomotive system with a closed loop electric drive employing separately excited traction motor and wheel rail interaction has been carried out by R. Mathew et al. [9]. Another important area of study is slip control strategies. There are a number of strategies available for slip control. Yoichi Hori et al. [12] suggest design of Model based Controller and optimal slip ratio controller for slip controller and experimental implementation of the scheme. They also introduce the concept of gradient control for effective slip control. This concept is further expounded by Kiyoshi Ohishi et al. [19] & Yoshiki Ishikawa et al. [20].

### **1.3 Objectives of the present work**

The primary objectives of this study are

1. To simulate a closed loop DC drive employing half controlled converter and study the improvement in performance using two stage half controlled converters.
2. To model the Traction load.
3. To model an Electric Traction drive employing wheel slip control.
4. To study the behavior of electric traction drive for different conditions such as operation on flat track, inclined track and variable track.

### **1.4 Approach adopted for mathematical modeling**

The simulation of closed loop DC drive and traction load has been carried out using SIMULINK environment of MATLAB. A major approach of this exercise is that electric drive system and mechanical load systems are simulated independent of each other. This provides a flexibility to make changes in any one of them to incorporate new features without disturbing other.

### **1.5 Outline of the dissertation.**

Chapter two starts by expounding the natural behavior of DC series motor and some general discussions about converter fed dc motor drive. This chapter culminates at the simulation of a closed loop dc drive with braking capabilities. It also demonstrates the superiority of two stage sequence control of series connected half controlled converters over single stage half controlled converter. Chapter three explains the mechanics of traction load, various factors affecting wheel- rail interaction including factors affecting the coefficient of adhesion. It also derives the equations governing wheel and train dynamics and finally culminates at the evolution of traction load model. Chapter four implements an electric traction drive with wheel slip control. The two wheel slip control strategies implemented are slip control to the reference value and gradient control.

Chapter five is the conclusion chapter and ties up everything together by presenting important points of the study and some recommendations for improvement of existing model and further work that can be carried out.



## Modeling of Converter fed DC Series motor Drive

---

### 2.1 DC Series Motor and its characteristics.

A DC machine can operate as either a generator or a motor but at present its use as a generator is limited because of the widespread use of AC power. Large DC motors are used in machine tools, printing presses, conveyors, fans, pumps, hoists, cranes, paper mills, textile mills and so forth. Small DC machines (in fractional horsepower rating) are used primarily as control devices such as tacho-generators for speed sensing and servomotors for positioning and tracking. DC motors still dominate as traction motors used in transit cars and locomotives as their torque-speed characteristics can be varied over a wide range while retaining high efficiency. The DC machine definitely plays an important role in industry.

DC motor may be classified as separately excited, shunt motor, series motor and compound motor. In a separately excited DC motor, the field and armature voltage are controlled independently of each other. In a shunt motor field and armature are connected to the common source. In case of series motor, the field winding is connected in series with the armature; hence the field current is equal to armature current. All DC motors are governed by following basic equations.

$$\bullet \quad V = E + I_a * R_a \quad (2.1)$$

$$\bullet \quad E = K * \omega \quad (2.2)$$

$$\bullet \quad T = K * I_a \quad (2.3)$$

Where

$$K = K_e * \phi. \quad (2.4)$$

From the above equations we can show that  $\omega = (V / K_e * \phi) - (R_a / K_e * \phi) * I_a$ .

Both series and separately excited motors have been used as Traction motors with each motor having its own advantages to justify its use as a traction motor.

The DC traction motor that has been used to carry out further modeling is a DC series motor (for further specifications, see Appendix A).

The motor dynamics are governed by the following equations

$$E = V - I_a(R_a + R_{se}) - (L_a + L_{se}) \frac{dI_a}{dt} \quad (2.5)$$

$$T_e = T_l + B_m \omega + J \frac{d\omega}{dt} \quad (2.6)$$

Where

$L_a$  = armature inductance.       $L_{se}$  = field inductance.  
 $R_a$  = Armature resistance.       $R_{se}$  = Field resistance.  
 $J$  = moment of inertia.       $B_m$  = coefficient of viscous friction

Under steady state

$$(L_a + L_{se}) \frac{dI_a}{dt} = 0 \quad (2.7)$$

$$\text{and } J \frac{d\omega}{dt} = 0 \quad (2.8)$$

Therefore steady state equation becomes

$$E = V - I_a(R_a + R_{se}) \quad (2.9)$$

$$T_e = T_l + B_m \omega \quad (2.10)$$

Further, from equation 2.2, 2.3, and 2.4, we get,

$$E = K_e \varphi \omega \quad (2.11)$$

$$\text{and } T_e = K_t \varphi I_a \quad (2.12)$$

Assuming a linear model, we get,

$$\varphi = K_f I_f \quad (2.13)$$

For a series motor  $I_a = I_f$ , therefore

$$\varphi = K_f I_a \quad (2.14)$$

From equation 2.11, 2.12 & 2.14, we get

$$E = K_e K_f I_a \omega \quad (2.15)$$

$$\text{and } T_e = K_t K_f I_a^2 \quad (2.16)$$

Using equation 2.9, 2.15 & 2.16, we get,

$$\omega = \frac{V}{\sqrt{K_e * K_f}} \frac{1}{\sqrt{T}} - \frac{(R_a + R_{se})}{K_e * K_f} \quad (2.17)$$

Using this equation, a theoretical steady state torque-speed characteristic of this motor is obtained below

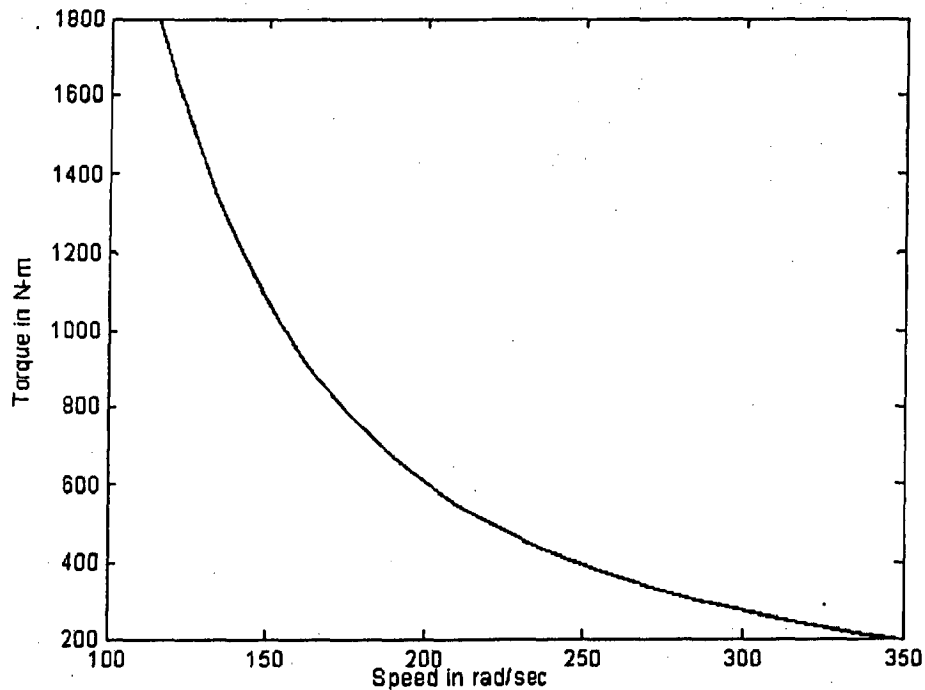


**Figure 2.1** Torque-Speed characteristic of DC series motor.

In terms of field-armature mutual inductance, 2.15 & 2.16 can be written as [8]

$$E = (P/2)L_{af}I_a \omega \quad (2.18)$$

$$\text{and } T_e = (P/2)L_{af}I_a^2 \quad (2.19)$$

where  $L_{af}$  = field-armature mutual inductance.

$P$  = number of poles.

The SimPowerSystem blocksets to the MATLAB provides a dc motor model which is governed by the equations obtained above. A check on the validity of the model for our machine is obtained by comparing the simulated steady state torque-speed characteristic of the motor by the theoretical torque speed characteristic obtained in figure 2.1.

This is given in figure 2.2.

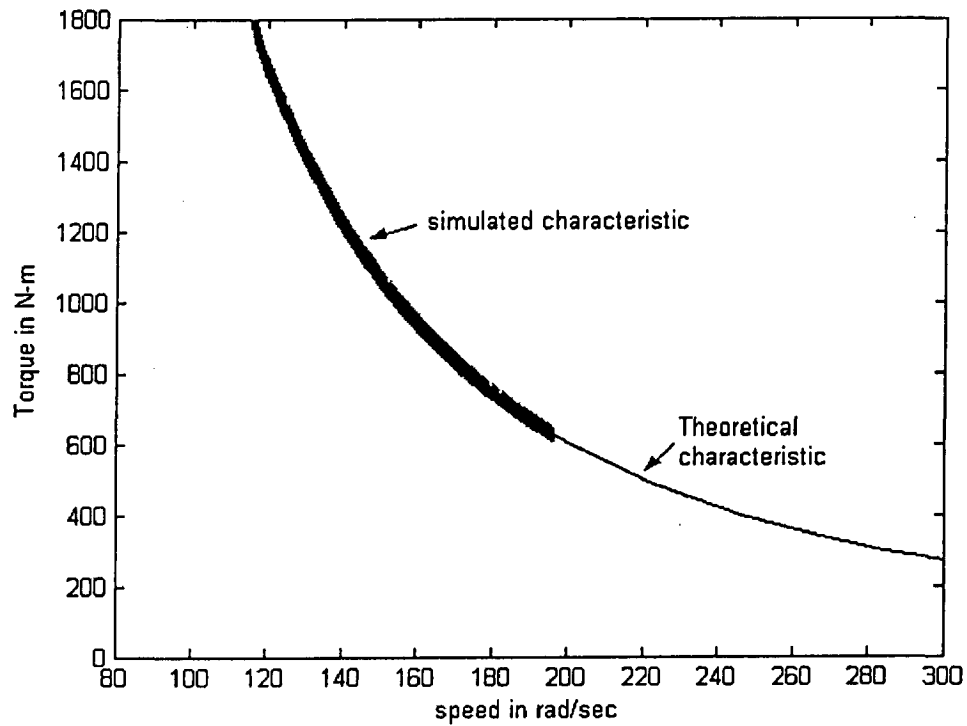


**Figure 2.2** Simulated and Theoretical Torque-Speed Characteristic.

Once the validity of the motor model of confirmed, it would be natural to look into the speed control of the motor.

## 2.2 Speed control of DC motor

From the discussion in last chapter, it follows that there can be two control strategies for controlling the speed of the machine.

1. Armature Voltage Control.
2. Field Flux control.

Armature voltage control yields high efficiency, good transient response and good speed regulation. However, it can provide speed control only below base speed because the armature voltage cannot be allowed to exceed rated value. For speed above base speed, field flux control is employed.

### **2.2.1 Armature Voltage Control**

If the armature voltage of a separate or series excited dc motor running at steady speed is reduced by a small amount, then, the armature current and hence the motor torque will decrease. As the motor torque is less than the load torque, the motor will decelerate, causing speed to decrease. It will finally settle at a lower speed at which torque equals load torque[1].

On the other hand, if the armature voltage of a DC motor running in steady state speed is increased, the armature current and therefore the motor torque will increase. The motor torque now exceeds the load torque, the motor accelerates. The motor speed increases causing the back emf to increase. The motor finally settles at higher value of speed when motor torque becomes equal to load torque.

Armature voltage control for a DC motor can be obtained any of the following methods

- Using Ward-Leonard schemes.
- Using Transformer with taps and uncontrolled rectifier bridge.
- Using Controlled rectifiers.

### **2.2.2 Field Flux Control**

If the field of a DC motor running at a particular speed is weakened, its emf decreases. Because of low armature resistance, the current increases by a amount much more than the decrease in the field flux. As a result, in spite of the of the weakened field, the motor torque increases by a large amount, considerably exceeding the load torque. The surplus torque thus available causes the motor to accelerate and back emf to rise. The motor will finally settle down to a new speed higher than the previous one, at which the motor torque with weakened field becomes equal to the load torque. The highest speed that is achievable by field weakening is restricted by the instability of machine due to demagnetizing effect of armature reaction [1]. Field control of a separately excited DC motor is simple as the field connections are independent of armature connections. In case of series excited dc motor, field weakening can be achieved by employing a field diverter.

However, in our schemes, only armature control has been simulated for the DC series motor with a view that the rated speed of the motor can offer the maximum speed of the train.

### 2.3 Open loop speed control of DC Series motor using half controlled converter

#### 2.3.1 Theory

Single phase half controlled rectifier fed DC series motor is often used in electric traction. This is shown in the figure below.

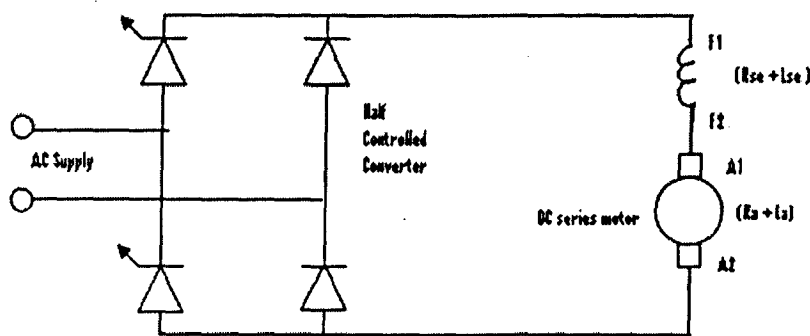


Figure 2.3 Schematic layout of converter fed DC series motor.

Figure 2.4 shows the controlled voltage from the converter being applied to the motor.



Figure 2.4 Output voltage of converter.

The motor operation for the duty and the free wheeling intervals respectively, are given by the following equations.

$$Vm \sin \omega t = (R_a + R_{se})i_a + (L_a + L_{se})\frac{di_a}{dt} + E \quad \text{for } \alpha \leq \omega t \leq \pi. \quad (2.20)$$

$$\text{And } (R_a + R_{se})i_a + (L_a + L_{se})\frac{di_a}{dt} + E = 0 \quad \text{for } \pi \leq \omega t \leq \pi + \alpha \quad (2.21)$$

Taking average over the entire duty cycle we get,

$$\frac{V_m}{\pi}(1 + \cos \alpha) = (R_a + R_{se})I_{av} + E_{av} \quad (2.23)$$

$$\text{or } E_{av} = \frac{V_m}{\pi}(1 + \cos \alpha) - (R_a + R_{se})I_{av} \quad (2.24)$$

The figure 2.5 shows the steady state torque speed characteristic for two values of firing angles.

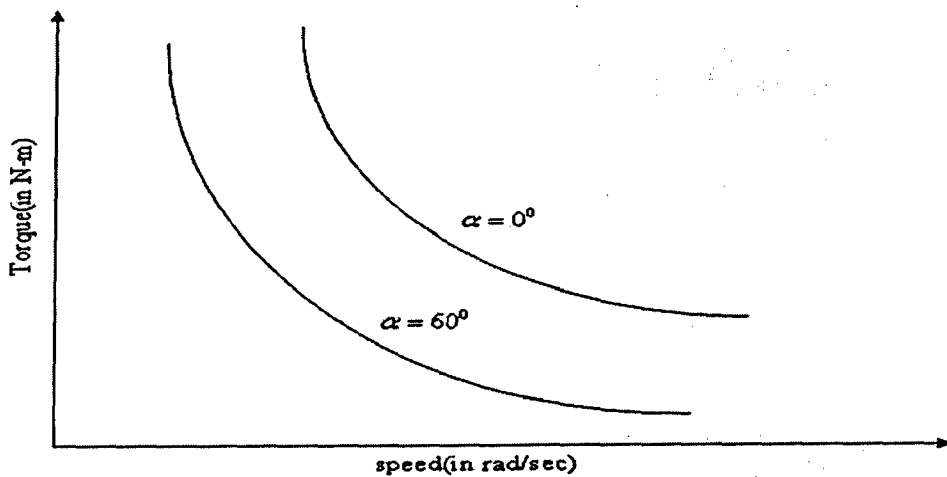


**Figure 2.5** Torque-Speed Curves of converter fed dc series motor at different firing angles.

### 2.3.2 Simulation with MATLAB

The open loop control of DC series motor fed from half controlled converter has been simulated using SimPowerSystem blocksets of MATLAB to demonstrate the behavior of the traction motor with converter fed supply. The figure 2.6 shows the MATLAB implementation of the open loop control. The load torque is assumed to be proportional to speed of the motor.

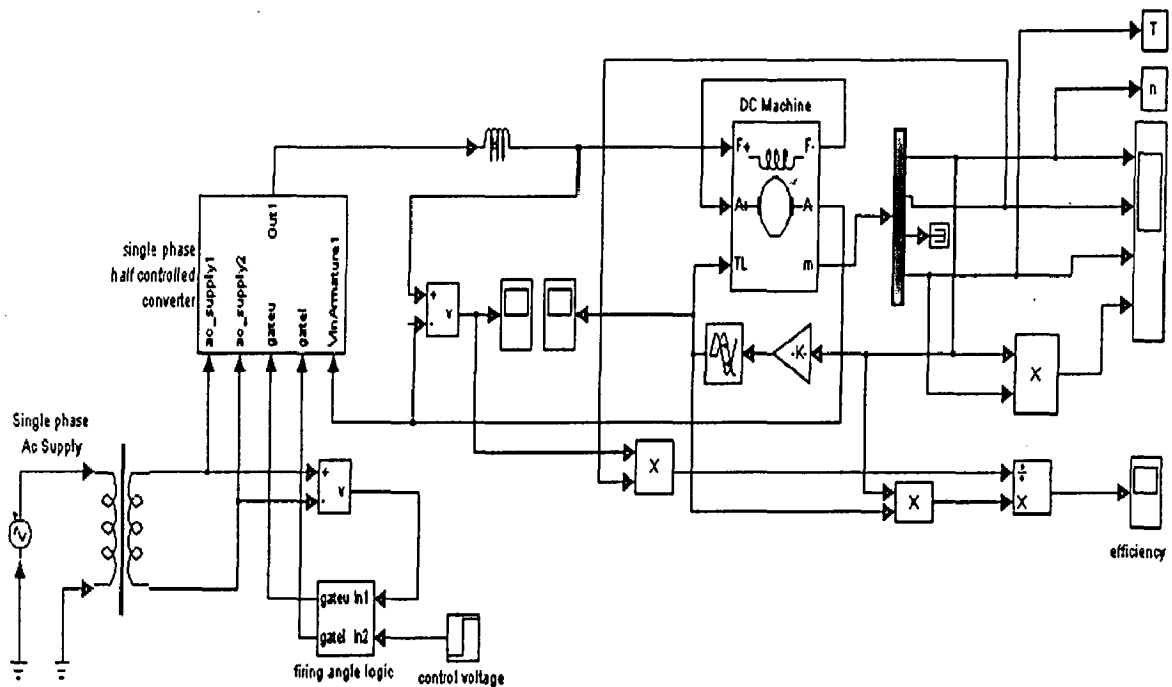


**Figure 2.6** SIMULINK implementation of open loop control of half controlled converter fed DC series motor.

The important components this scheme are discussed in detail below

### 2.3.2.1 DC Series motor

This has been discussed in detail in section 2.1.

### 2.3.2.2 Single phase Half Controlled Converter

The single phase half controlled converter used in the scheme has been designed in asymmetrical configuration as this configuration has a number of advantages over symmetrical configuration. Some of these advantages are listed below [3].

1. For large firing angle delays, commutation failure may occur due to limited time available in symmetrical configuration. This may result in half waving effect.
2. In symmetrical configuration, the thyristor conduct for longer interval and therefore they must have higher average current rating than the ones required for asymmetrical configuration.

The SIMULINK implementation of this converter is given in figure 2.7



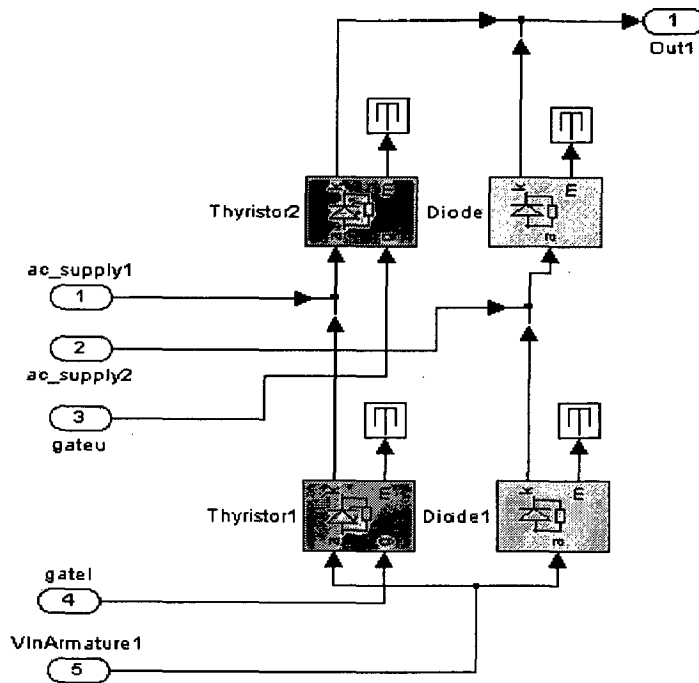


**Figure 2.7** SIMULINK block for Single Phase Half Controlled Converter

For a single phase half controlled converter, the average output voltage is given as

$$V_{ao} = \frac{\sqrt{2}V(1 + \cos \alpha)}{\pi} \quad (2.25)$$

Now if the firing angle is produced at the intersection of control voltage  $V_c$  and the timing wave,  $V_r = V_{rm}(1 + \cos \omega t)$

$$\text{Then, } V_{rm}(1 + \cos \alpha) = V_c \quad (2.26)$$

If the converter has a linear transfer characteristic with respect to control voltage, then the average output voltage of converter can be given as

$$V_{ao} = K_r V_c \quad (2.27)$$

$$\text{or } \frac{\sqrt{2}V(1 + \cos \alpha)}{\pi} = K_r V_{rm}(1 + \cos \alpha) \quad (2.28)$$

$$\text{or } K_r = \frac{\sqrt{2}V}{\pi V_{rm}} \quad (2.29)$$

The average delay time for a single phase converter is given by

$$T_r = 1/(4f).$$

Where  $f$  = frequency of ac supply voltage.

Thus a mathematically, a half controlled converter can be represented as

$$G(s) = K_r e^{-sT_r}. \quad (2.30)$$

where

$K_r$  = gain of converter.

$T_r$  = average delay in implementation of new firing angle command.

Equation (2.30) can be approximated as a first order time lag and given as

$$G_r(s) = \frac{K_r}{(1 + sT_r)} \quad (2.31)$$

### 2.3.2.3 Firing Circuit Logic

The firing circuit used in the scheme is designed such that the converter gain is linearized. For this the timing wave is made proportional to  $(1 + \cos \omega t)$ . This has already been discussed in section 2.3.2.2. The intersection of control signal with the timing wave yields the instant at which the thyristor should be triggered. This is given by the equation given 2.26

The output of single phase half controlled converter is given by

$$V_{ao} = \frac{\sqrt{2}V(1 + \cos \alpha)}{\pi} \quad (2.32)$$

$$\text{Or} \quad V_{ao} = \frac{\sqrt{2}V}{\pi V_{rm}} V_c \quad (2.33)$$

Thus we see that output of the converter becomes a linear function of the controller output.

This firing circuit logic with above mentioned considerations has been implemented in SIMULINK environment of MATLAB as given below

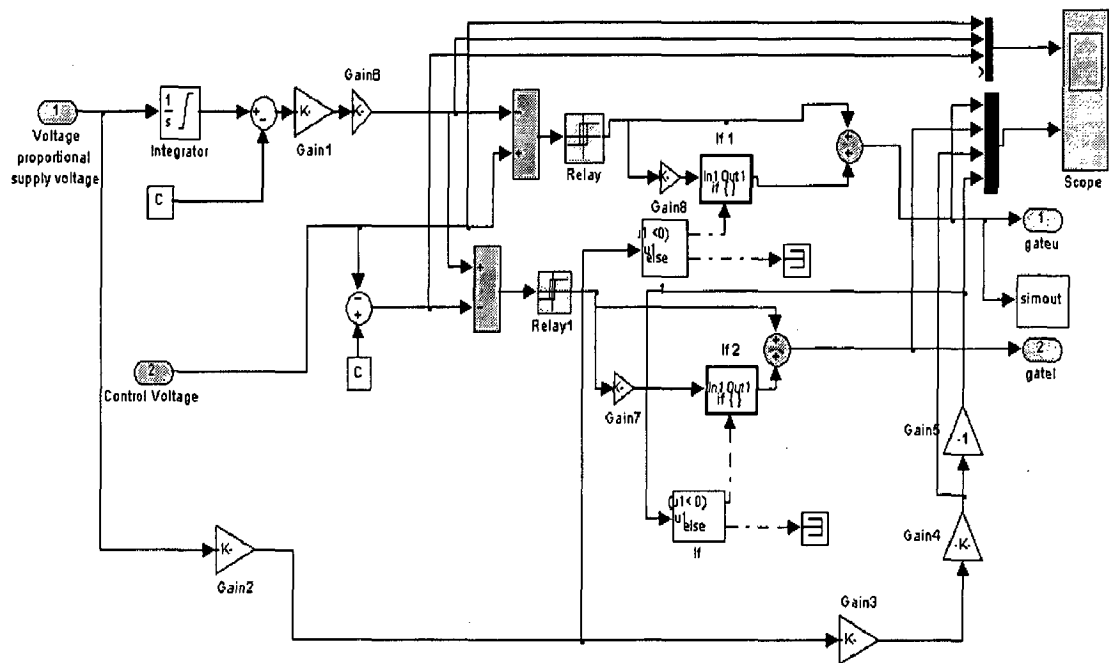


**Figure 2.8** SIMULINK block implementing firing circuit logic

The sample output of this firing circuit logic for a particular simulation is given below

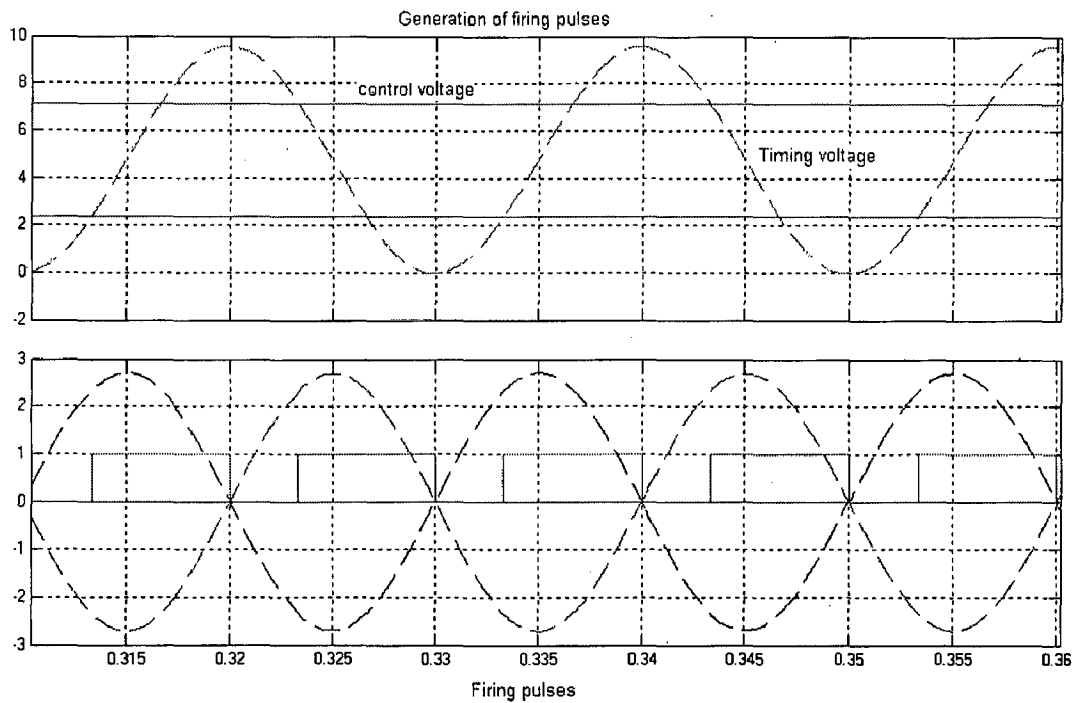


**Figure 2.9** Generation of firing pulses.

### 2.3.3 Results

The scheme was simulated for various values of firing angles of the converter. The results hence obtained shows the capability of the series motor when fed with single phase half controlled converter.

For  $\alpha=0^\circ$ .

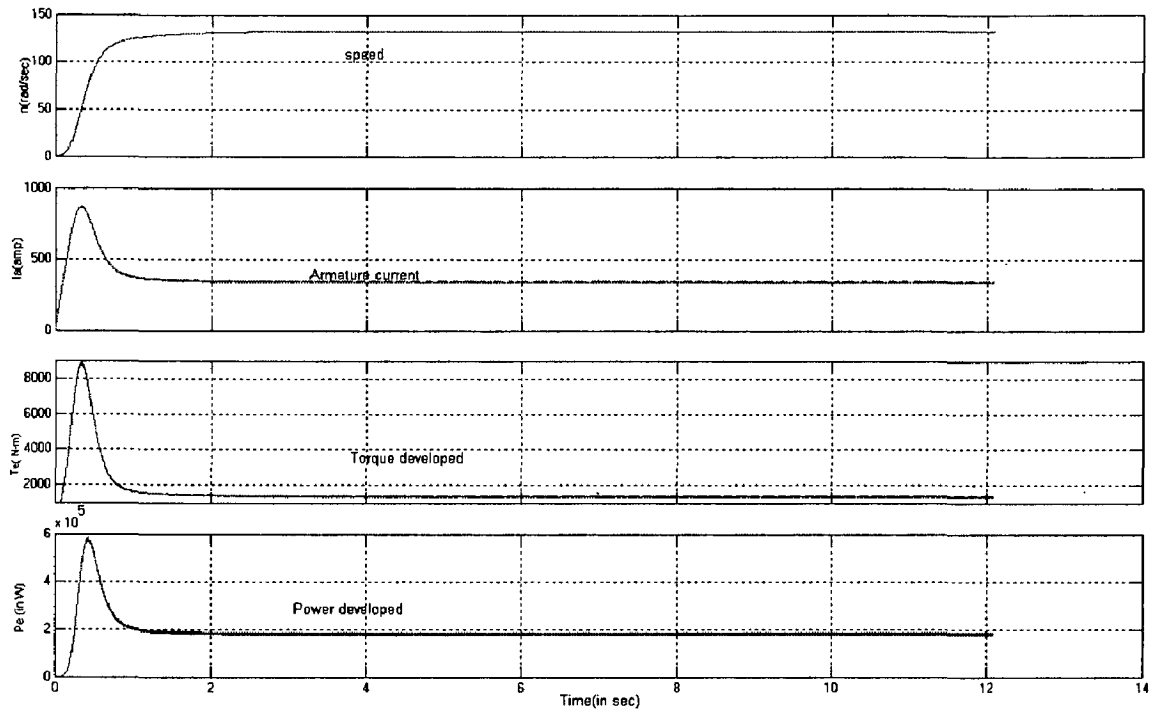


**Figure 2.10.** Performance of DC series motor when fed from converter with  $\alpha=0^\circ$ .

The variation of efficiency as the motor builds up towards the rated speed is given below

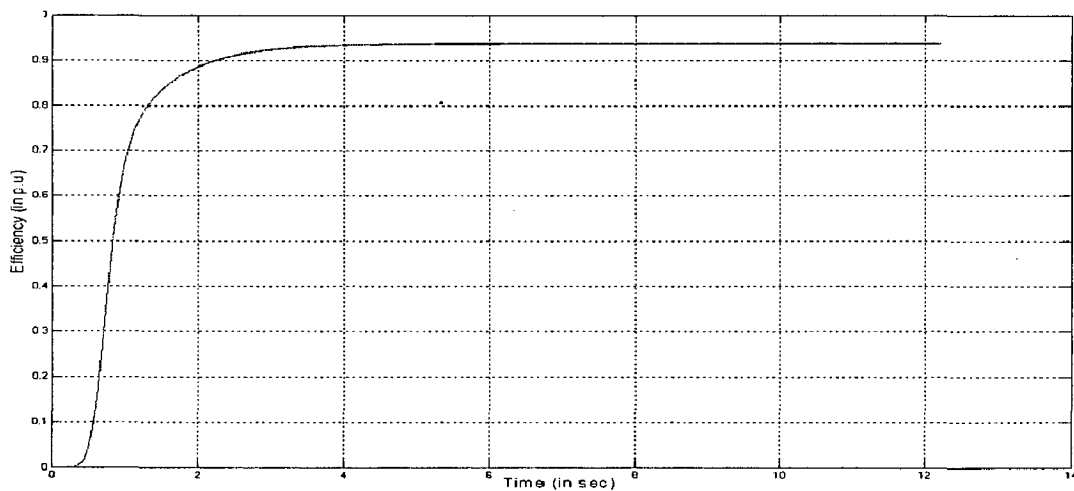


**Figure 2.11.** Efficiency of DC series motor when fed from converter with  $\alpha=0^\circ$ .

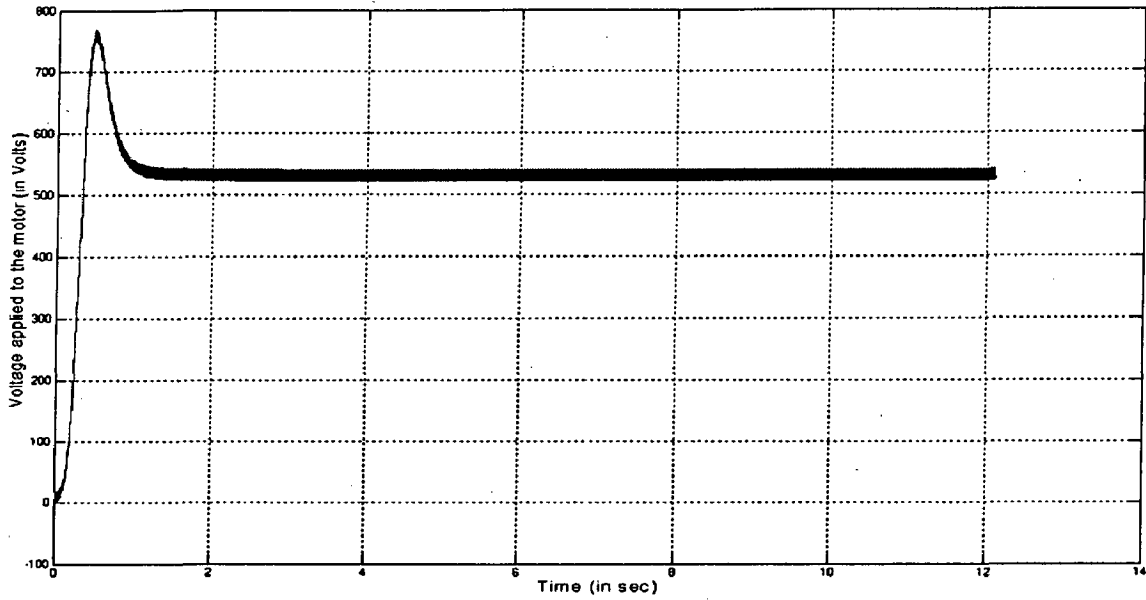


Figure 2.12 Voltage applied to the DC series motor.

For  $\alpha = 60^\circ$

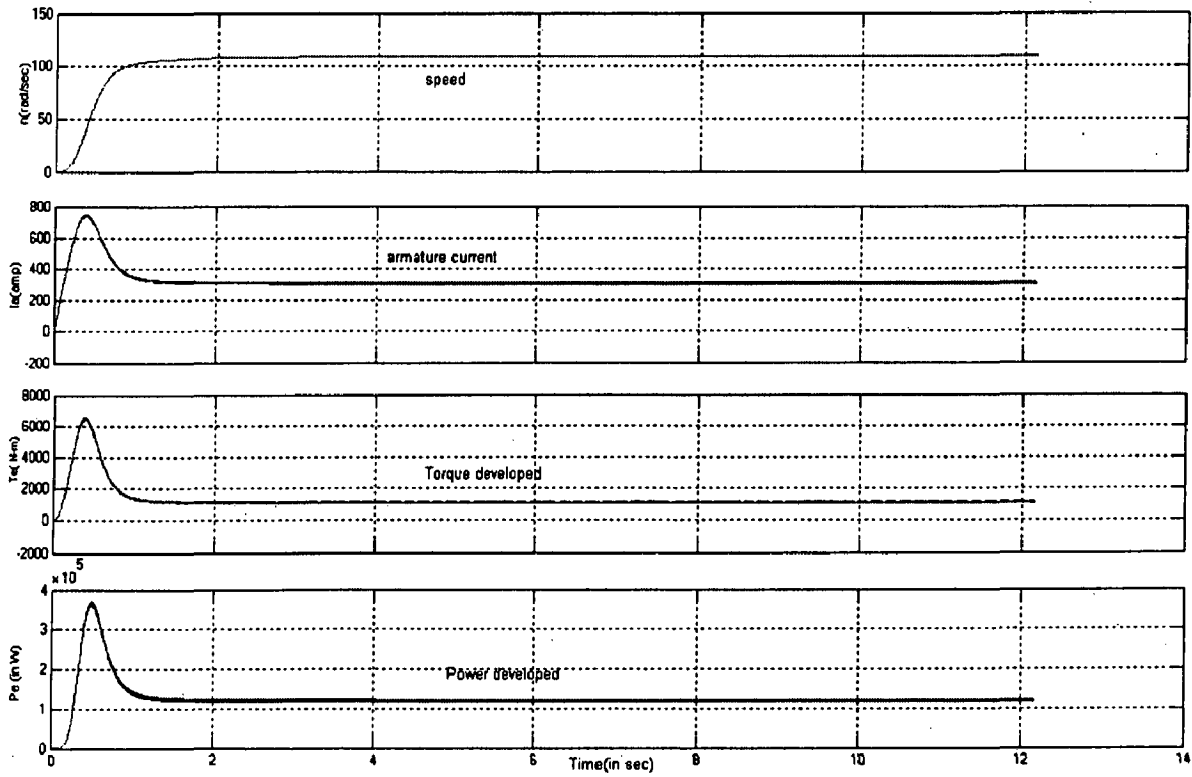
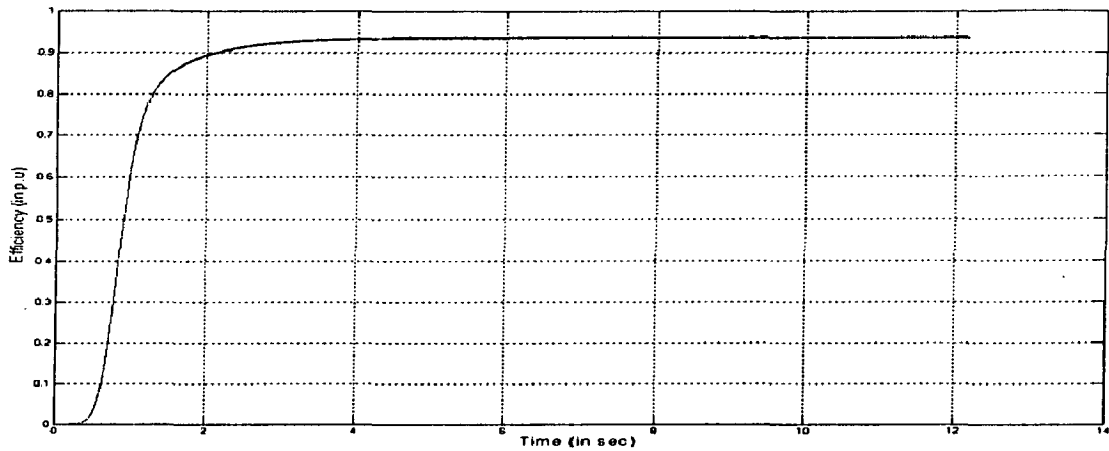
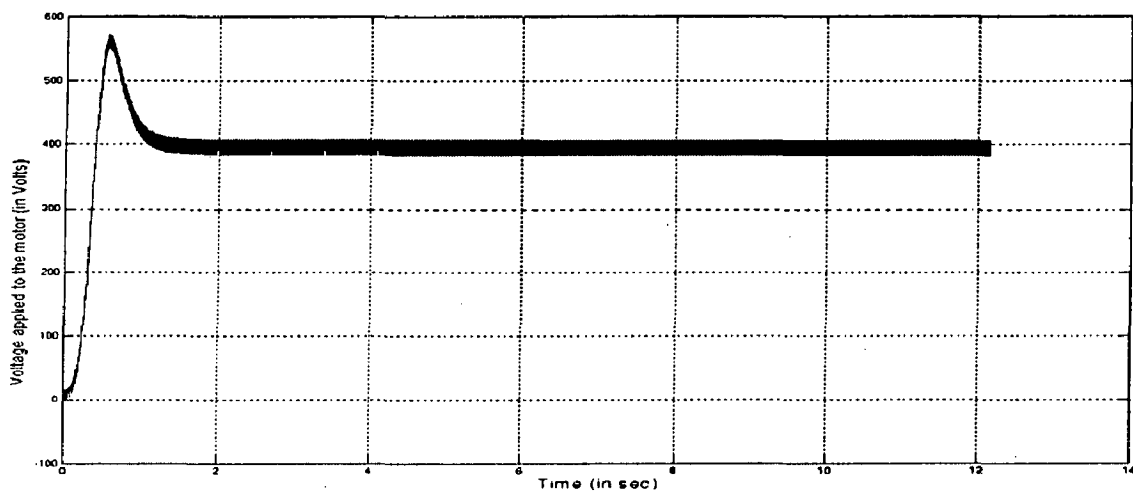


Figure 2.13 Performance of DC series motor when from converter with  $\alpha = 60^\circ$ .



**Figure 2.14** Efficiency of DC series motor when fed from converter with  $\alpha = 60^\circ$ .



**Figure 2.15** Voltage applied to the DC series motor.

The steady state torque-speed characteristic of the motor for two firing angles is simulated below

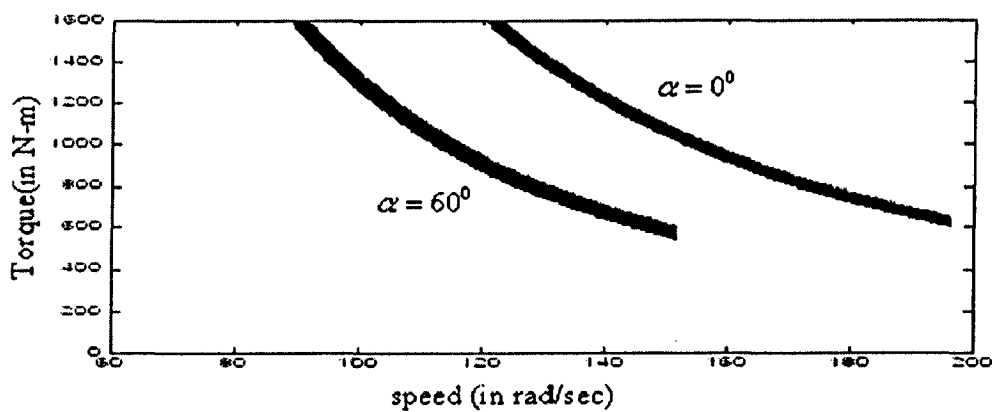


**Figure 2.16** Simulated Torque-Speed Curves of converter fed DC series motor at different firing angles.

## 2.4 Closed loop Control of DC Series motor.

### 2.4.1 Theory

The scheme employs an inner current loop with an outer speed loop. The advantage of using such a scheme is that the machine builds up towards desired speed without ever exceeding the current limit. The inner current loop also reduces the effect of non linearity in the converter-motor system on the drive performance. This is given in figure 2.17.

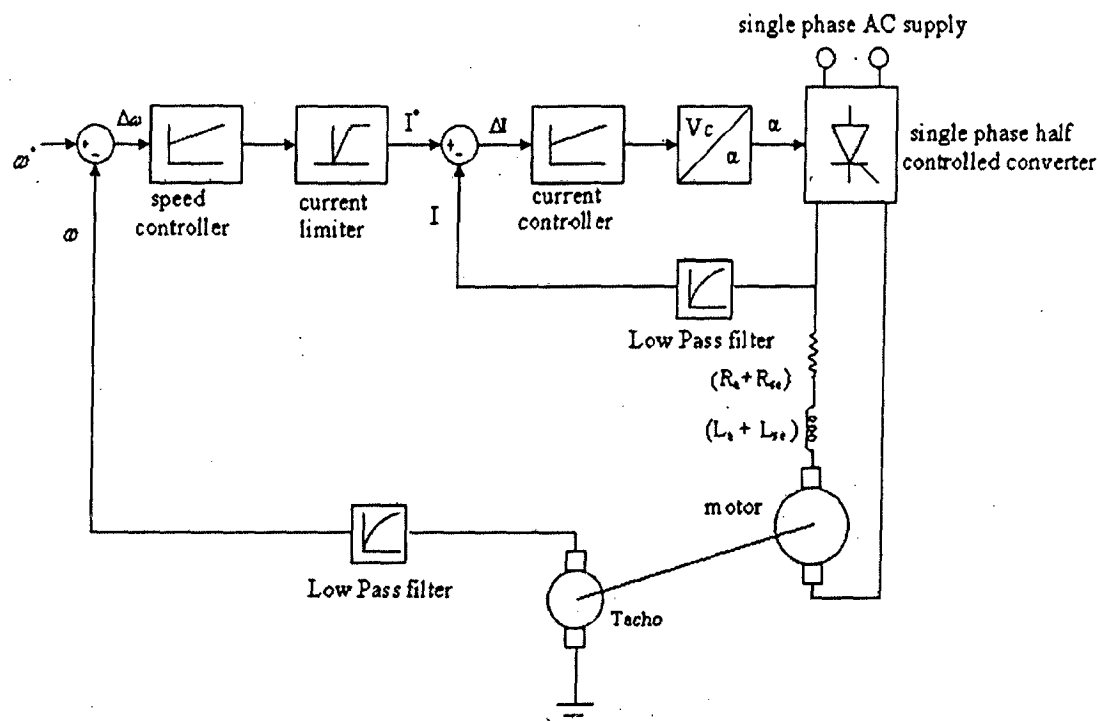


**Figure 2.17** Schematic layout of closed loop dc drive with inner current loop and outer speed loop.

The speed error is processed through a speed controller. The output of the speed controller yields torque command which is processed to form a current reference. The actual armature current is then fed to the current controller after smoothing the current signal. The current error is processed to produce a firing angle command for the firing circuit. The gate trigger pulses from the firing circuit controls the triggering instant of the converter and hence the voltage fed to the armature is controlled.

Any positive speed error, caused either by an increase in speed command or an increase in load torque produces a higher current reference  $I_a^*$ . The motor accelerates due to an

increase in  $I_a$ , to correct the speed error and finally settles at a new  $I_a^*$  which makes the motor torque equal to load torque and the speed error close to zero. If the speed error is large, the current limiter saturates and sets the current reference at rated value. The drive therefore accelerates at rated value of current and torque. For a negative speed error the current reference is set to zero because negative  $I_a^*$  is of no use and it charges the PI controller. When the speed reference becomes positive again, the charged PI controller takes longer time to respond.

#### **2.4.2 Implementation of the closed loop control of DC series motor**

The closed loop scheme discussed above is simulated using SIMULINK blockset of MATLAB. This is illustrated in figure 2.18. The model developed can exhibit both braking and motoring mode.

In the motoring mode, the output of speed controller forms current reference for the current controller. The current controller processes the speed error and the drive accelerates under controlled torque. Since half controlled converter is used to simulate the electric drive, dynamic braking is used. In this form of braking the electric supply to the armature of the motor is cut off and the motor is connected across a resistor thus allowing the kinetic energy of the motor to get dissipated. A change of mode from motoring to braking can be made with the help of a 'manual switch' provided in the scheme. Whenever a transition of zone is made, i.e. motoring to braking or vice-versa, the circuit connections are changed with the help of switches. The circuit connection for the motoring and braking mode will be discussed in section 2.4.2.2.

A number of functional subsystems blocks have been designed to implement this model. Some of the most important subsystems are half controlled converter, PI controllers and firing circuit logic. The details of these functional subsystem blocks are discussed in detail.



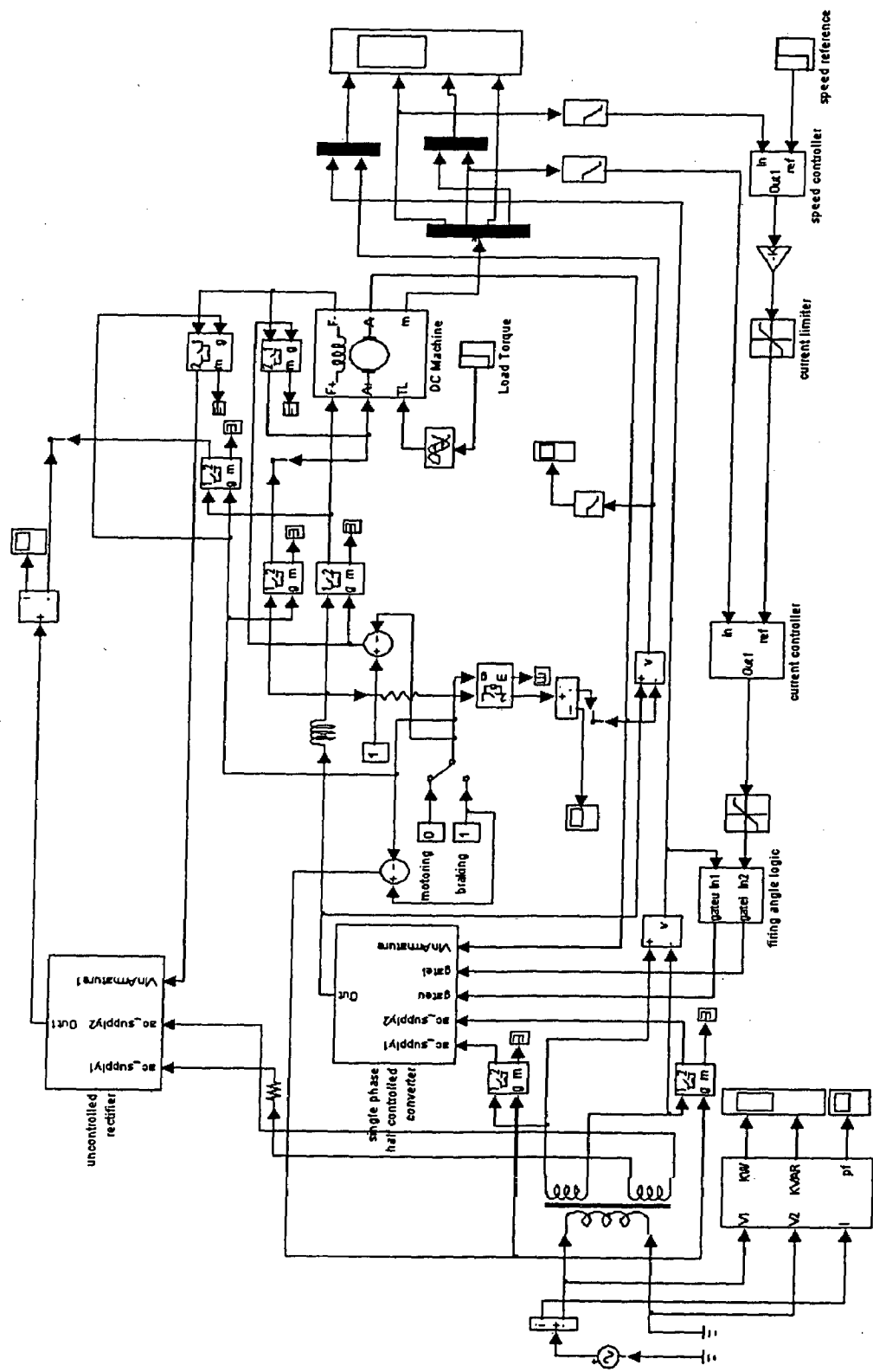


Figure 2.18 Simulink implementation of closed loop DC motor drive with braking capability.

### 2.4.2.1 Motoring mode

This has been explained in detail in article 6.

### 2.4.2.2 Braking mode

Since the supply is fed from a half controlled converter, regenerative braking is not possible. Therefore dynamic braking has been simulated.

Dynamic braking of a DC series motor can be achieved in two ways.

- **Field reversal**

In this, the motor is disconnected from the supply and is connected across a resistor with field connections reversed such that the direction of field current does not change. Thus the motor now acts as generator and all its kinetic energy is dissipated across the external resistor. It is important to note that the value of external resistance should be less than the critical resistance, otherwise there would be no excitation of motor as generator. The schematic layout of this scheme is given in the figure below.

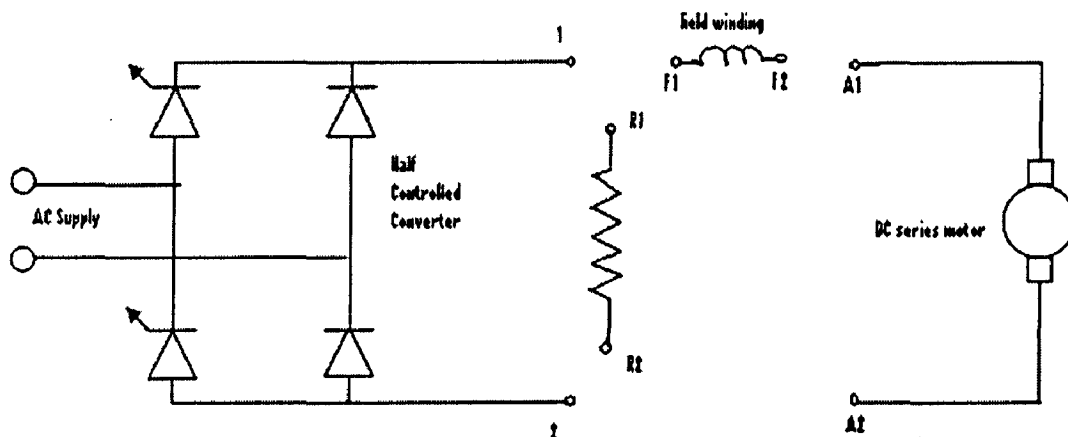


**Figure 2.19**

Braking with field reversal.

*Connection in motoring mode*

1-F1, F2-A1, A2-2.

*Connection in braking mode*

F1-A1, F2-R1, R2-A2.

- *Field is connected to a separate dc source during braking.*

In this scheme the field winding is separately excited during braking. This is illustrated by figure below

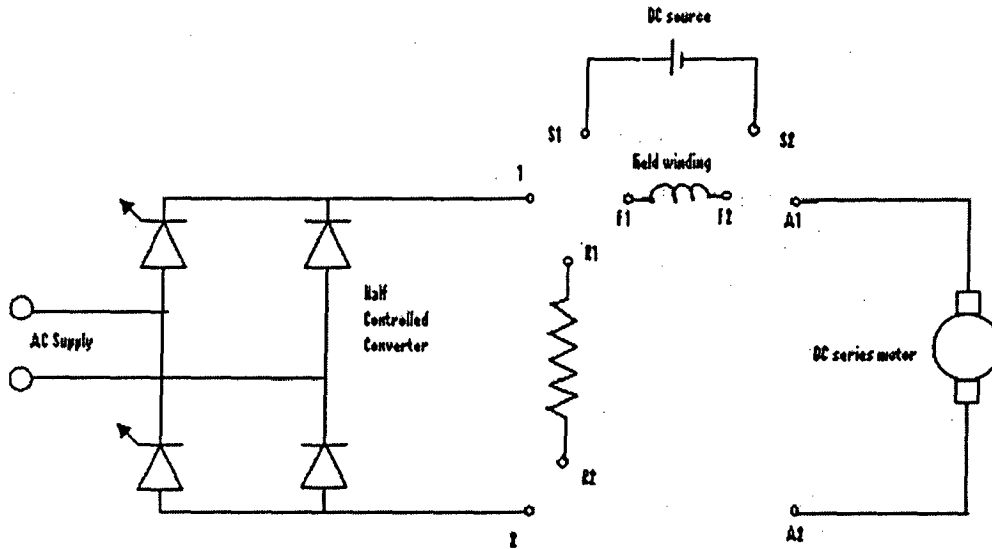


Figure 2.20 Braking with field connected to separate dc source.

*Connection in motoring mode*

1-F1, F2-A1, A2-2.

*Connection in braking mode*

S1-F1, S2-F2, A1-R1, R2-A2.

This mode of dynamic braking is more common in traction applications and has therefore been adopted further in the simulations. The DC source is derived by rectifying AC source voltage using uncontrolled bridge rectifier.

Some of the important subsystem blocks to simulate the entire closed loop scheme with braking capability are discussed below

### Single phase half controlled converter

Asymmetrical configuration of converter has been used due to inherent advantages it yields over the symmetrical configuration [3]. This has been discussed in detail in section 2.3.2.2. A SIMULINK implementation of half controlled converter is given in figure 2.7.

### Firing circuit logic.

The firing circuit used in the scheme is designed such that the converter gain is linearized. This has been discussed in section 2.3.2.3. A SIMULINK implementation of this firing circuit logic has been discussed in figure 2.8.

### PI Controllers

The PI controller is an effective means of regulating quantities to the desired values. It also improves the steady state error. This is achieved by providing a gain for the error term with an integral component correction.  $K_p$  is the proportional gain and  $K_i$  is the integral gain of the feedback loop. A SIMULINK block diagram for PI controller is given below

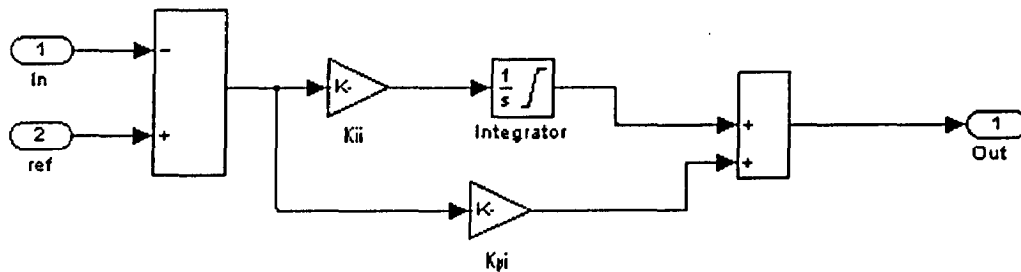
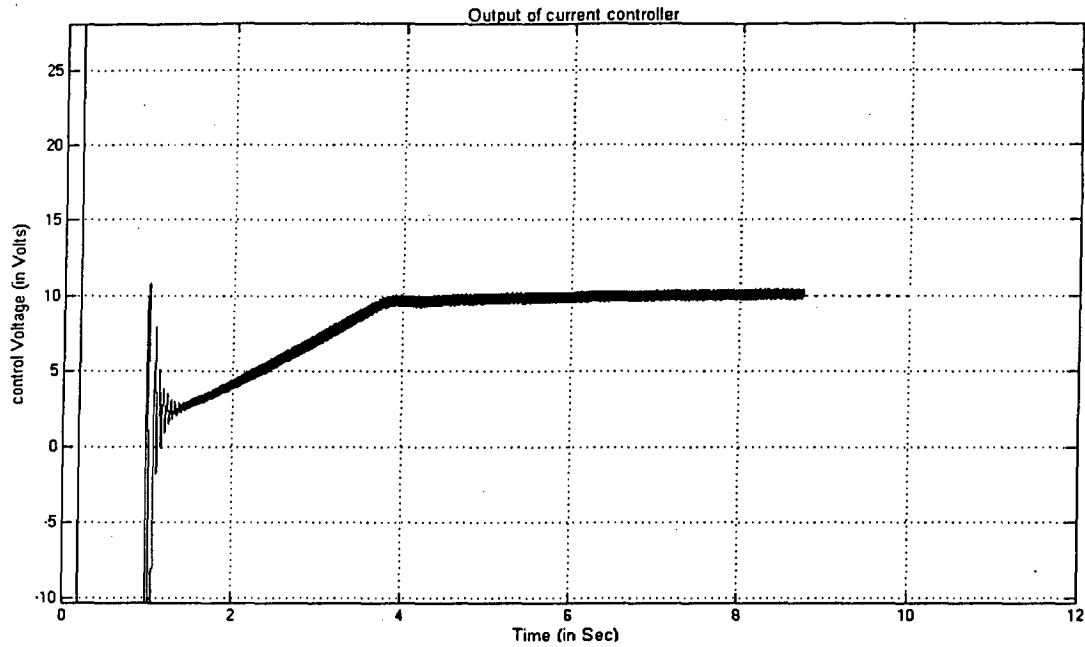


Figure 2.21 A SIMULINK block diagram representation of PI Controller



**Figure 2.22** Sample response of current controller.

The values of  $K_p$  and  $K_i$  for speed and current controllers have been found by trial and error. The values of current and speed controllers are as following

*Speed Controller*

$K_p = 146$ ,  $K_i = 585$ .

*Current Controller*

$K_p = 2.25$ ,  $K_i = 5.3$ .

A brief analysis of current and speed response for different values of current and speed controllers gains is presented with simulated results with the reference speed set at 125 rad/sec.

The current response at different values of controller gains is shown in figure 2.23 and 2.24.

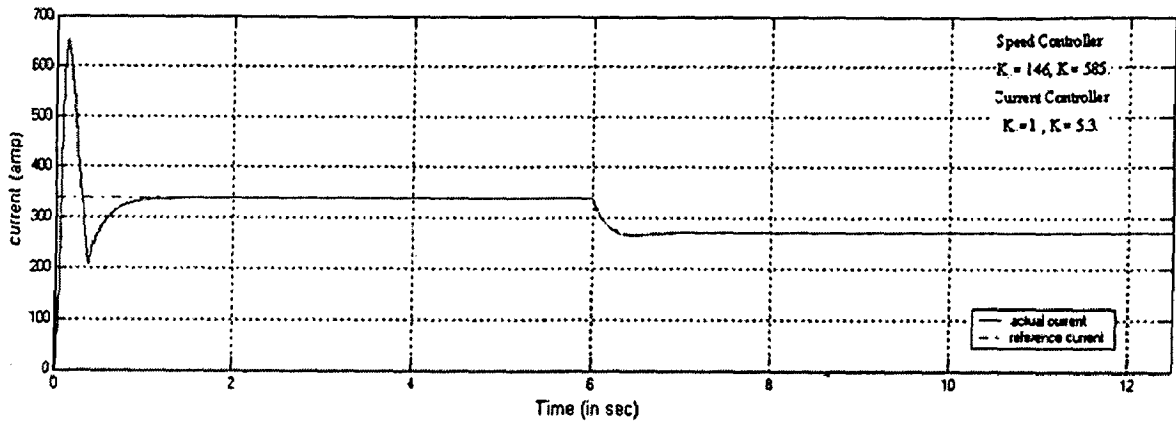


**Figure 2.23** Current response when proportional gain of current controller,  $K_p=1$ .

Now if the current controller's proportional gain is made equal to 2.25, then the current response is as shown below in figure 2.25.

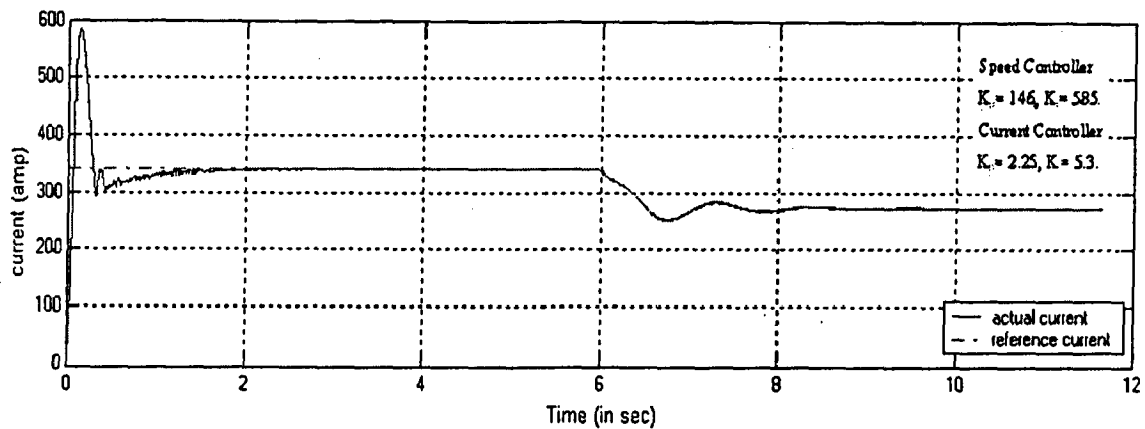


**Figure 2.24** Current response when proportional gain of current controller,  $K_p=2.25$ .

It may be observed that the peak overshoot has decreased. It was observed that the system worked more satisfactorily when operated with a proportional gain,  $K_p=2.25$ .

The speed response at set values of speed controller gains is given in figure 2.25 and 2.26.

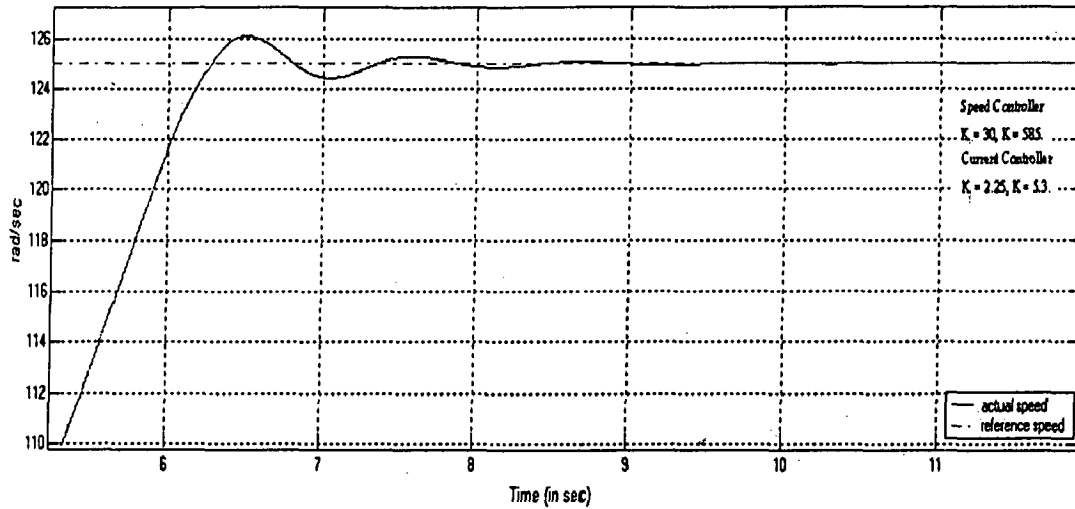


**Figure 2.25** speed response when proportional gain of speed controller,  $K_p=30$ .

The response in figure 2.25 reflects that the transient response of the system is poor. The peak percentage overshoot is approximately 0.8% and also the settling time is approximately 3.2 sec

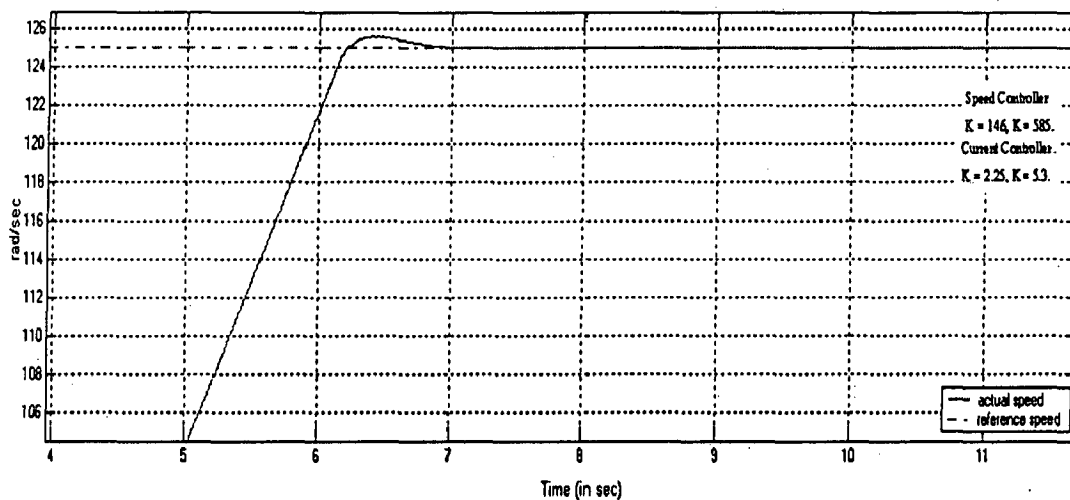


**Figure 2.26** Magnified view of speed response when proportional gain of speed controller,  $K_p=146$ .

From the figure 2.26, it may be observed that the peak percentage overshoot is 0.32% and the settling time is approximately 1.25 sec. Thus there was an improvement in transient response.

### 2.4.2.3 Results

The scheme was simulated for a reference speed of 125 rad/sec with a load torque  $T_l = 800$  N-m. During the acceleration mode, the armature current is maintained constant at rated value. Once the desired speed is reached, the armature current falls such that the torque developed by the motor is equal to the load torque.

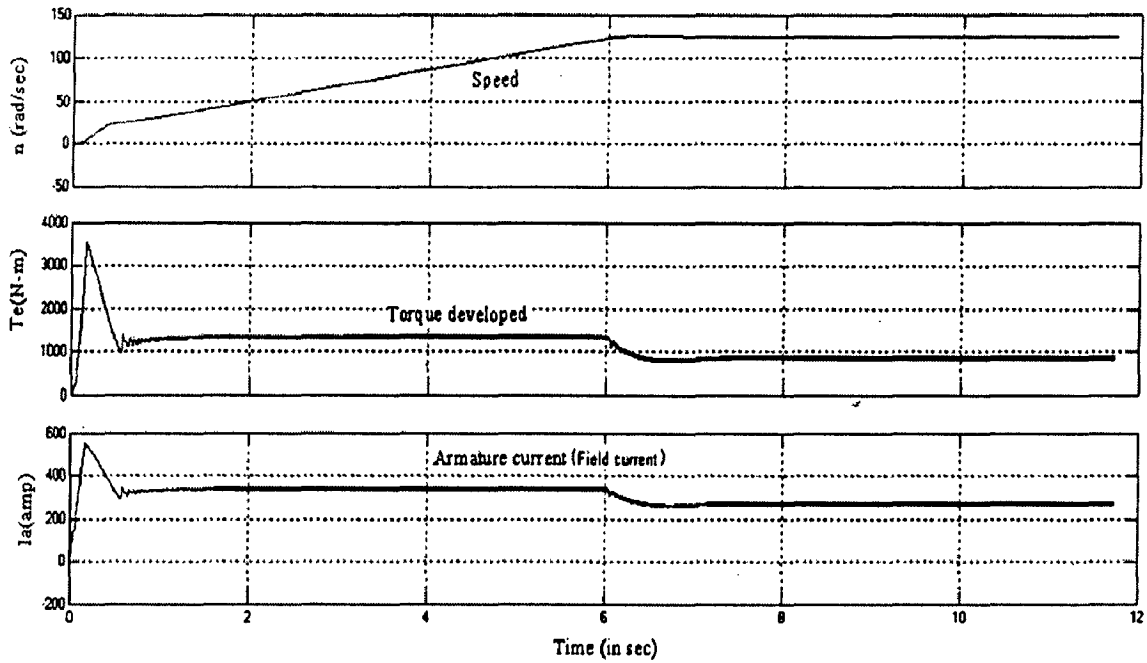


Figure 2.27 Performance of DC series motor under closed loop control.

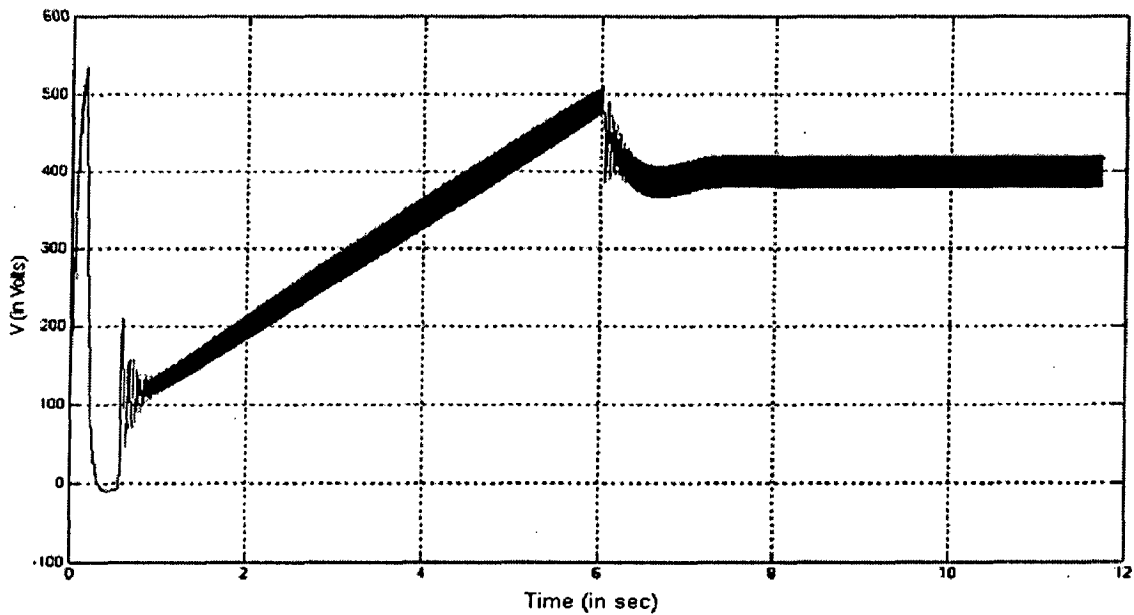
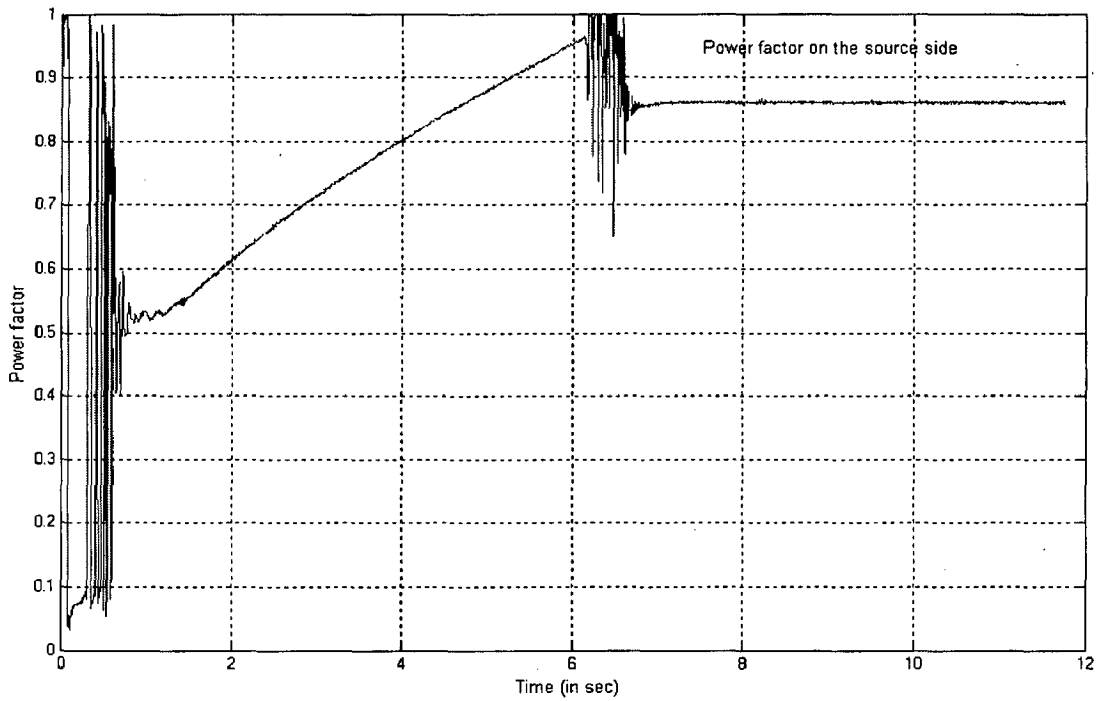
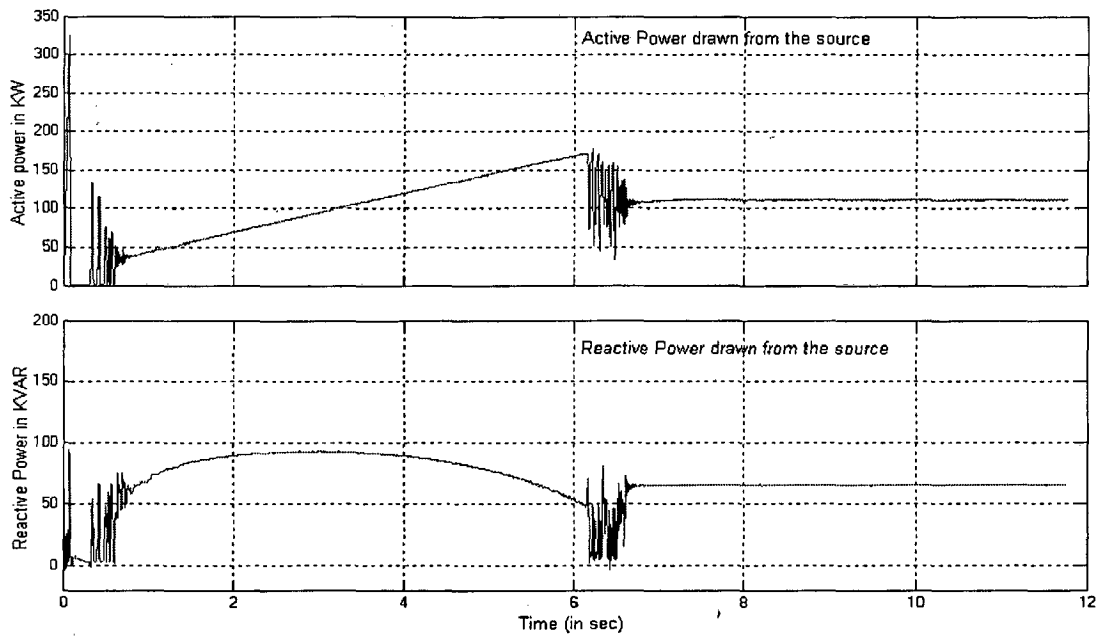


Figure 2.28 Voltage applied to the DC series motor.





**Figure 2.29** Variation of Power factor on the source side.



**Figure 2.30** Active and Reactive Power drawn by the motor from the supply.

The results obtained above were exclusively for motoring mode. In figures 2.31 to 2.34, braking mode has also been demonstrated. The reference speed is set at 125 rad/sec and the applied load torque  $T_l = 800\text{N}\cdot\text{m}$ . The motor can be toggled from motoring mode to braking mode using a manual switch.

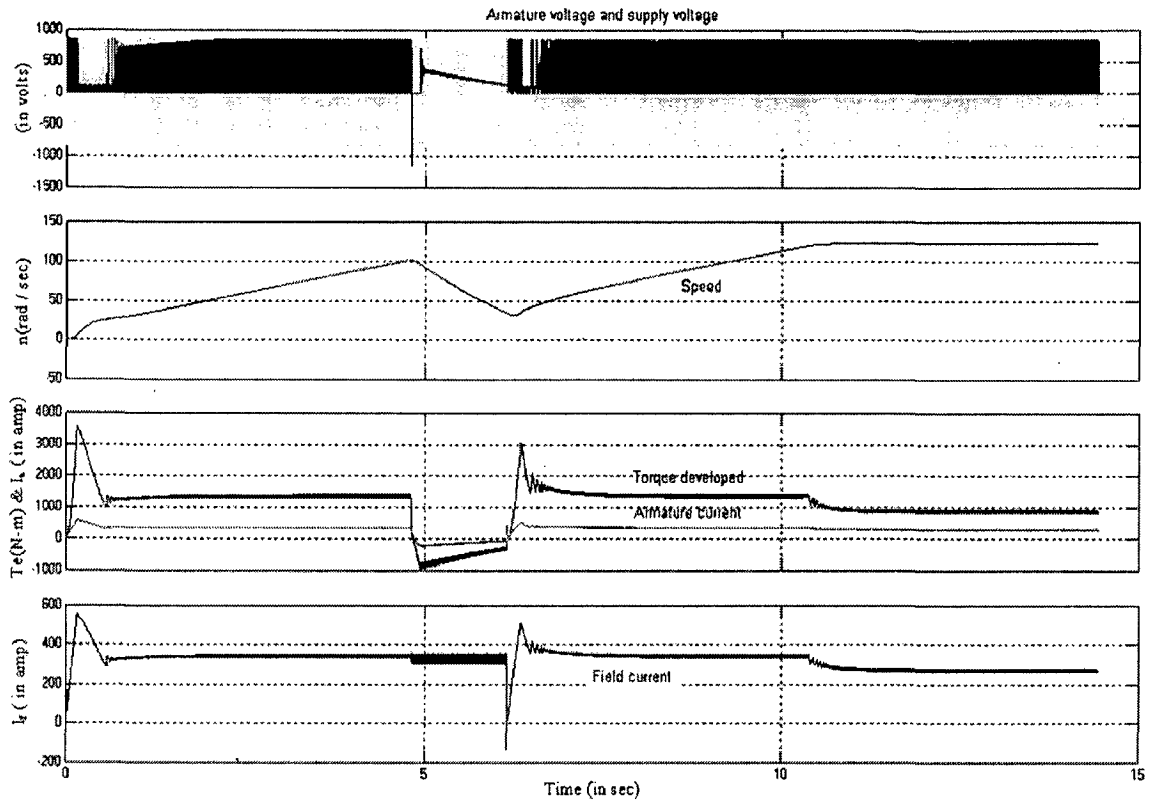


**Figure 2.31** Performance of drive when toggled from motoring to braking and back to motoring mode.

The motor was switched onto braking mode at  $t = 4.813$  sec and was switched back to motoring mode at  $t = 6.166$  sec. It may be noted that a reflection of back emf can be seen during the braking mode. This back emf falls as the speed of the motor falls. Further, it may be noted that the field current has higher ripples during the braking mode as unsmooth voltage from uncontrolled rectifier voltage is fed to the field winding.

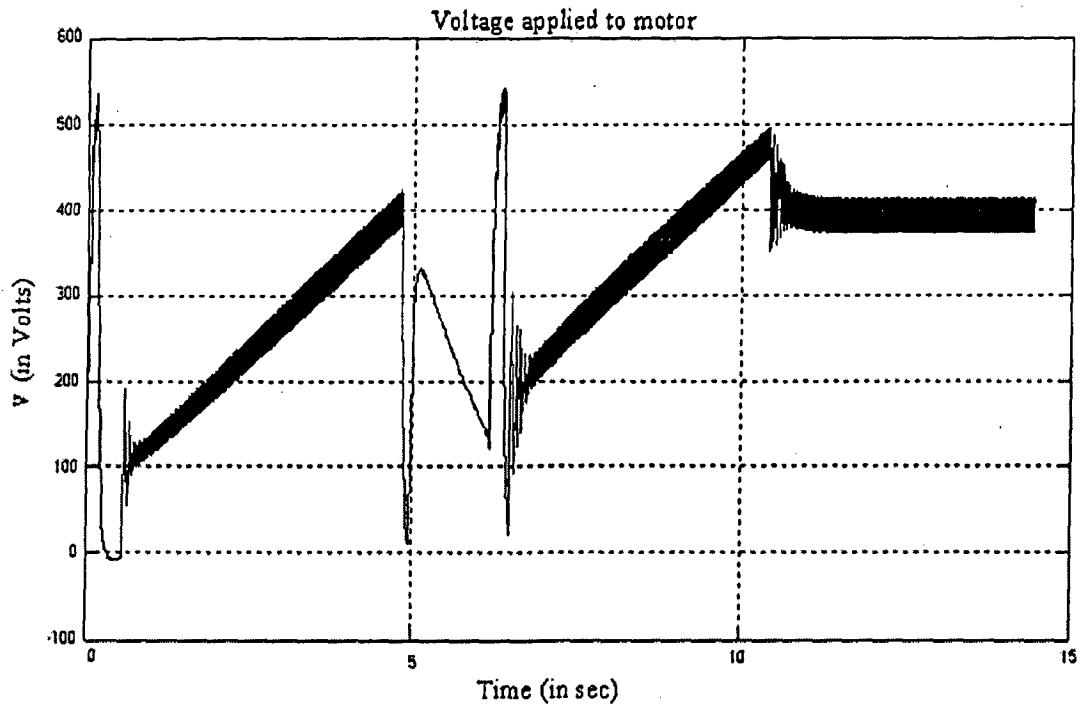


Figure 2.32 Voltage applied to the motor

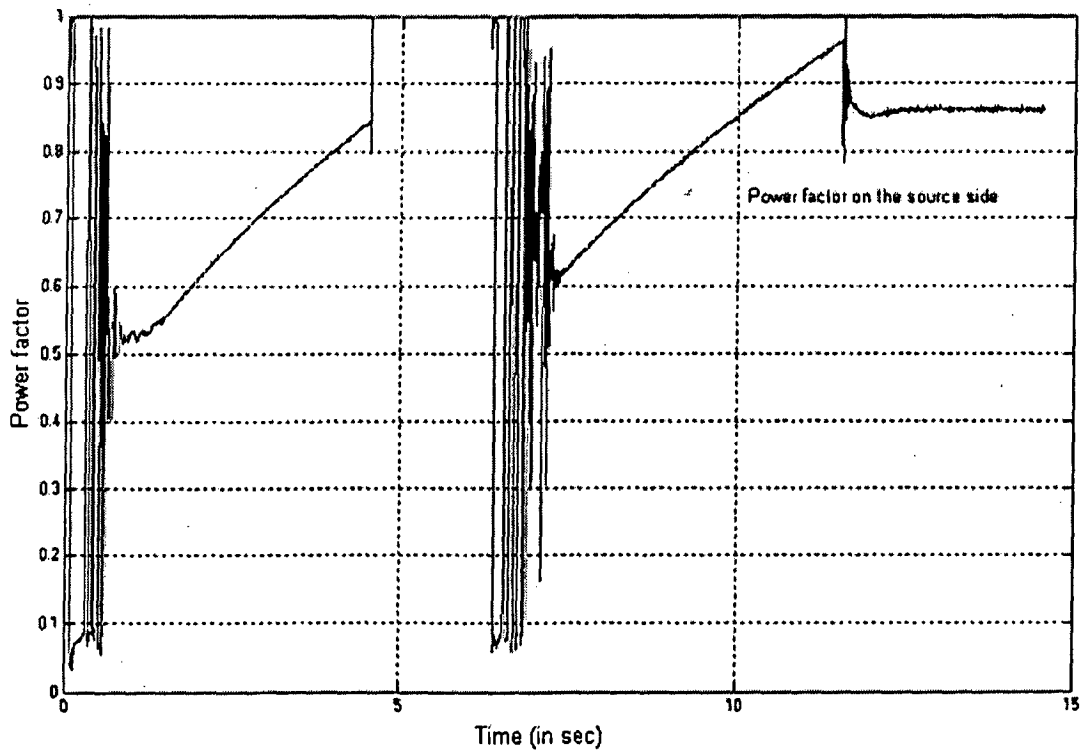
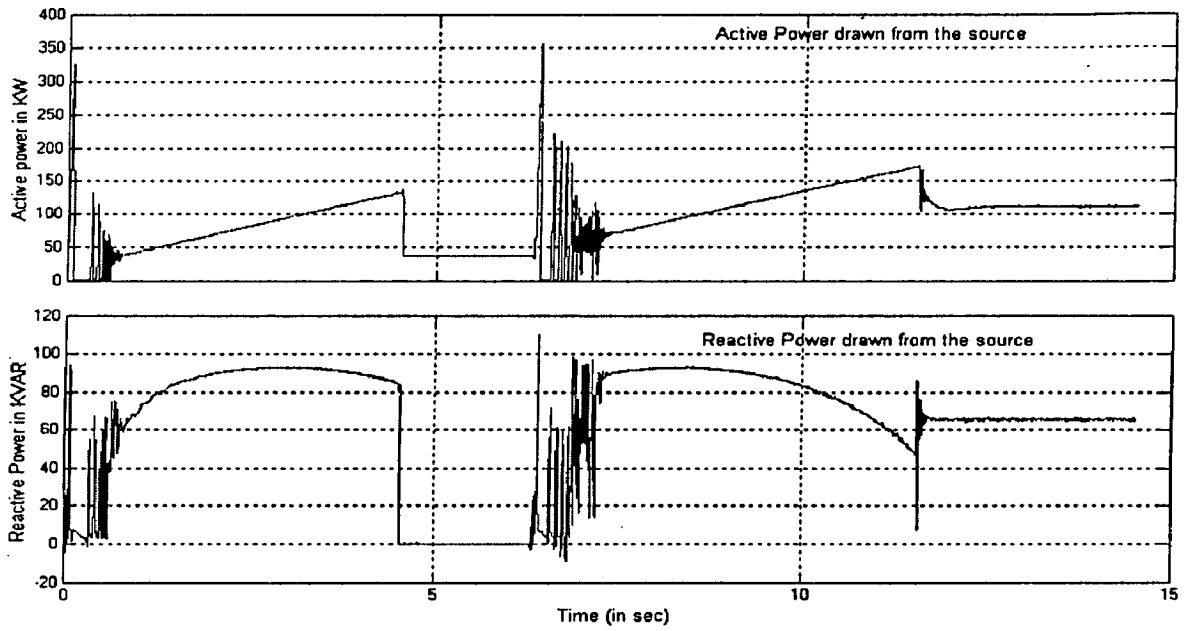


Figure 2.33 Variation of Power factor on the source side.



**Figure 2.34** Active and Reactive Power drawn by the motor from the supply.

### 2.4.3 Two-Stage sequence control of half Controlled converters

This scheme employs two half controlled converters connected in series as shown in figure 2.35. This converter can be employed in a sequence control to improve the overall power factor of the drive.

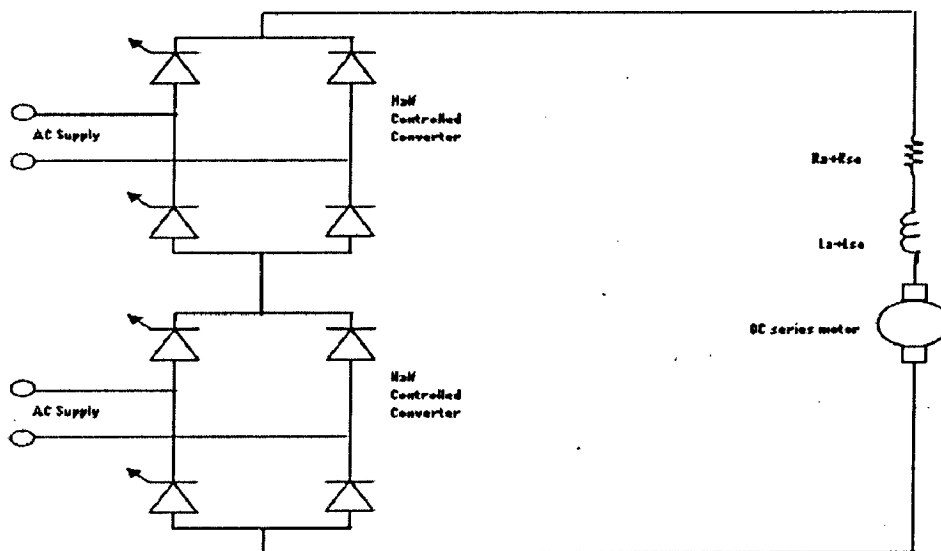


**Figure 2.35** Two half controlled converters connected in series for two stage control.

### *Two stage sequence control half controlled converters*

In a two stage sequence control, for the output voltage from zero to half the maximum, only one converter (say converter I) is controlled and the other is not operated. Load current bypasses converter II through two diodes. The load voltage is mainly decided by the firing angle of converter I. At half the maximum voltage converter I would be at full advance (zero firing angle). For the output voltage more than half of the maximum, converter I is maintained at full advance and converter II is controlled. Thus voltages from 0 to  $V_{ao}/2$  is controlled by converter I (converter II bypassed) and voltage from  $V_{ao}/2$  to  $V_{ao}$  is controlled by converter II (converter I in full advance).

The per unit output voltage versus reactive power variation is shown in figure 2.36 For comparison reactive power variation from single stage converter is also shown.

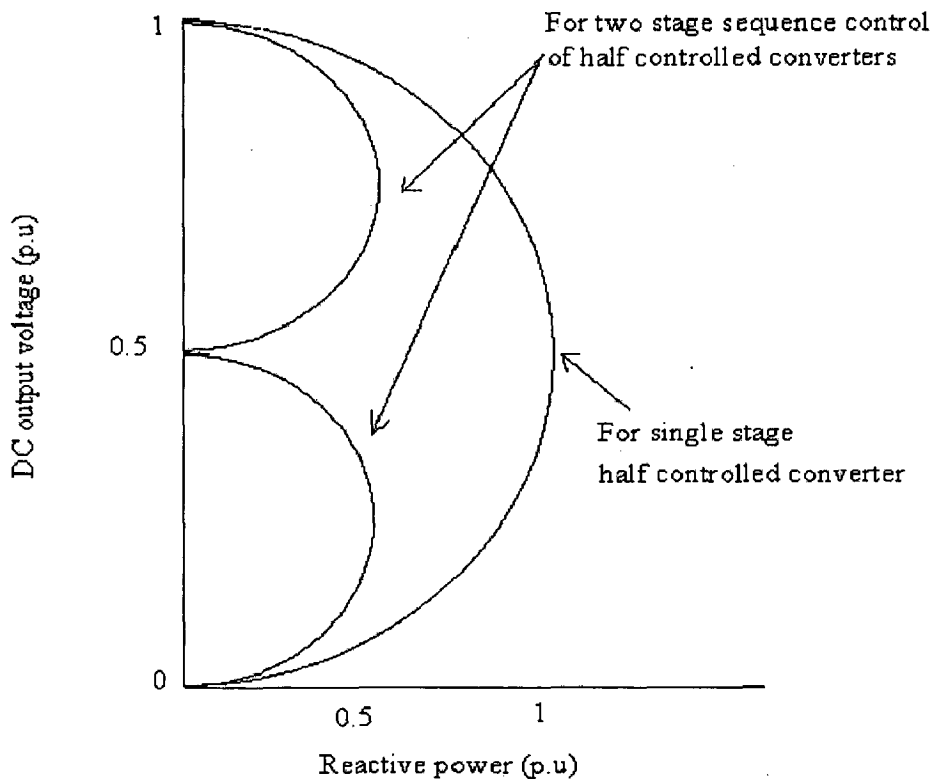


**Figure 2.36** Variation of reactive power with DC output voltage

Thus as compared to single stage half controlled converter, the maximum reactive power is reduced to half. Thus there is a considerable improvement in the power factor. The sequence control also yields an additional advantage of reducing the torque ripple.

### 2.4.4 Implementation of two stage sequence control of half controlled converters

Two half controlled converters connected in series for two stage control are modeled in MATLAB as shown in figure 2.37.

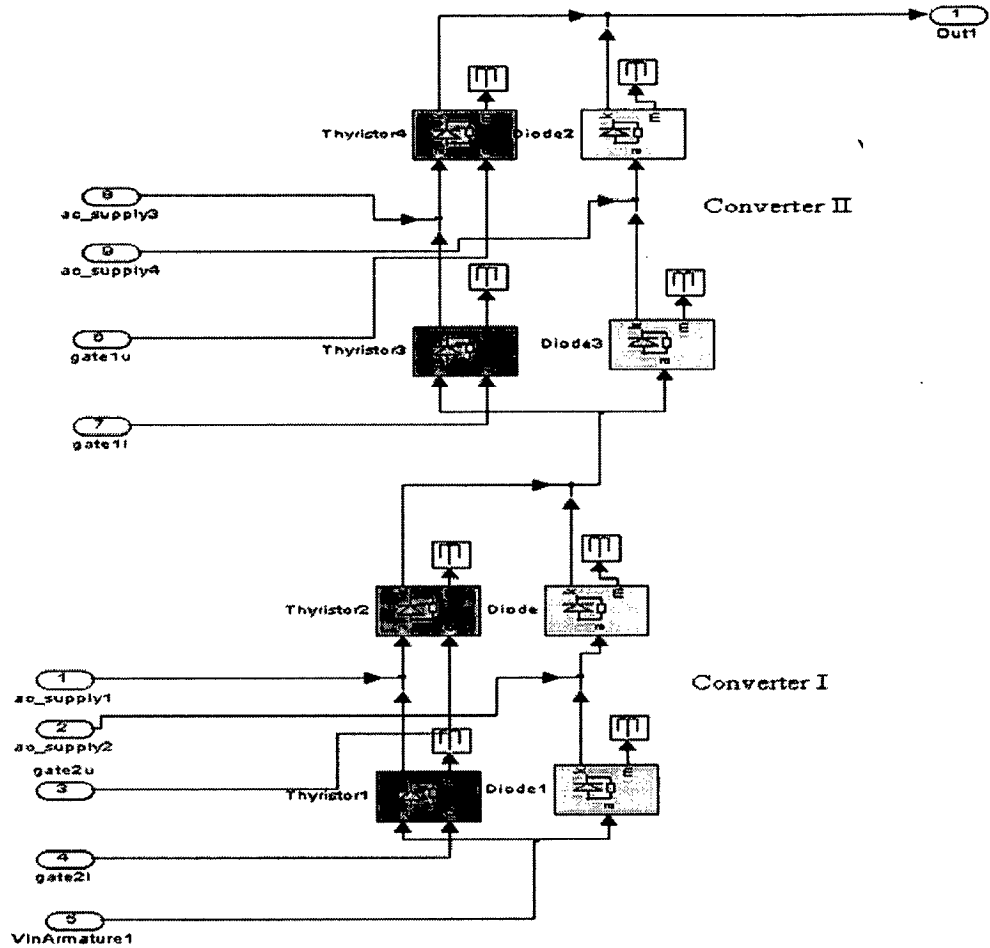


**Figure 2.37** SIMULINK implementation of Two half controlled converters connected in series.

The MATLAB implementation of closed loop scheme employing two stage sequence control of half controlled converters is shown in the figure 2.38. In this scheme the firing circuit logic has been split into two parts, one for converter I and other for converter II.

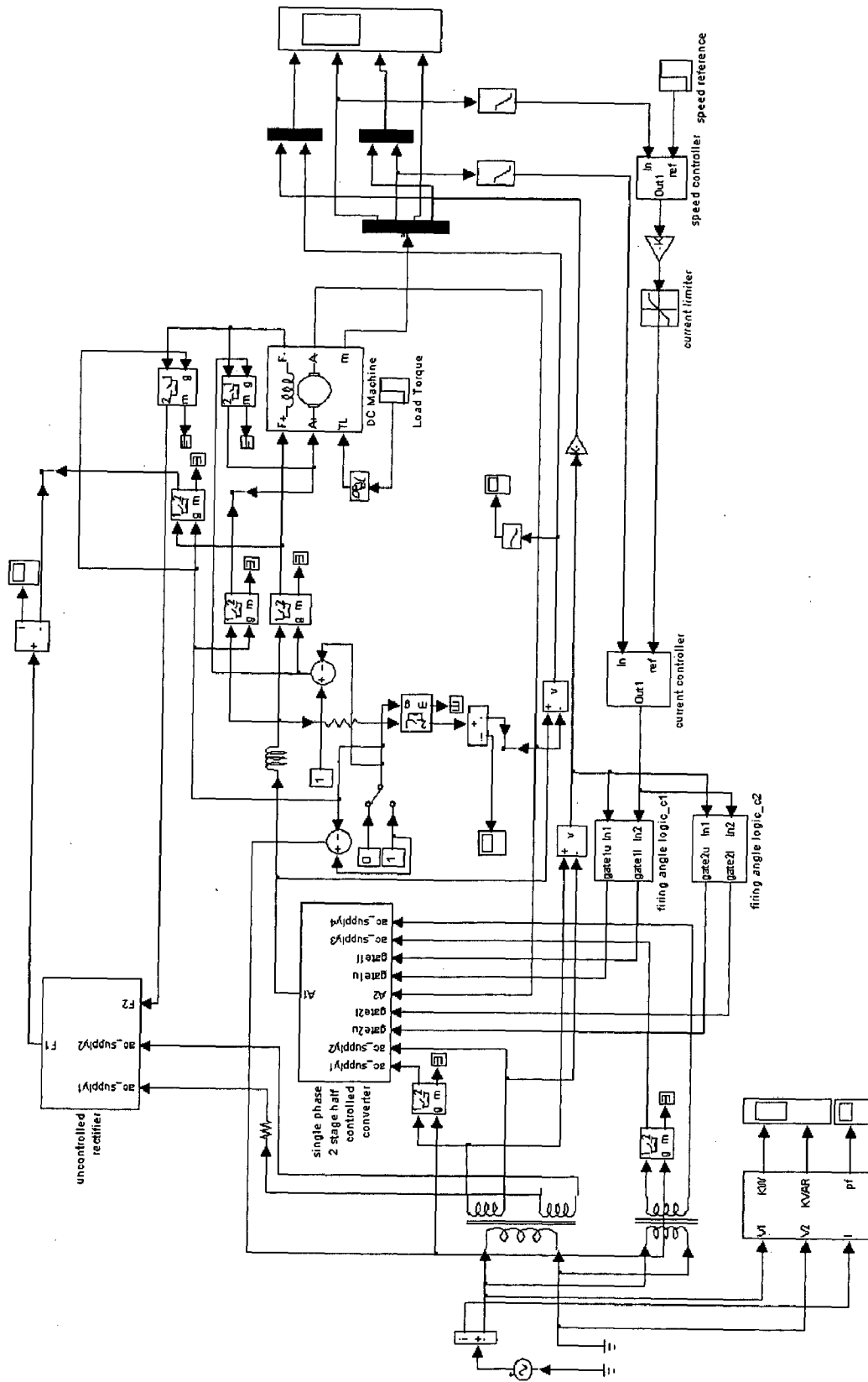
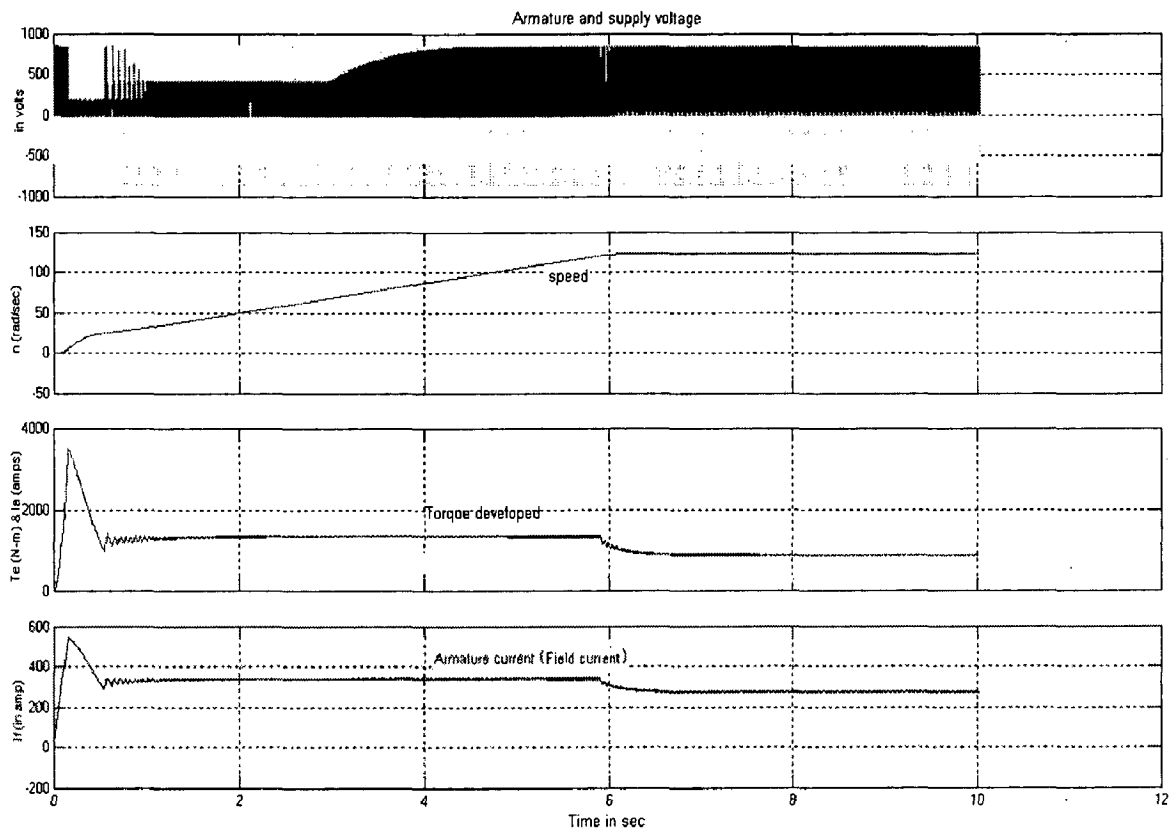


Figure 2.38 Simulink implementation of closed loop DC drive employing two stage sequence control of half controlled converters

### 2.4.4.1 Results

The scheme was simulated for a reference speed of 125 rad/sec and load torque of 800N-m. The response of the drive is given in the figure below. Initially only one converter was feeding the motor and other was bypassed through diodes. At  $t = 2.85$  sec, the converter II starts operating with converter I in full advance. This is shown in figure 2.39 and 2.40.



**Figure 2.39** Performance of closed loop drive when fed from two stage sequence controlled half controlled converters.

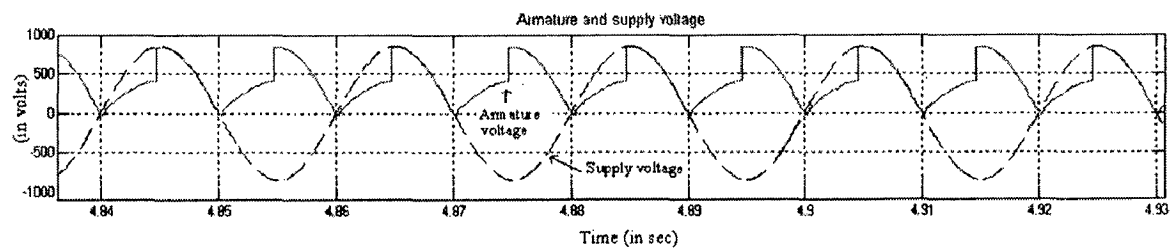


**Figure 2.40** Spread out view of armature and supply voltage showing converter I in full advance and converter II is being controlled.



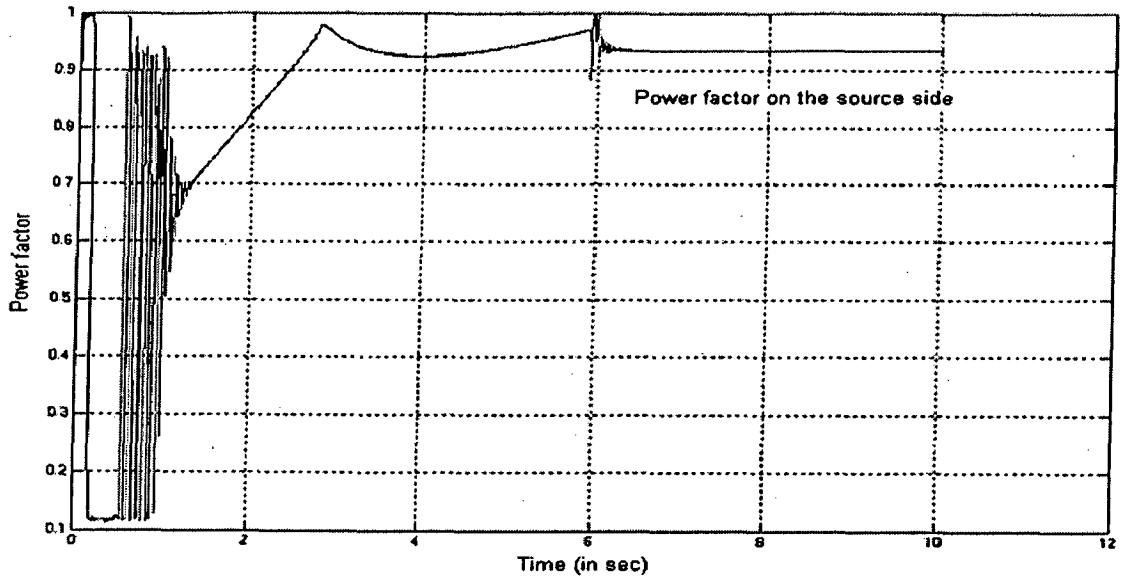


**Figure 2.41** Variation of Power factor on the source side.

If we compare figure 2.29 and figure 2.41, we observe that there is a definite improvement in the power factor on the source side.

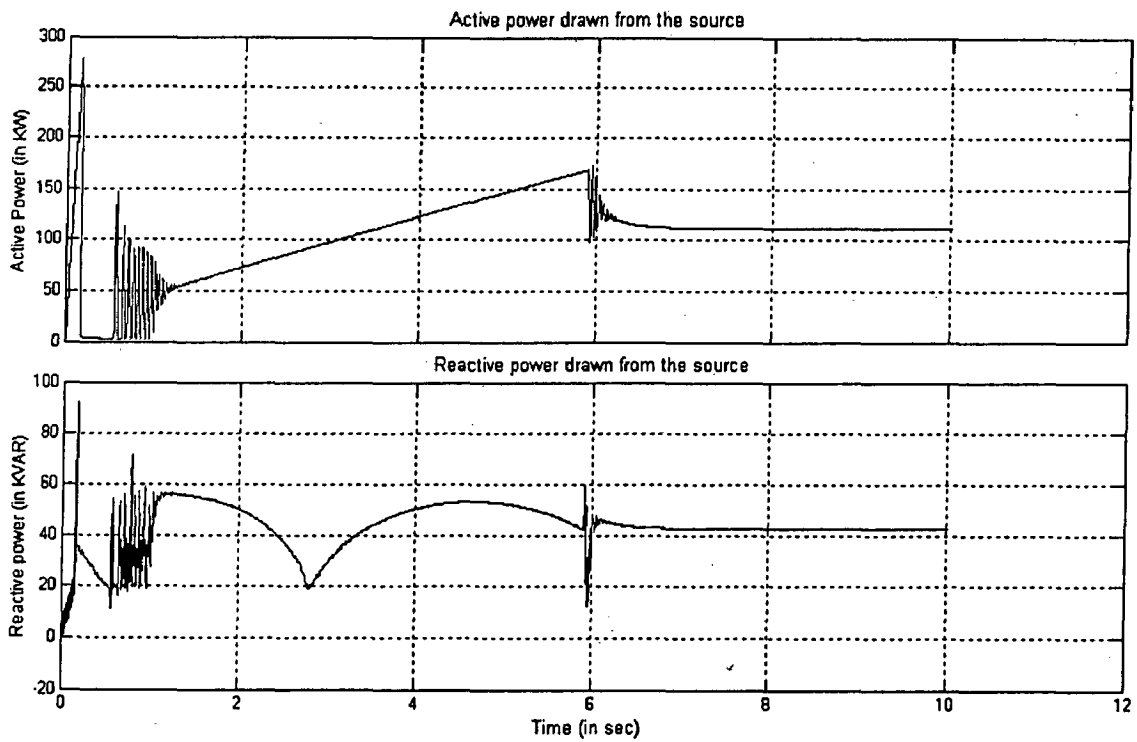


**Figure 2.42** Active and Reactive Power drawn by the motor from the supply.

## Mechanics of Traction load

---

The mechanics of traction deals with the nature of traction load and the dynamics of wheel–rail interaction. This includes slip- spin effects of the wheel on the track. These effects are governed by the complex interaction between motor, its controller and wheel-rail adhesion characteristics. This interaction is crucial to the motion of the locomotive but it can also introduce certain characteristics which are undesirable, such as wheel slip/spin.

### 3.1 Motion of locomotive

The motion of the locomotive is induced by the force created when the wheel pushes against stationary track. The torque applied by the motor is transferred as a force at the rim of the wheel. This force at the rim of the wheel is transferred to a force which propels the train through a mechanism known as adhesion.

Adhesion may be defined as the ability of the wheel to exert the maximum tractive effort without sliding on the rail. This adhesion force is the virtue of friction between the two surfaces (the wheel and the rail). Under the condition of acceleration there is a dynamic unbalance in the adhesion force and force exerted by the motor. This causes slipping and sliding motion of the train. Friction causes the wheel to catch up and prevents the sliding and slipping motion. However, the surface could not possibly have such an effect on the wheel once the wheel has achieved pure rolling motion and constant angular and linear velocity. Thus friction becomes zero when the train moves on a flat track at constant velocity. Under pure rolling the train moves under the effect of rolling friction.

Rolling friction is caused primarily by the interference of small indentations formed as one surface rolls over another. This is because the wheel and the surface will undergo deformations due to their particular elastic characteristics. This is illustrated in the figure

3.1

$f_r$  = rolling friction.

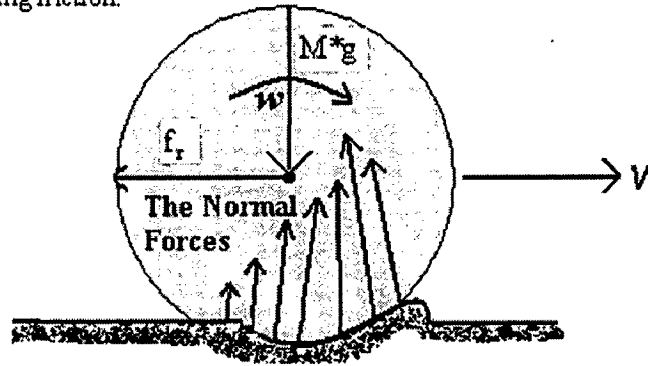


**Figure3.1** The actual forces acting on the wheel and the surface of the rail. In this exaggerated view, both the wheel and the surface undergo deformation to an extent determined by the elastic properties of the two surfaces [22].

At the contact points, the wheel flattens out while a small trench is formed in the surface of the rail. The normal force is now distributed over the actual contact area rather than the point just below the center of the wheel. The load seen by the motor is also the result of adhesion as the force transferred by the adhesion is also seen as the load on the motor.

### 3.2 Coefficient of Adhesion

As defined earlier, adhesion is the ability of the wheel to exert the maximum tractive effort on the rail and still maintain the persistence of the contact without sliding. Thus the coefficient of adhesion can be approximately defined as the ratio of maximum tractive effort that can be developed without slipping and the weight on the driving axle. Thus, the force of adhesion is given by

$$F_a = \mu N. \quad (3.1)$$

Where  $\mu$  = coefficient of adhesion

$N$  = normal reaction force at the point of contact.

It may be noted that the coefficient of adhesion is not same as coefficient of friction. While the latter forms an undesirable resistive force, the former forms a coupling force and is extremely desirable for traction purposes. The coefficient of adhesion is affected by following factors.

1. **Contaminants:** Contaminants like oil, grease, water, snow and mud reduces the value of coefficient of adhesion.

2. **Wheel slip:** The value of coefficient of adhesion decreases slowly with wheel slip after initial sharp rise. The rate of decrease depends upon the track condition. The measure of wheel slip is provided by a factor called wheel slip ratio which is given by

$$\lambda = \frac{V_w - V_t}{V_w} \quad (3.2)$$

Where  $V_w$  = peripheral velocity of wheel (referred as wheel velocity).

$V_t$  = velocity of train.

A change in slip ratio causes change in coefficient of adhesion. This is given in figure 3.2

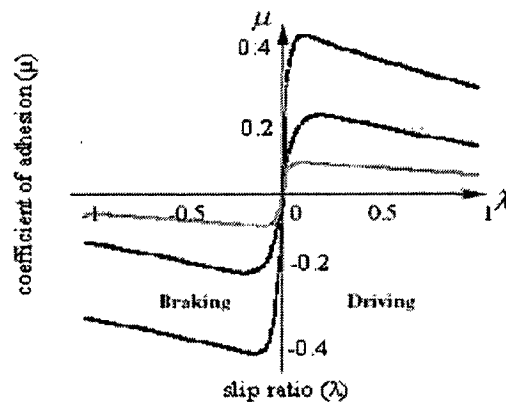


**Figure3.2** Variation of coefficient of adhesion with wheel slip ratio for various track conditions.

**Speed of the vehicle:** Generally speaking, the coefficient of adhesion decreases with wheel speed. The actual behavior however is given in the figure below.

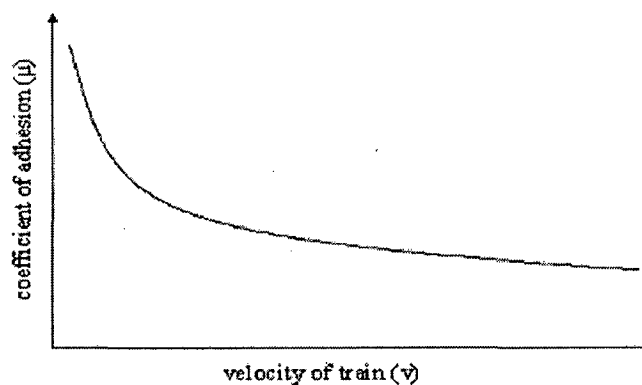


**Figure 3.3** Variation of coefficient of adhesion with velocity of the train.

3. *Nature of motor speed torque characteristic:* The motor with lower speed regulation has higher value of coefficient of adhesion.

### **3.3 Nature of Traction Load**

The traction load comprises of the various frictional forces that act on the system and the gravitational pull that act if the train is moving on an inclined track. The various frictional forces that act on the traction system can be classified as

- Internal friction: This comprises of the friction at the bearings, guides etc.
- External friction: It comprises of the rolling friction between the wheels and the rails, and friction between wheel flanges and rail. This depends upon the nature of the track.
- Air friction: This is independent of the weight of the train but depends upon the shape and the size of the train, velocity and direction of wind and speed of the train.

All these components collectively form the train resistance. The train resistance can also be identified in terms of common classification of friction such as windage, viscous friction, coulomb friction and stiction which has a very large value. However, owing to large value of the inertia, particularly due to the weight of the vehicle, accelerating torque forms the major component of total torque in the accelerating range.

### **3.4 Dynamic Mechanical model**

The overall dynamics of the train can be broadly classified as

22. Wheel Dynamics.
22. Train Dynamics.

#### **3.4.1 Wheel dynamics**

The wheel dynamics is nothing but dynamics of a rotating mass. This can be generally represented by a first order system comprising of the load and the inertia. The load torque can be split into two components, the conventional frictional elements and windage, and the component unique to the wheel (torque due to adhesion force).

Thus the differential equation defining the wheel dynamics is given as

$$T_e = J \frac{d\omega}{dt} + T_l + F_a r. \quad (3.3)$$

Where  $F_a = \mu N$ .

$T_e$  = motor torque referred to the wheel.

$T_l$  (load torque contributed by friction (external friction), windage and gravitational component) =  $F_{ext} + Mg \sin(\theta) * k$ .

Where  $k$  = minimum distance between the radius of the wheel and the horizontal line passing through the centre of gravity.

$F_{ext}$  = external friction.

$J$  = combined moment of inertia of the wheel and motor referred to the wheel.

$r$  = radius of the wheel.

Equation 3.3 can be further solved as

$$\omega = \int \frac{T_e - T_l - F_a r}{J} dt \quad (3.4)$$

This equation can be represented in the form of block diagram as shown below.

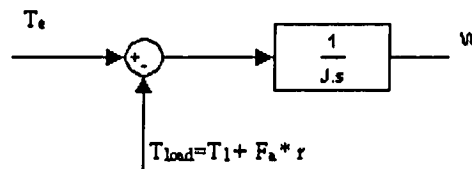


**Figure 3.4** Control block diagram representation of wheel dynamics.

The angular velocity of the wheel yields the peripheral speed of the wheel which will be addressed as wheel speed.

$$V_w = \omega r. \quad (3.5)$$

### 3.4.2 Train Dynamics

The Train dynamics governs the translational motion of the train (vehicle). This can be given by a first order equation in terms of mass, train resistance and tractive effort. This is given as

$$M \frac{dv}{dt} = TE - R - Mg \sin \theta. \quad (3.6)$$

Where  $M$  = mass of the train.

$TE$  = total tractive effort.

$R$  = train resistance.

This equation can be solved as

$$V_t = \int \frac{TE - R - Mg \sin \theta}{M} dt \quad (3.7)$$

Thus the entire mechanical model is represented by figure 3.5

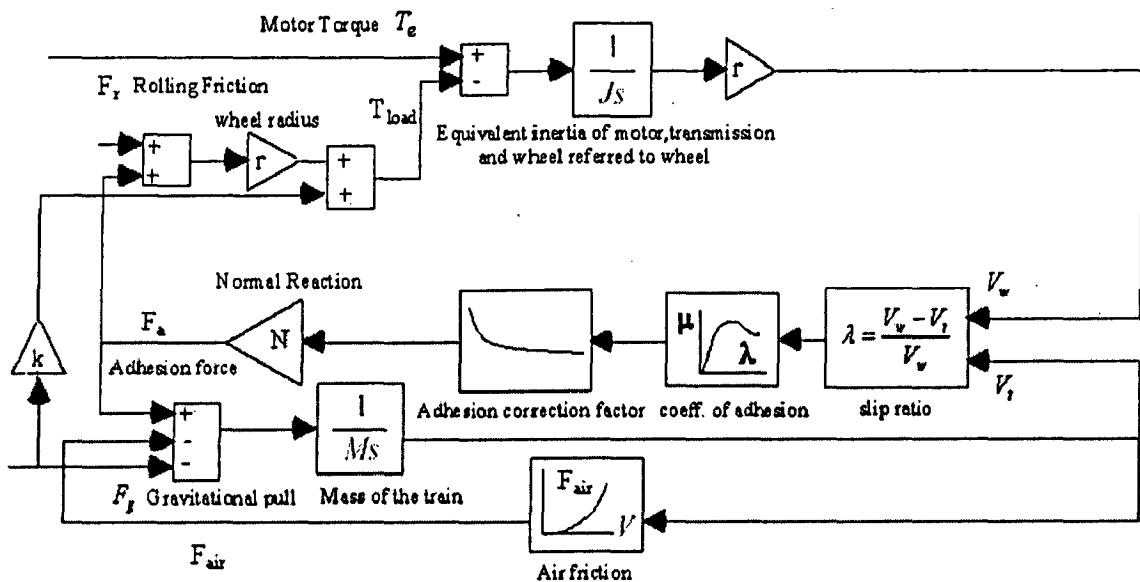


Figure 3.5 Block diagram for entire mechanical system.

When the train reaches the desired speed, a controller takes over and maintains the speed constant.

### 3.5 MATLAB Implementation of Mechanical load

The load torque subsystem in the main figure represents the mechanical system. While designing the mechanical system some assumptions have been taken due to lack of adequate data (or relationships) for their modeling. Some of them are as follows

- The air resistance which depends on size and shape of the train (vehicle), speed of the train and velocity of wind has been taken as a constant value.

- The look up table for rolling (external) friction and stiction and coefficient of adhesion has been assumed after referring relevant literature discussing their behavior upon the dependent quantities.

The load torque model has then been simulated and is given in figure below.

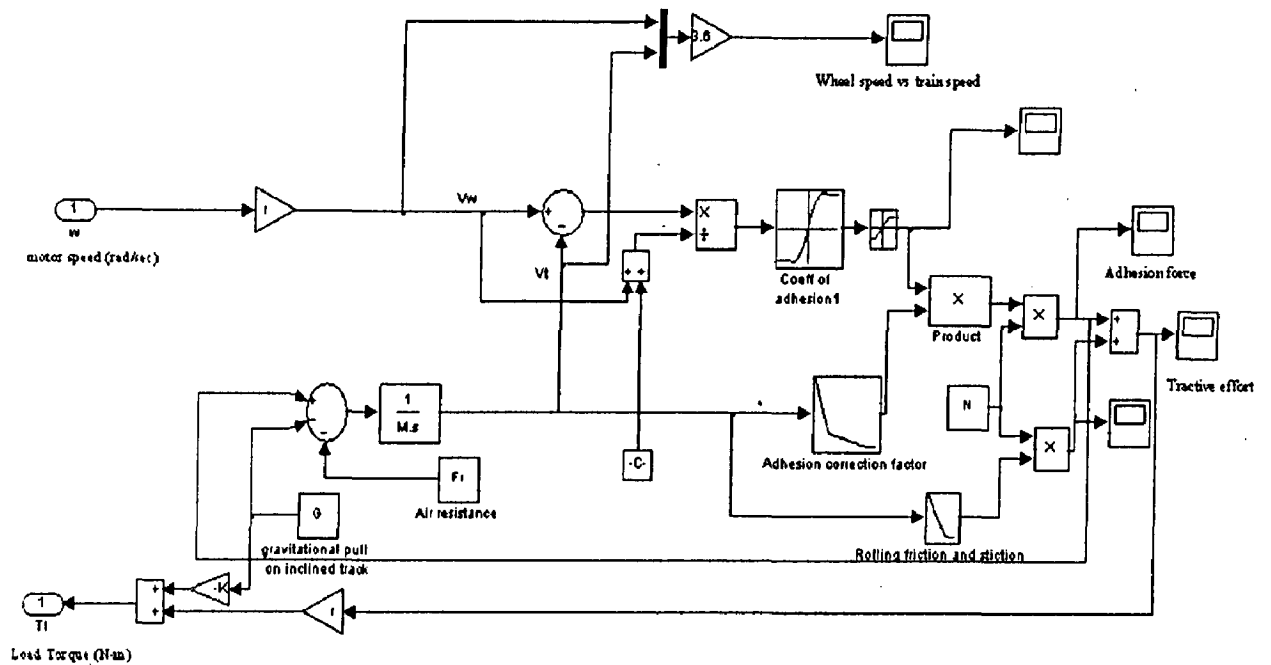


**Figure 3.6** SIMULINK block diagram of mechanical load.



## **Electrical Traction Drive with wheel slip control**

---

All traction closed loop schemes are essentially closed loop torque control schemes. This is important because an excessive amount of torque leads large wheel speed resulting in the rotation of wheel, all of which is not converted into translational motion. Consequently, there occurs slipping of the wheel on the track resulting in excessive wear of the wheels and also wastage of electrical energy. Thus there has to be a torque control. This is achieved by a controller which would form a current reference for the current loop. When the speed of the train reaches the desired speed, i.e. at the end of acceleration period, the speed controller maintains the speed at constant value.

In this part of the thesis an attempt has been made to integrate the mechanical load model and the electric drive model with different wheel slip control strategies.

### **4.1 Wheel Slip Control**

It may be observed from figure 4.1 that the entire slip range is divided into two regions, viz. stable and unstable region. In the stable region of operation the value of coefficient of adhesion increases with slip. In the stable region, as the motor torque increases, the wheel speed increases, resulting in immediate increase in the value of slip, which causes increase in force of adhesion. This results in increase of the mechanical load on the system causing wheel-slip to improve. Thus there is a self regulating action.

However, in the unstable region, coefficient of adhesion decreases with wheel-slip. In the unstable region, as the motor torque increases, the wheel-slip increases causing reduction in force of adhesion. This results in decrease of mechanical load on the system causing further acceleration of wheel. The slip ratio increases further. This is a cumulative action resulting in slipping of the wheel on the track.

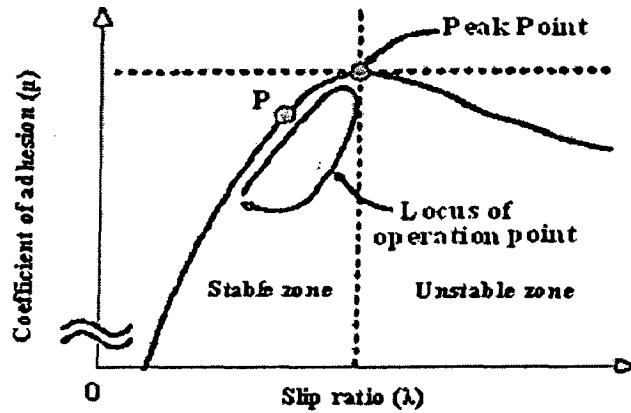


**Figure 4.1** Image of desired slip control.

The goal of all slip control methods is to control the slip in order to prevent wear of the wheels and the rail and to use the present adhesion effectively. Optimizing methods adds a search of the maximum adhesive force. This is achieved when the slip is controlled towards the peak of the slip curve within the stable region as shown in figure 4.1.

To be able to do this, two major problems must be solved:

- The slip present must be detected.
- The slip must be controlled towards the optimal slip.

Both of these issues are a lot more complex than they might seem at first. The two slip control strategies that are further discussed in this report are

- Slip control to the reference slip.
- Gradient control method.

In both the cases, the scheme has been simulated for maximum possible acceleration of the motor within the limits of permissible wheel slip.

## 4.2 Slip Control to the reference value.

### 4.2.1 Theory

In this scheme, the wheel slip is controlled using a slip ratio controller (a PI controller) which processes the slip error to produce the torque command for the motor. The slip controller generates a torque command for the motor which yields the current reference

for the current controller and the input power to the motor is controlled as per the traction requirements. Thus the motor accelerates at a reference slip under the stable region such that the adhesion force is optimally utilized. To obtain an optimal reference slip, it is sufficient to know the  $\mu$ - $\lambda$  characteristic of the track. Once this characteristic is known, the optimal slip can be estimated by choosing a value of slip which is near the peak of the  $\mu$ - $\lambda$  curve. This is illustrated in the figure 4.2.

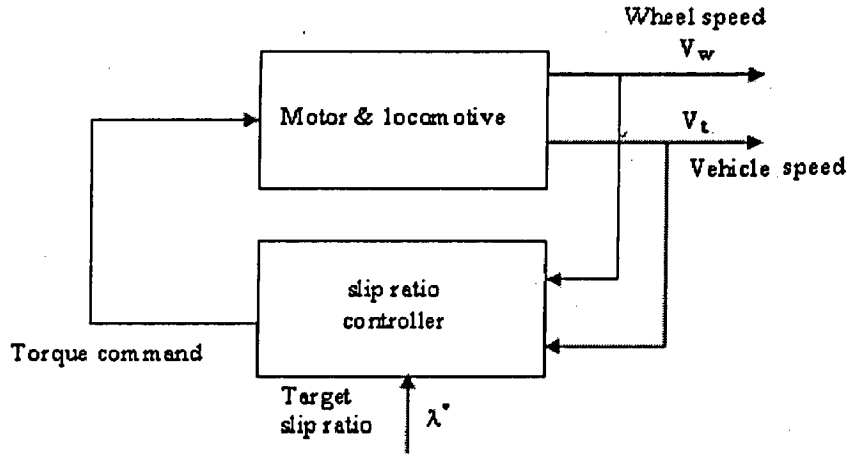


**Figure 4.2** Block diagram of slip ratio control to the reference value.

Assuming that rolling friction and air friction are very small, in practical schemes the coefficient of adhesion can be estimated as

$$\mu = M \frac{dv_t}{dt} \quad (4.1)$$

Further

$$\lambda = \frac{V_w - V_t}{V_w} \quad (4.2)$$

Using these two equations the track condition can be estimated.

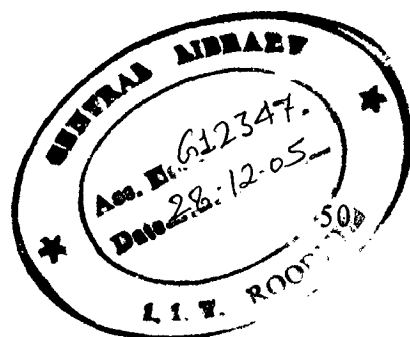
#### 4.2.2 Implementation with MATLAB

This slip control strategy has been implemented in MATLAB by combining electrical drive and mechanical load with a slip controller (a PI controller) forming an important link to achieve the desired traction control. As discussed above, the slip controller processes the slip error and produces a reference for the current controller and thus the

motor torque is controlled. The MATLAB implementation of the scheme is shown in the figure 4.3.

The scheme has been modeled to operate at any desired slip. The traction drive accelerates under the influence of slip ratio controller at the desired slip until the reference speed is reached. Once the train reaches the desired speed, the speed controller takes control and maintains the speed at desired value.

The electric motor drive in this scheme is assumed to be fed by two stage half controlled converter operating in sequence control because of its inherent advantage over single stage half controlled converter.



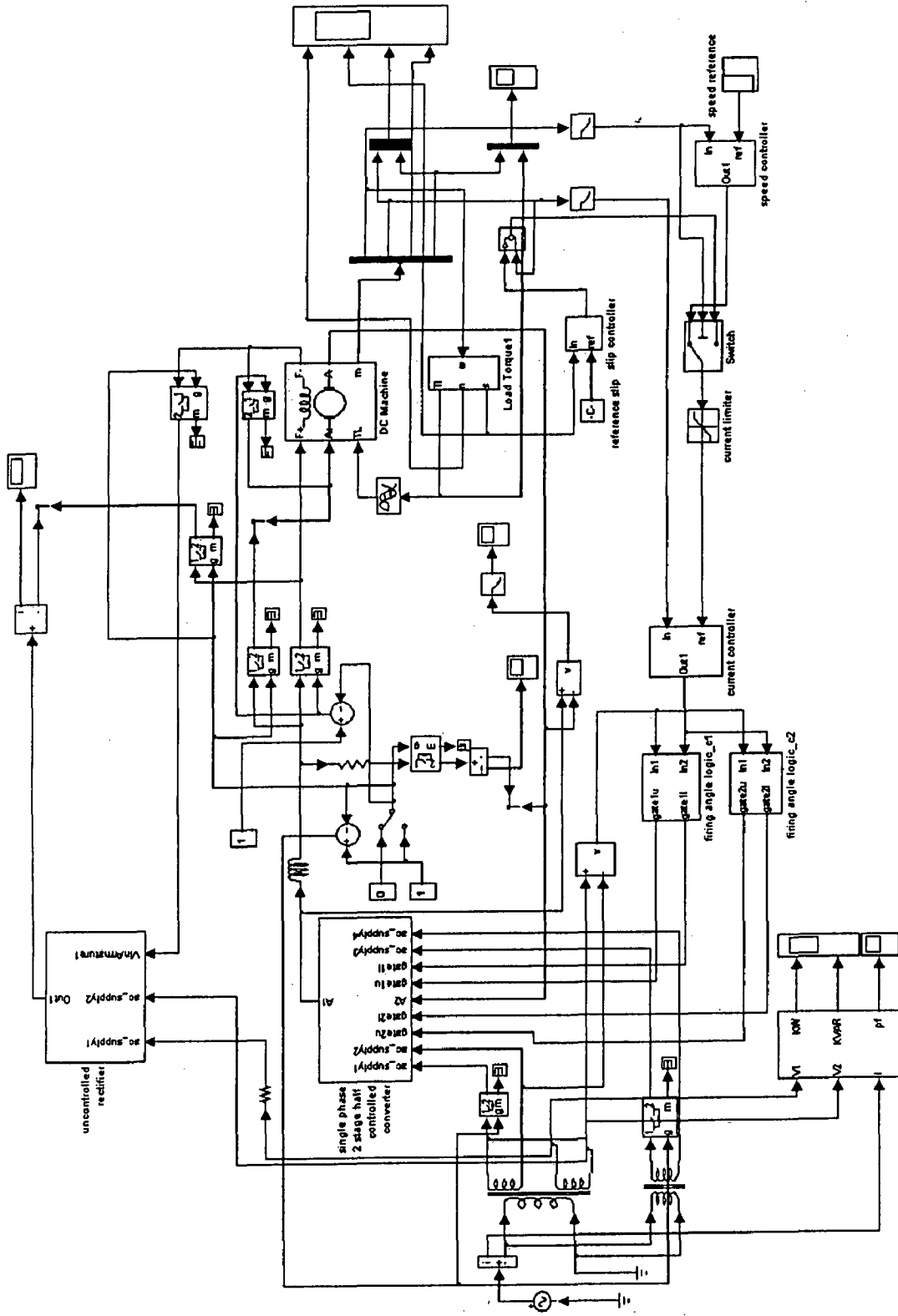


Figure 4.3 Simulink implementation Closed loop Traction scheme with slip control to the reference value.

### 4.2.3 Results

The simulation was carried out for a track whose  $\mu$ - $\lambda$  characteristic is simulated in figure 4.4

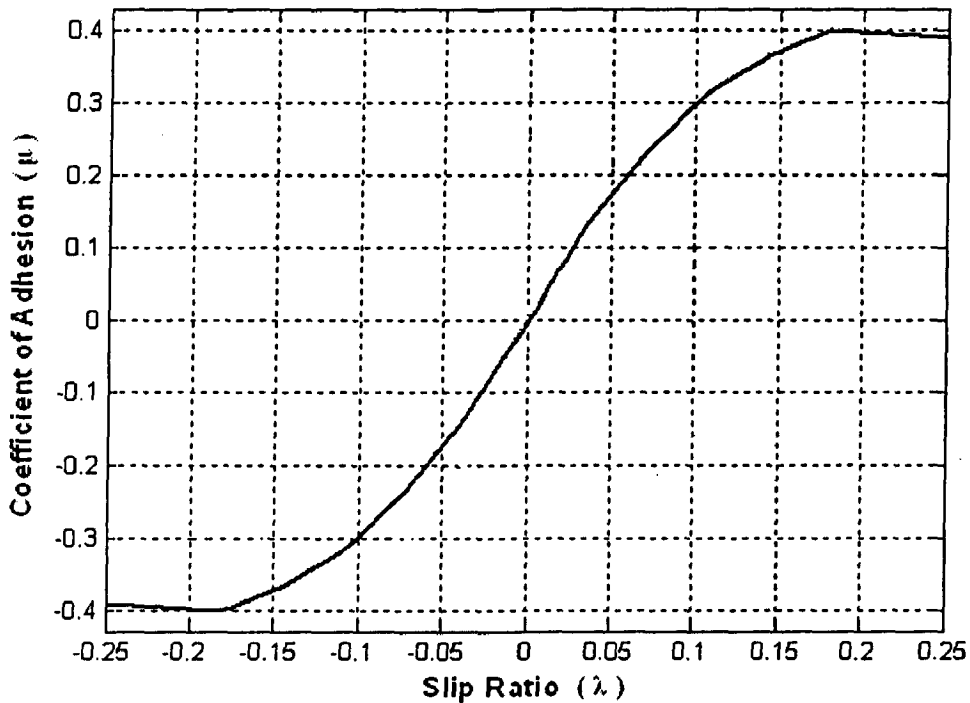


Figure 4.4

$\mu$ - $\lambda$  characteristic for the track.

This has been incorporated in the mechanical model as a lookup table. The reference slip fed to the controller is the slip at which the coefficient of adhesion is close to the peak value.

#### *Simulation for the flat track*

Parameter specifications

Reference slip = 0.07.

Desired speed = 75 Km/hr.

Nature of track = flat track.

The response of the system is given below.

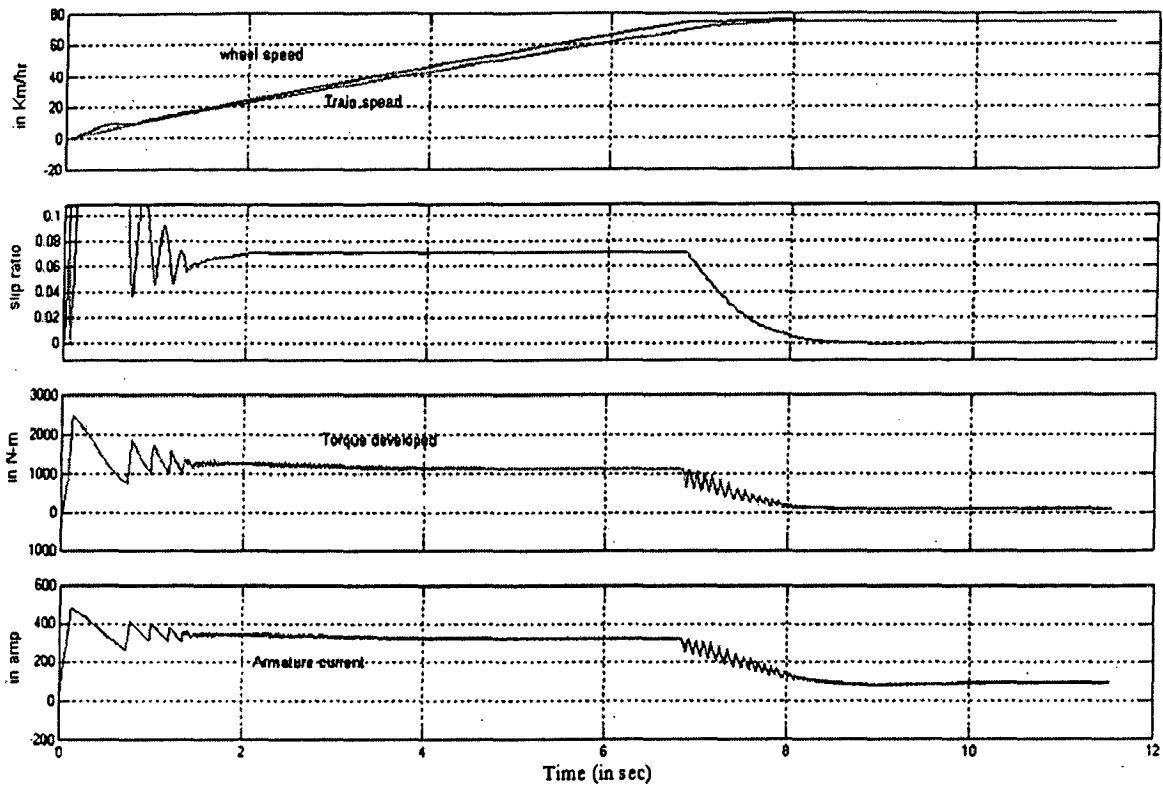


**Figure 4.5** The response of the system showing corresponding armature current and Torque developed by the motor as the slip ratio is being controlled to the commanded value while the train builds up to the desired value of speed on a flat track.

It may be noted the train accelerates such that the slip ratio is equal to the reference value. However once the train reaches the desired speed, the train moves at a constant velocity and the motion of the train becomes almost a purely rotational motion. Thus slip ratio decreases and settles at a value very close to zero. This results in drop of coefficient of adhesion from a near peak value to very low value (close to zero) when the train achieves desired speed. This is depicted in figure 4.6. It may also be noted that the value of coefficient of adhesion decreases even though the train moves at constant slip. This may be attributed to the fact that coefficient of adhesion decreases with velocity of train.

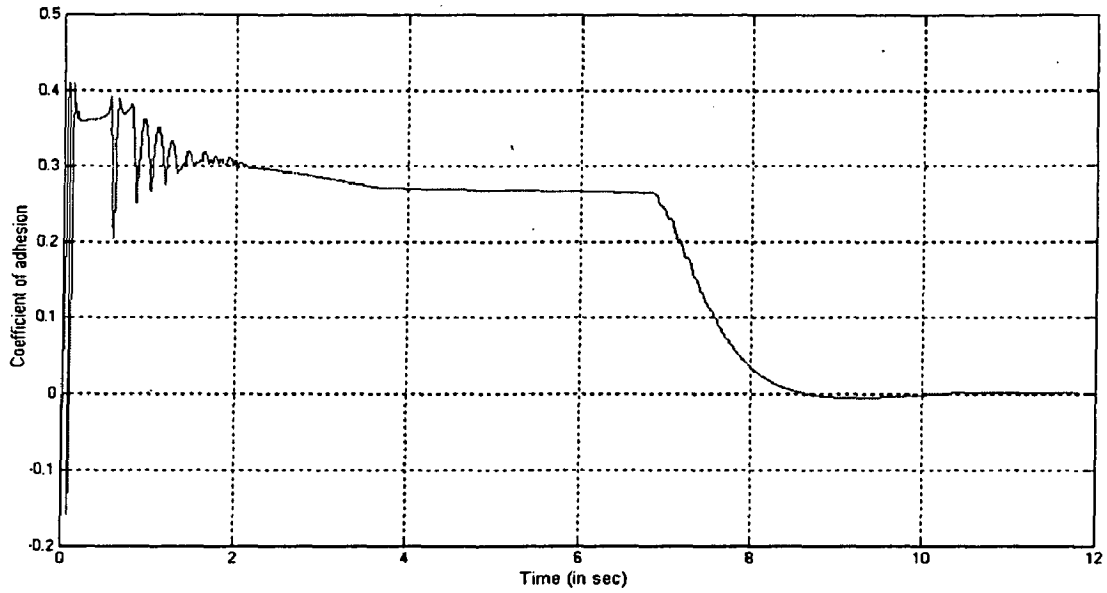


**Figure 4.6** Variation of Coefficient of adhesion with time.

The force of adhesion, which is directly proportional to the coefficient of adhesion, becomes close to zero when the train reaches the desired value (after a high value during acceleration), such that it is just sufficient to overcome frictional forces.

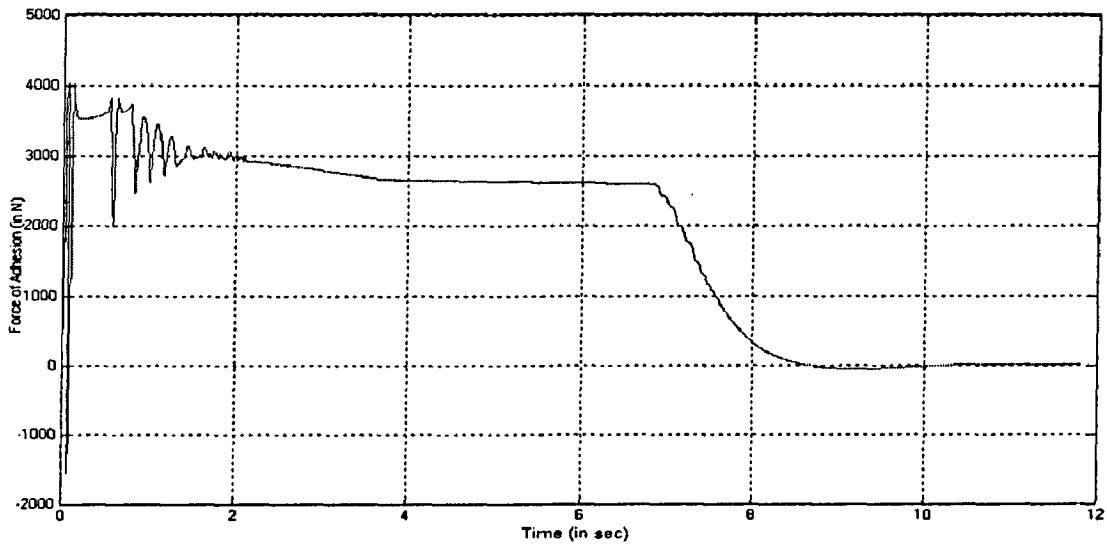


**Figure 4.7** Variation of force of adhesion with time

Thus from the above discussions it may be concluded that during acceleration the force of adhesion forms the major component of the total tractive effort required to drive the train.



However once the desired speed is reached, the external friction form the major portion of total tractive effort requirement.

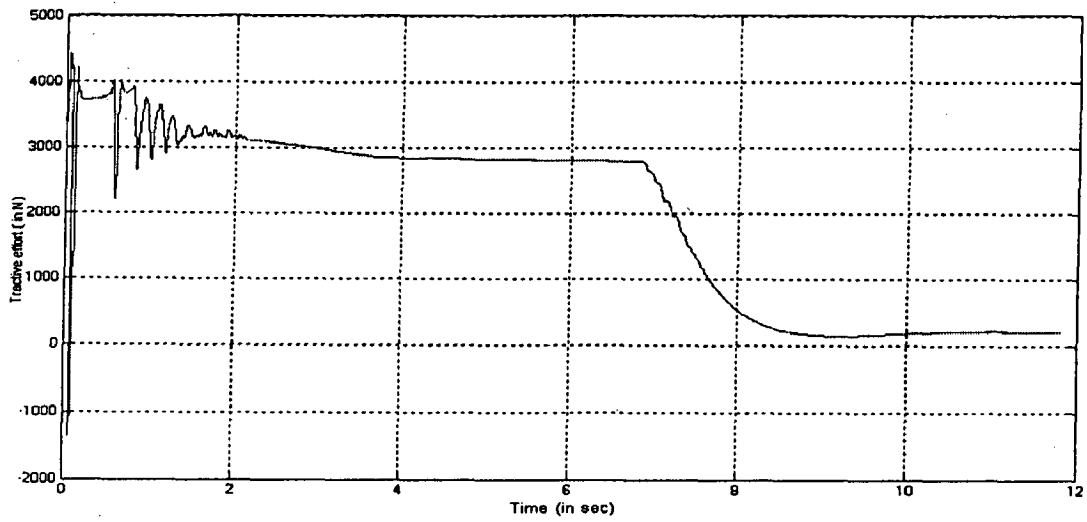


**Figure 4.8** Variation of Tractive effort with time

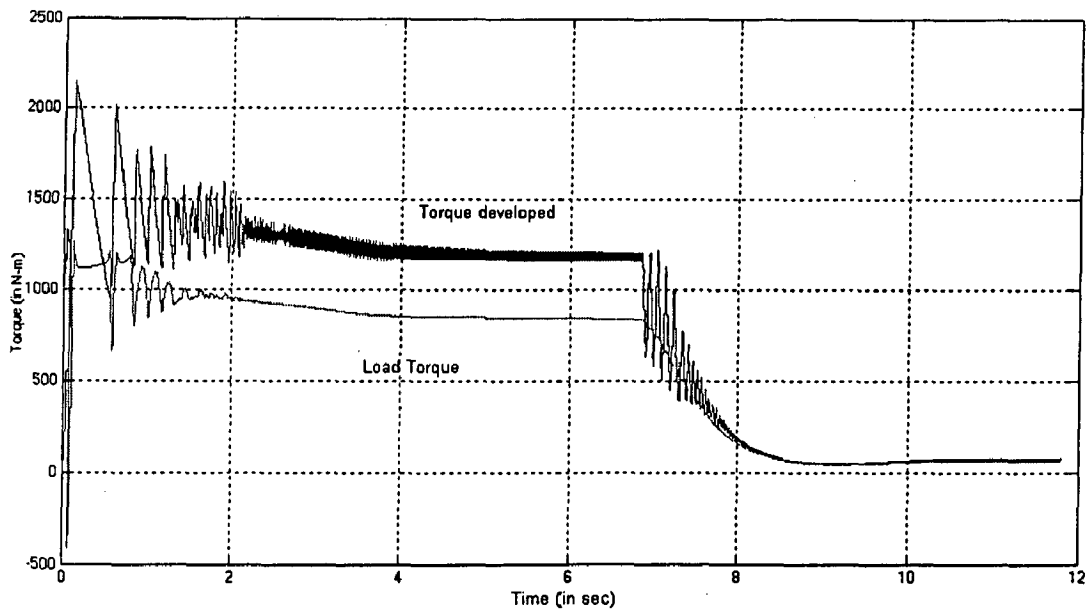


**Figure 4.9** This figure shows the torque developed by the motor and load torque on the drive on the same scale. The difference between the two curves during acceleration may be attributed to large value of  $J \frac{d\omega}{dt}$ .

As discussed above, the tractive effort requirement to drive the train falls once the desired velocity falls, thus it is likely that the motor drive would be much lightly loaded once it

starts moving at constant velocity. Thus the power factor falls drastically after a reasonably high value during acceleration.

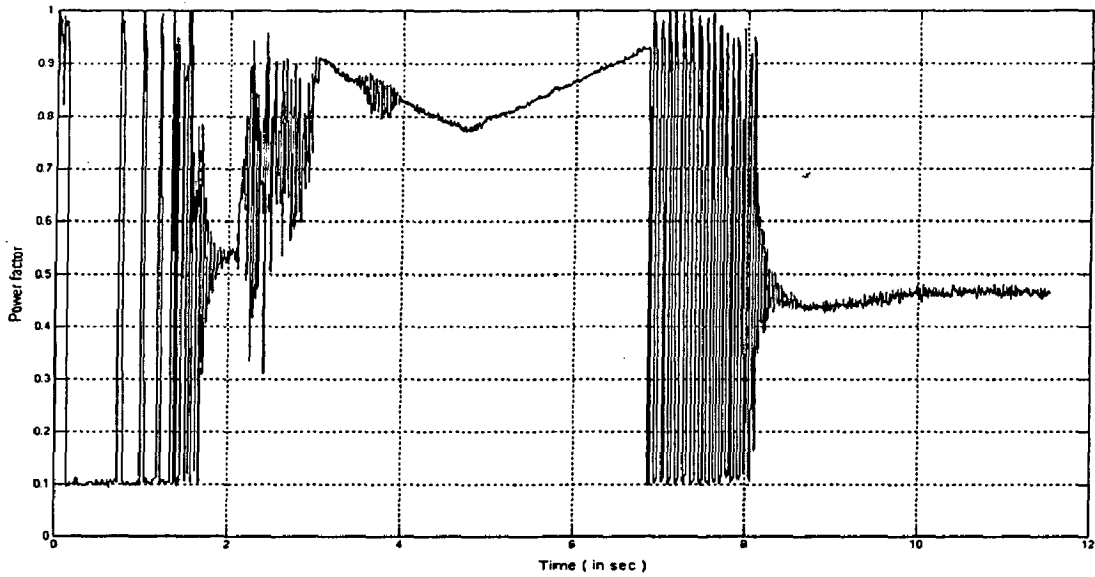


Figure 4.10 Variation of Power factor on the source side.

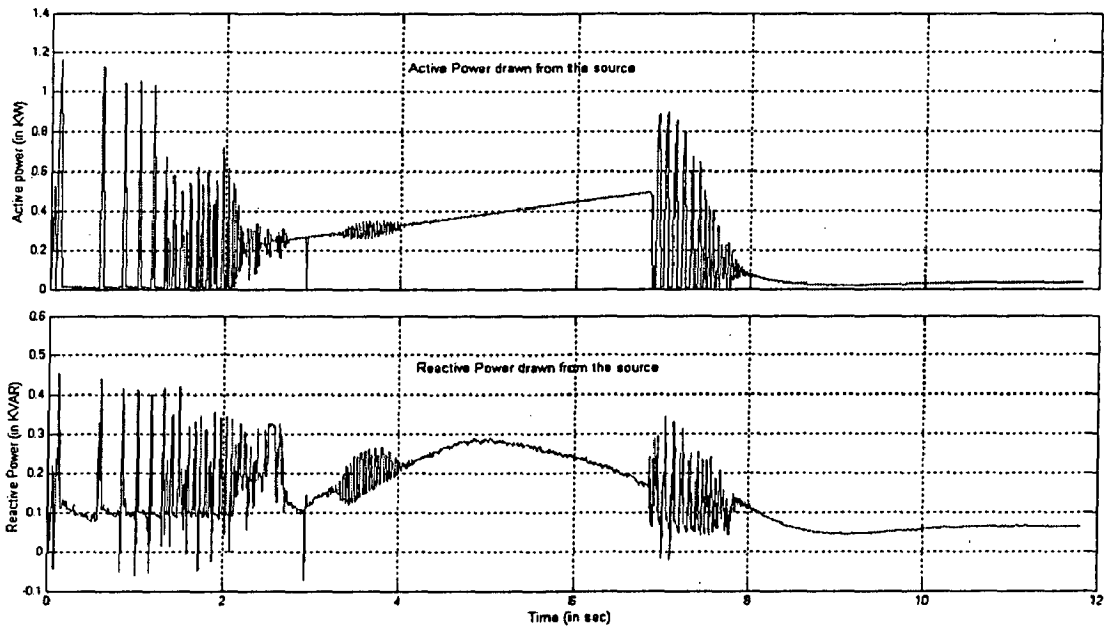


Figure 4.11 Active and Reactive Power drawn by the motor from the supply.

### *Simulation for the inclined track*

Parameter specifications:

Reference slip = 0.07.

Desired speed = 75 Km/hr.

Nature of track =  $2^{\circ}$  incline (up the hill).

The response of the system is given below.

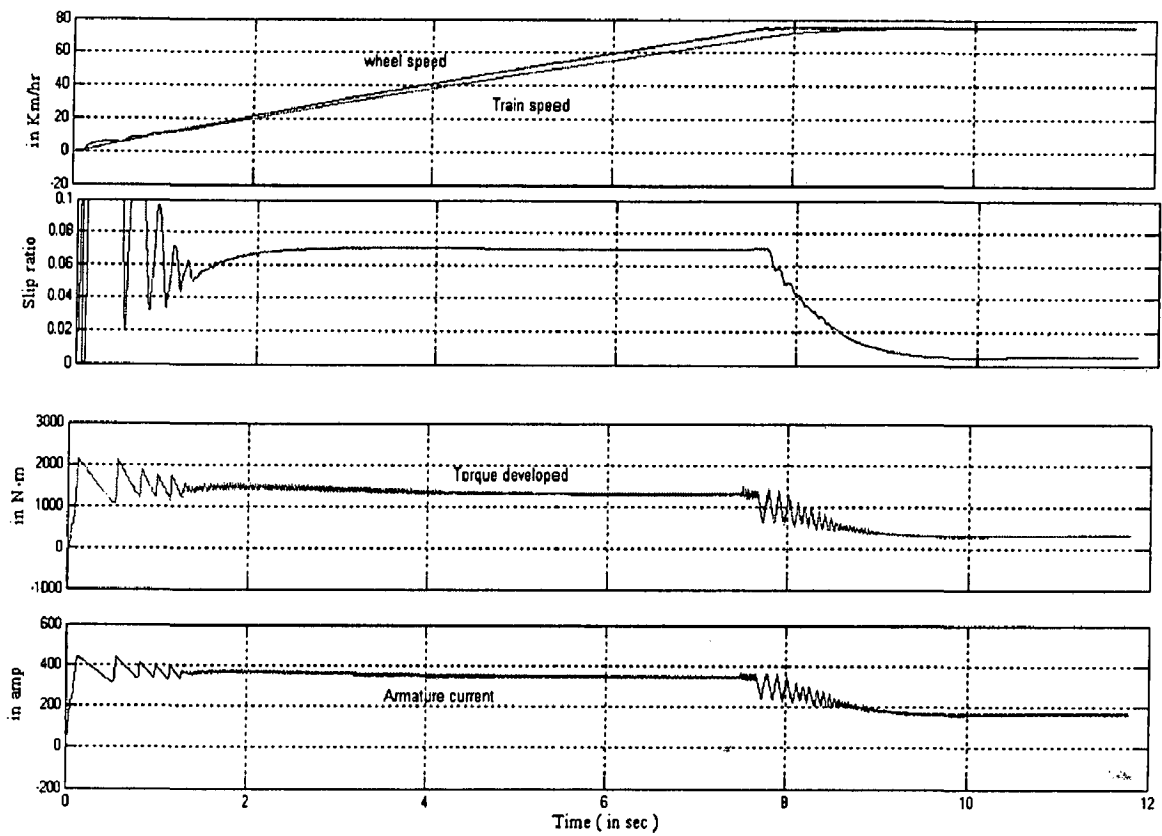


**Figure 4.12** The response of the system showing corresponding armature current and Torque developed by the motor as the slip ratio is being controlled to the commanded value while the train builds up to the desired value of speed on an inclined track.

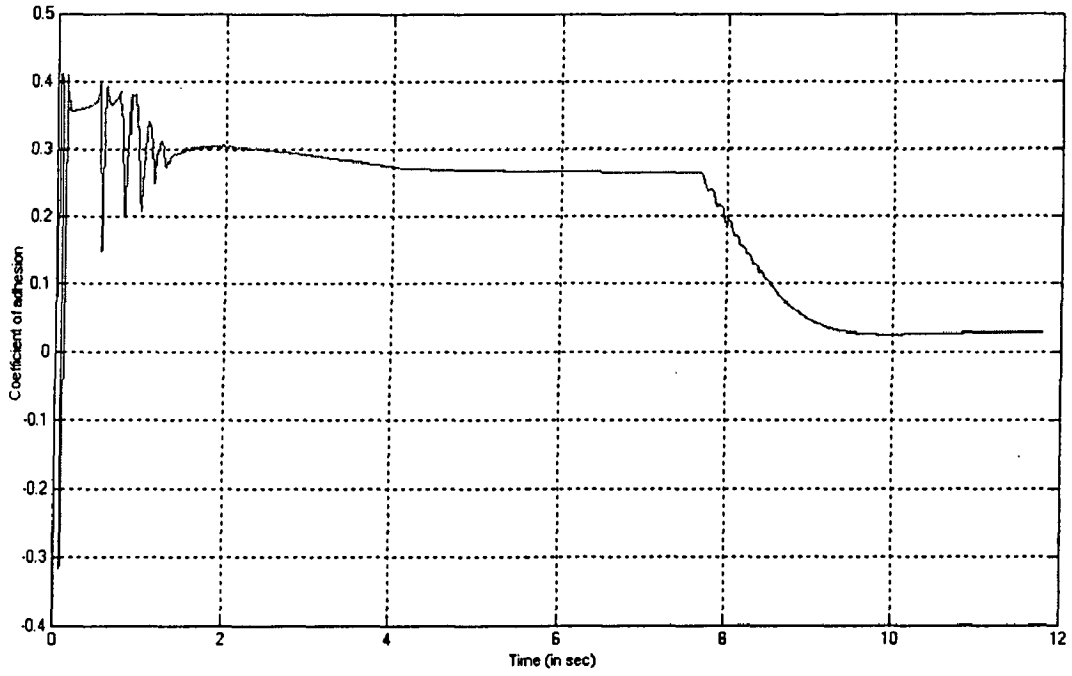


**Figure 4.13** Variation of coefficient of adhesion with time

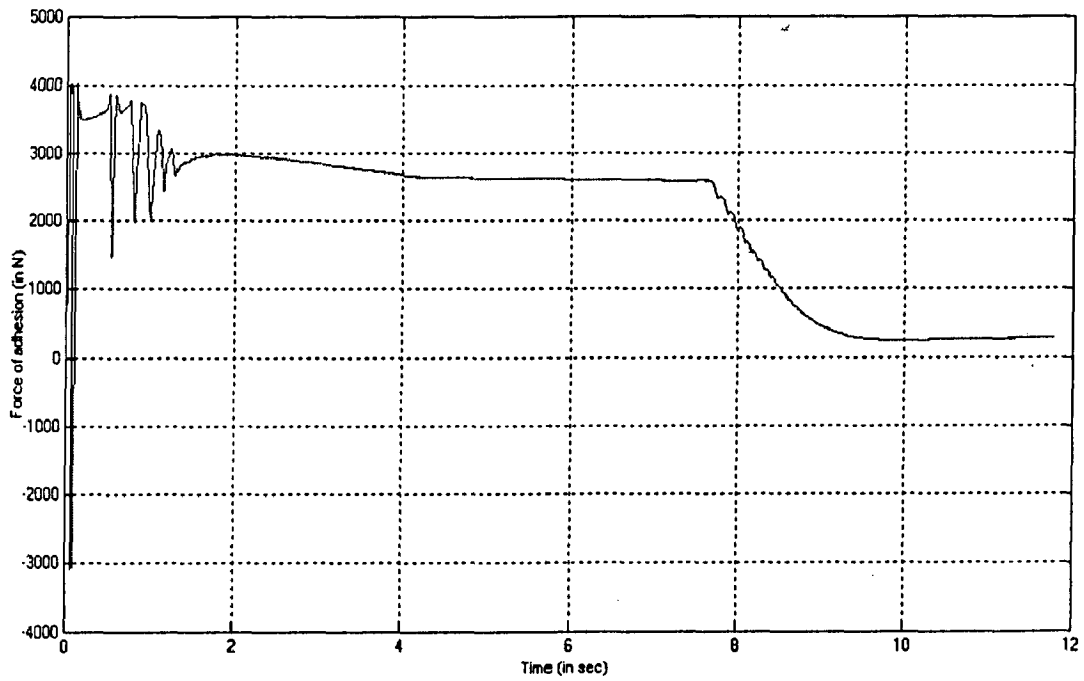


**Figure 4.14** Variation of force of adhesion with time.

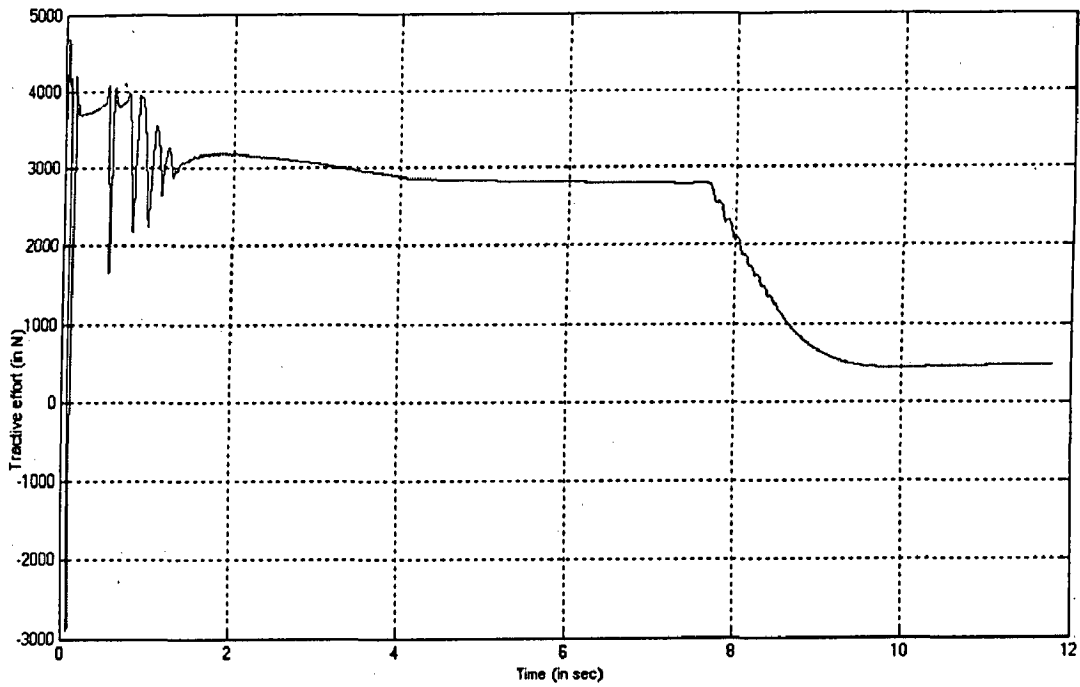


**Figure 4.15** Variation of Tractive effort with time.

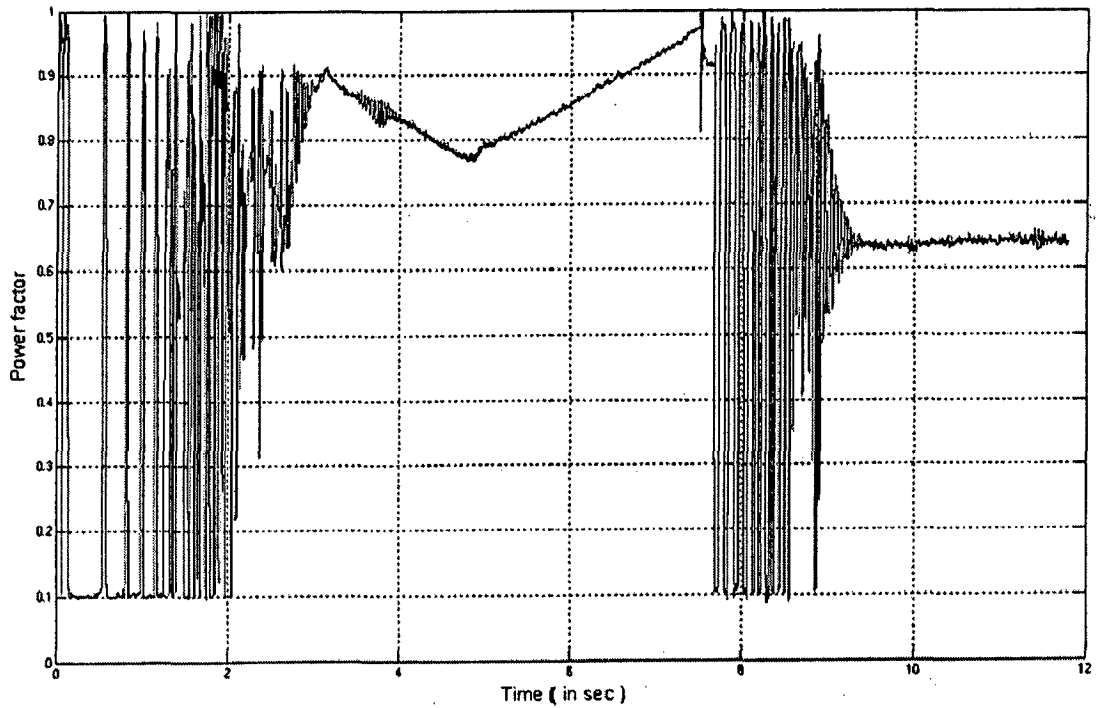


**Figure 4.16** Variation of Power factor on the source side.

It may be noted that the steady state power factor has improved. This is to be expected as steady state load increases.

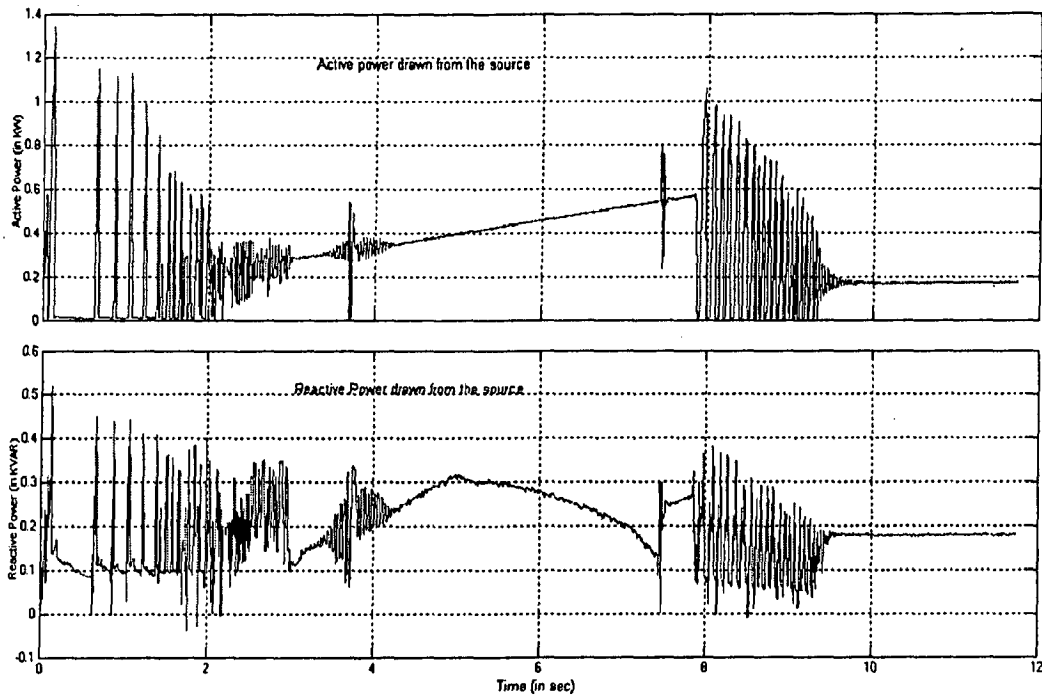


**Figure 4.17** Active and Reactive Power drawn by the motor from the supply.

**Simulation for the variable track**

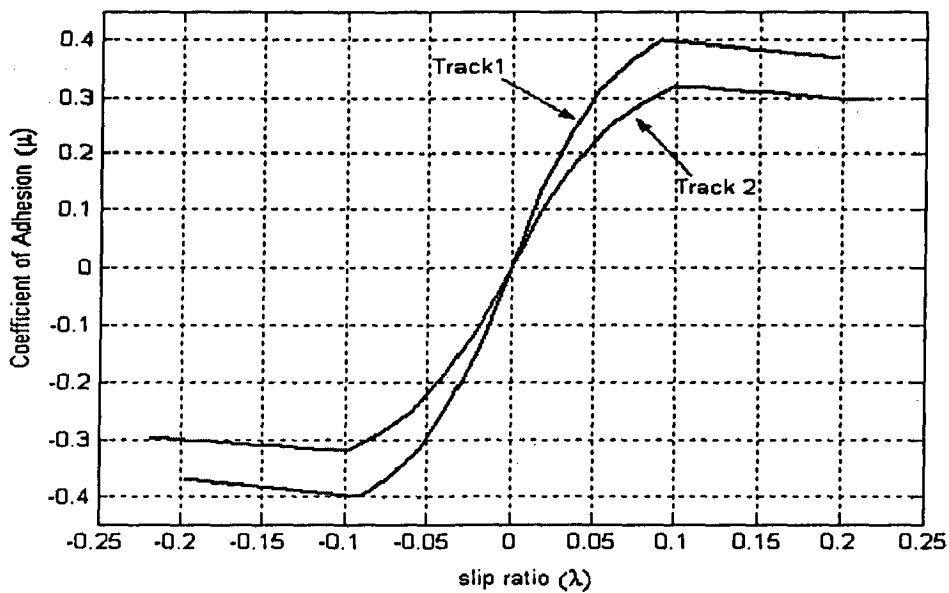
Parameter specifications:

Reference slip = 0.07.

Desired speed = 80 Km/hr.

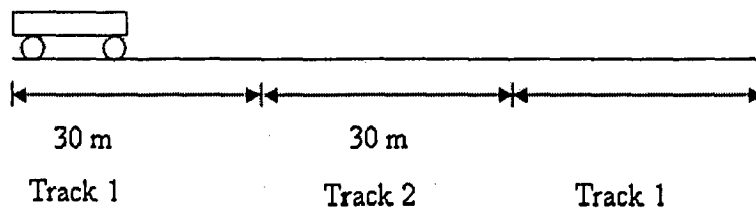
Nature of track = variable track.

The traction drive has been simulated to demonstrate how it re-adjusts itself to follow the reference slip when there is a change in track condition. The drive has been simulated for two track conditions shown in the figure 4.18



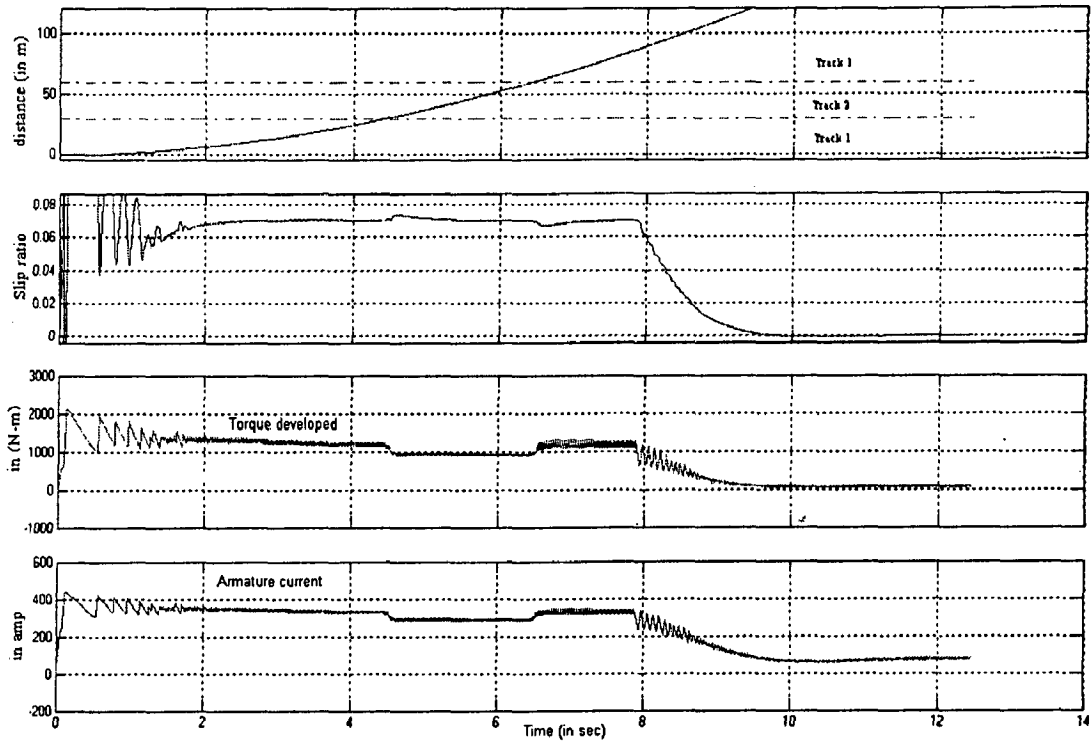
**Figure 4.18** The  $\mu$ - $\lambda$  curves for two tracks used in the simulation.

The train moves first 30 m on track 1. The track condition changes immediately at this point and the train moves on track 2 for next 30 m. It again shifts to track 1 after this. This is shown in figure 4.19.



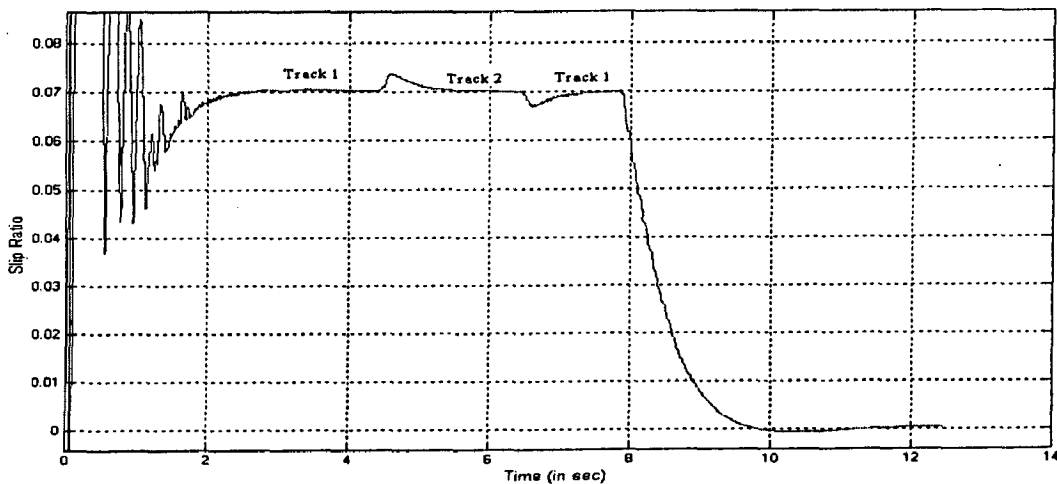
**Figure 4.19** Movement of train on the tracks.

The response of the system is shown below.



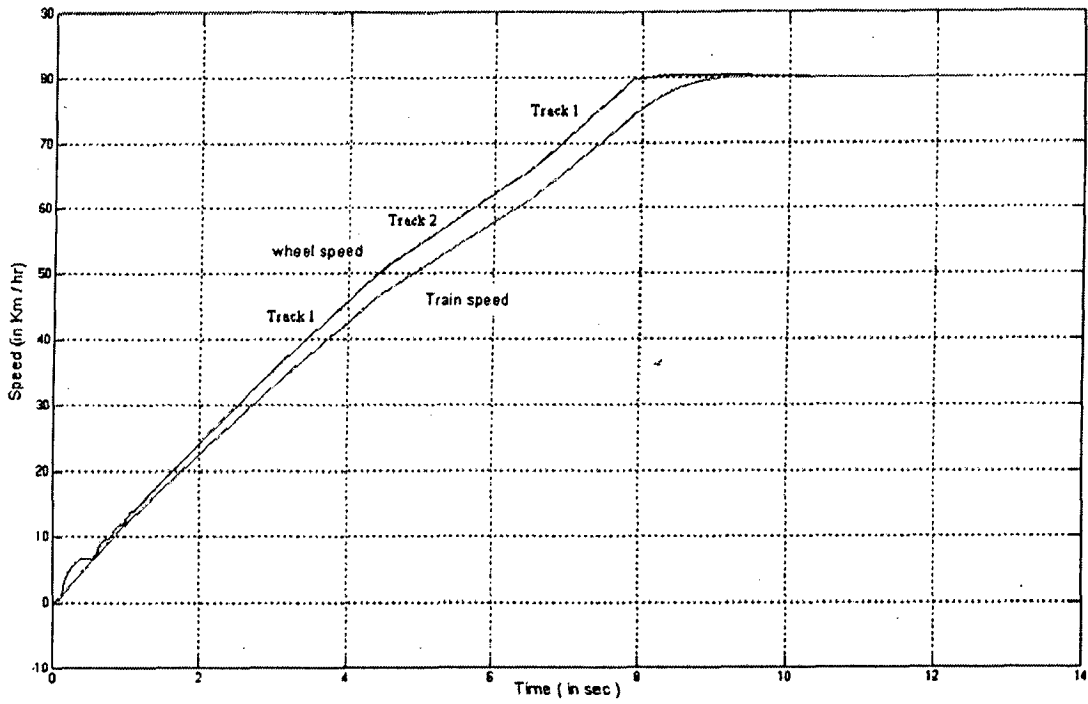
**Figure 4.20** The response of the system showing corresponding armature current and Torque developed by the motor as the slip ratio is being controlled to the commanded value while the train builds up to the desired value of speed on a variable track.

Figure 4.21 shows the zoomed in response of slip ratio variation with time.



**Figure 4.21** Variation of slip ratio with time.





**Figure 4.22** Variation of wheel speed and train speed with time.

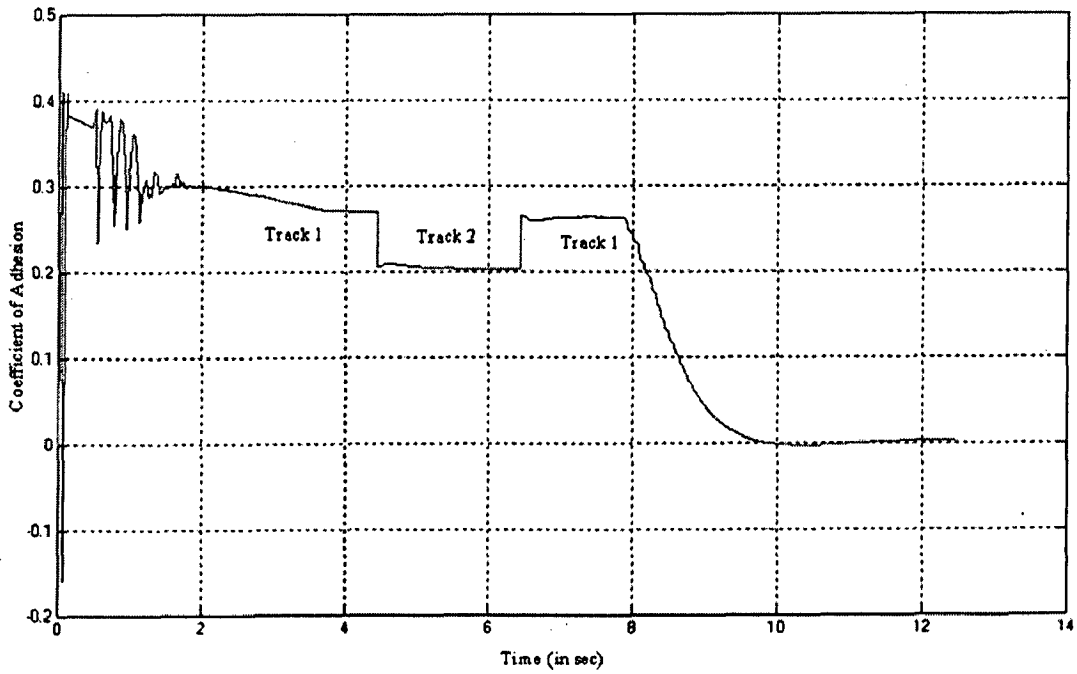


**Figure 4.23** Variation of coefficient of adhesion with time.

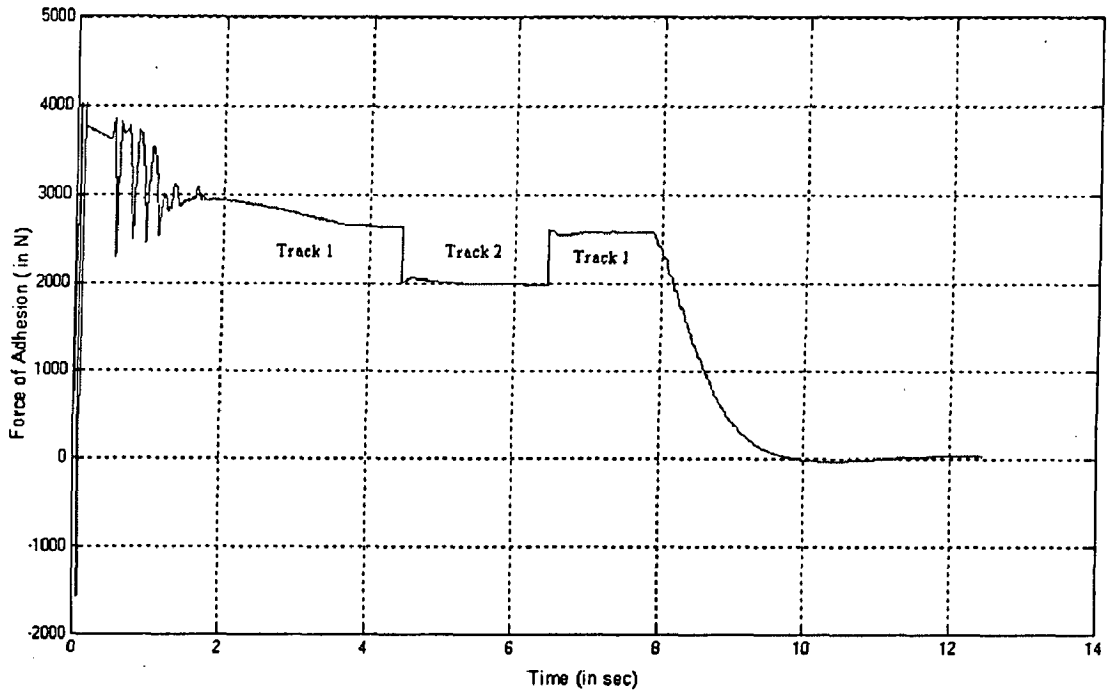


**Figure 4.24** Variation of force of adhesion with time.

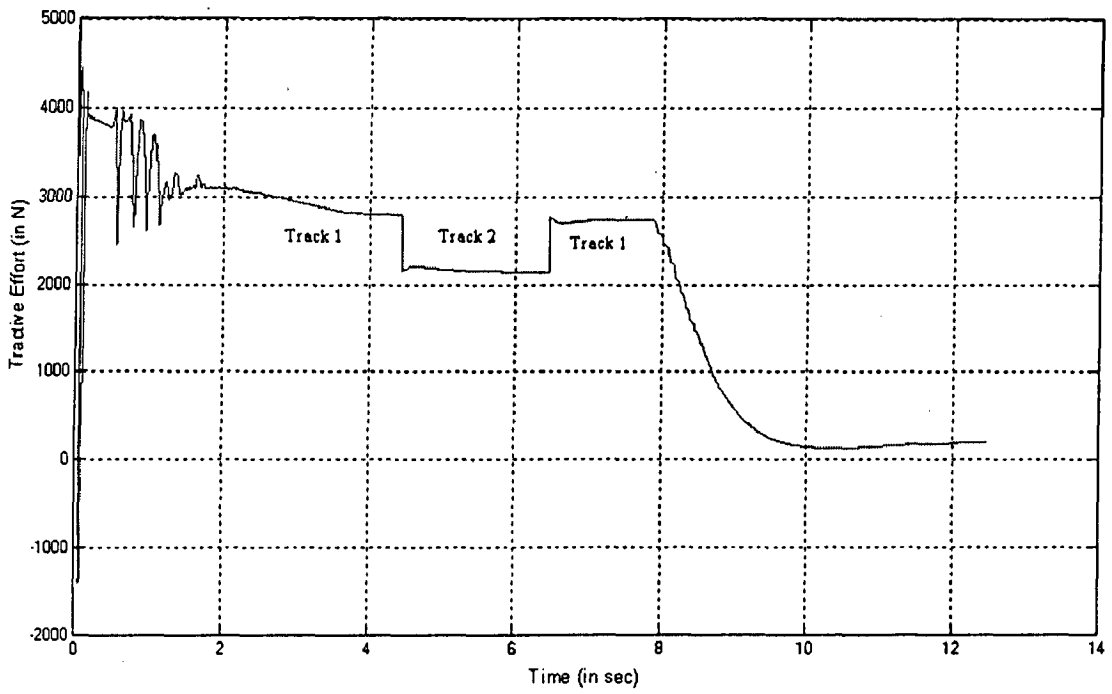


**Figure 4.25** Variation of Tractive effort with time.

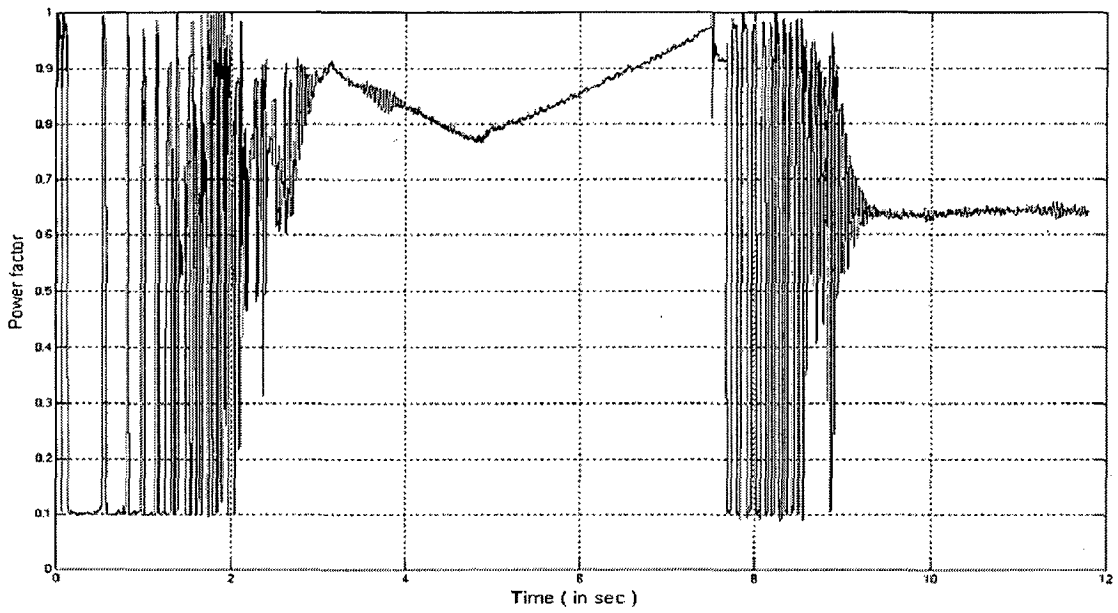


**Figure 4.26** Variation of Power factor on the source side.

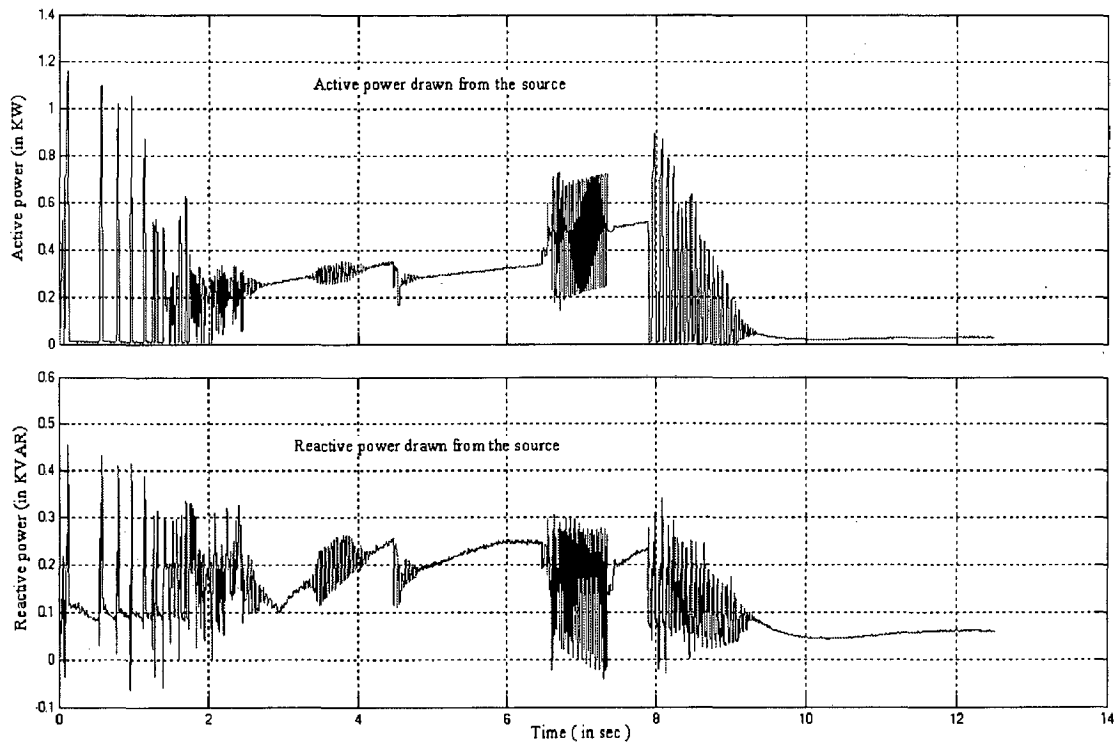


**Figure 4.27** Active and Reactive Power drawn by the motor from the supply.

However, this method has a drawback that when the track condition changes the reference slip may no longer be optimal and it may happen that the operating slip may lie in the unstable zone of operation. This is shown in figure 4.28.

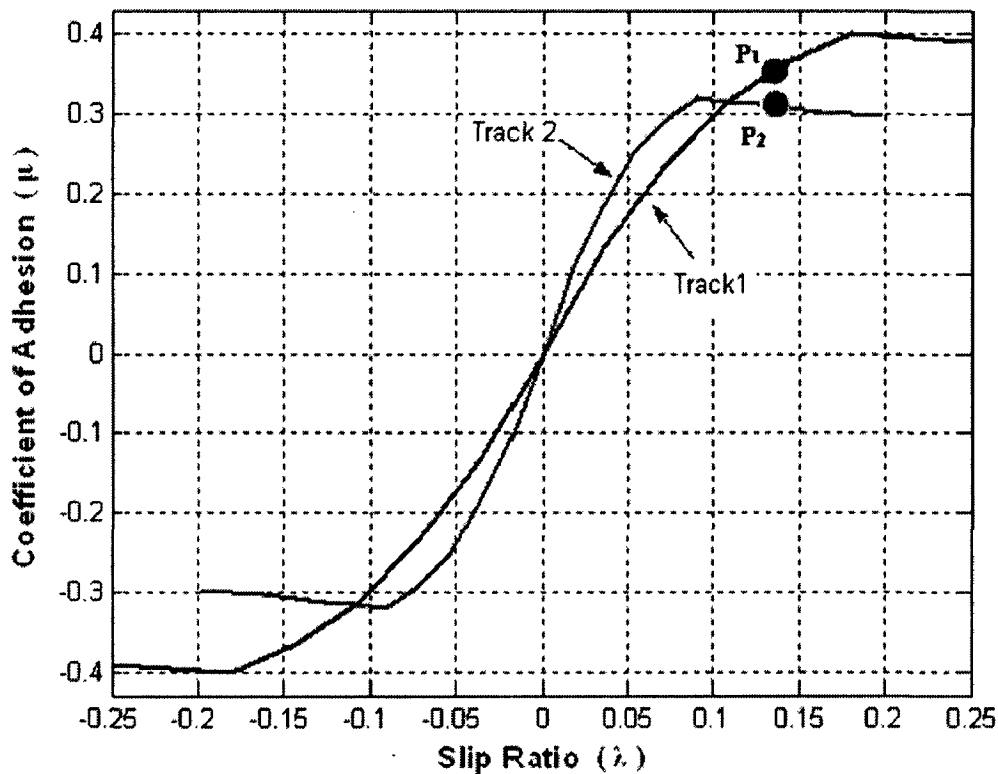


**Figure 4.28** The  $\mu$ - $\lambda$  curves for two tracks showing a possible shift into unstable zone.

Initially, when the train was moving on track 1, the slip was optimal and the operating point  $P_1$  was in the stable zone. However, when the track changed to track 2, then, at same slip the operating point  $P_2$  lies in the unstable zone of the  $\mu$ - $\lambda$  characteristic. Thus this scheme fails under such conditions.

To overcome this disadvantage, gradient control scheme is adopted.

## 4.3 Gradient Control Scheme

### 4.3.1 Theory

In this scheme, the gradient of  $\mu$ - $\lambda$  curve for the track is calculated and the operating point is controlled by a PI controller such that the gradient ( $d\mu/d\lambda$ ) at operating point is equal to the reference value. The idea of the scheme is to make the train operate at an operating point sufficiently high on the  $\mu$ - $\lambda$  curve such that the force of adhesion is optimally utilized without moving into the unstable zone of operation even when the track condition is changed.

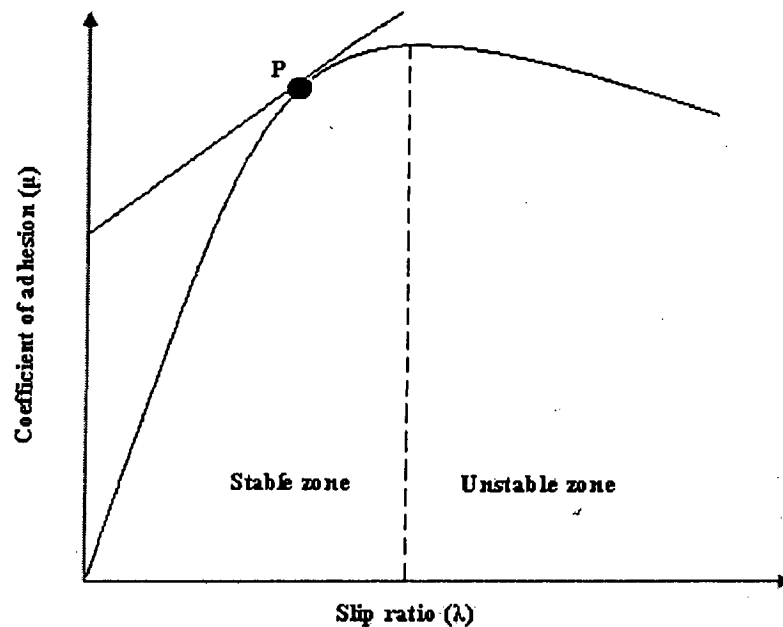


**Figure 4.29** The  $\mu$ - $\lambda$  curve showing stable and unstable regions and gradient at operating point.

It may be noted that the gradient of  $\mu$ - $\lambda$  curve is positive in the stable region and unstable in the negative region. Further, as one moves towards the peak of the curve, the slope continuously decreases and at the peak of the curve it becomes zero. Thus one can ensure an optimal utilization of adhesion force by selecting a small positive value of gradient as a reference value. A block diagram representation of a gradient control scheme is given in figure 4.30

The gradient detector detects the slope of the  $\mu$ - $\lambda$  curve at the point of operation. This slope is then made to follow up the reference gradient with the help of gradient controller.

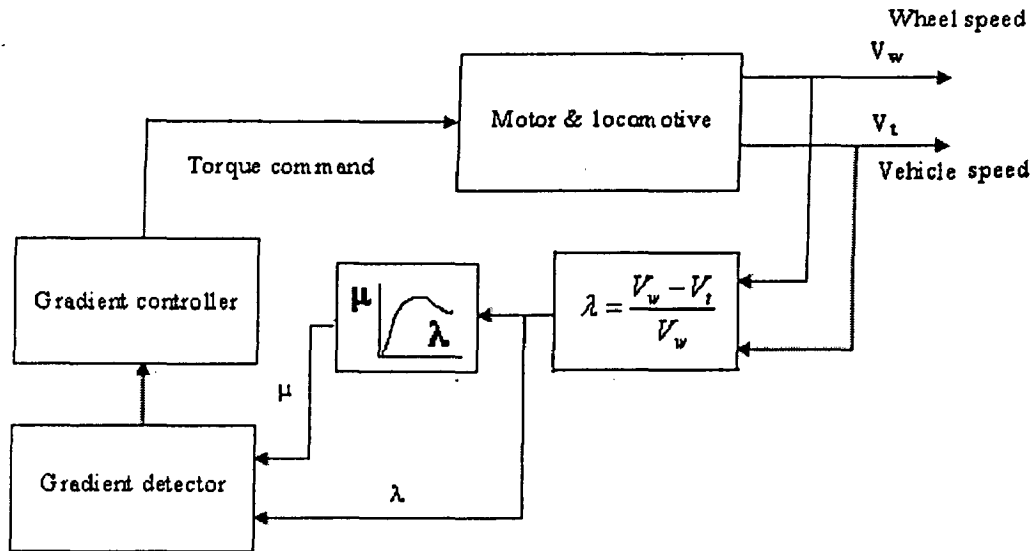


**Figure 4.30** Block diagram of gradient control Scheme.

#### 4.3.2 Implementation with MATLAB

The gradient control scheme has been simulated by combining electrical drive and mechanical load with a gradient controller ( a PI controller) forming an important link to achieve the desired traction control. Figure 4.31 shows the MATLAB implementation of this scheme.

An important subsystem developed for implementation of this scheme is gradient detector which detects the current gradient of the  $\mu$ - $\lambda$  curve. Figure 4.32 shows the MATLAB implementation of gradient detector.

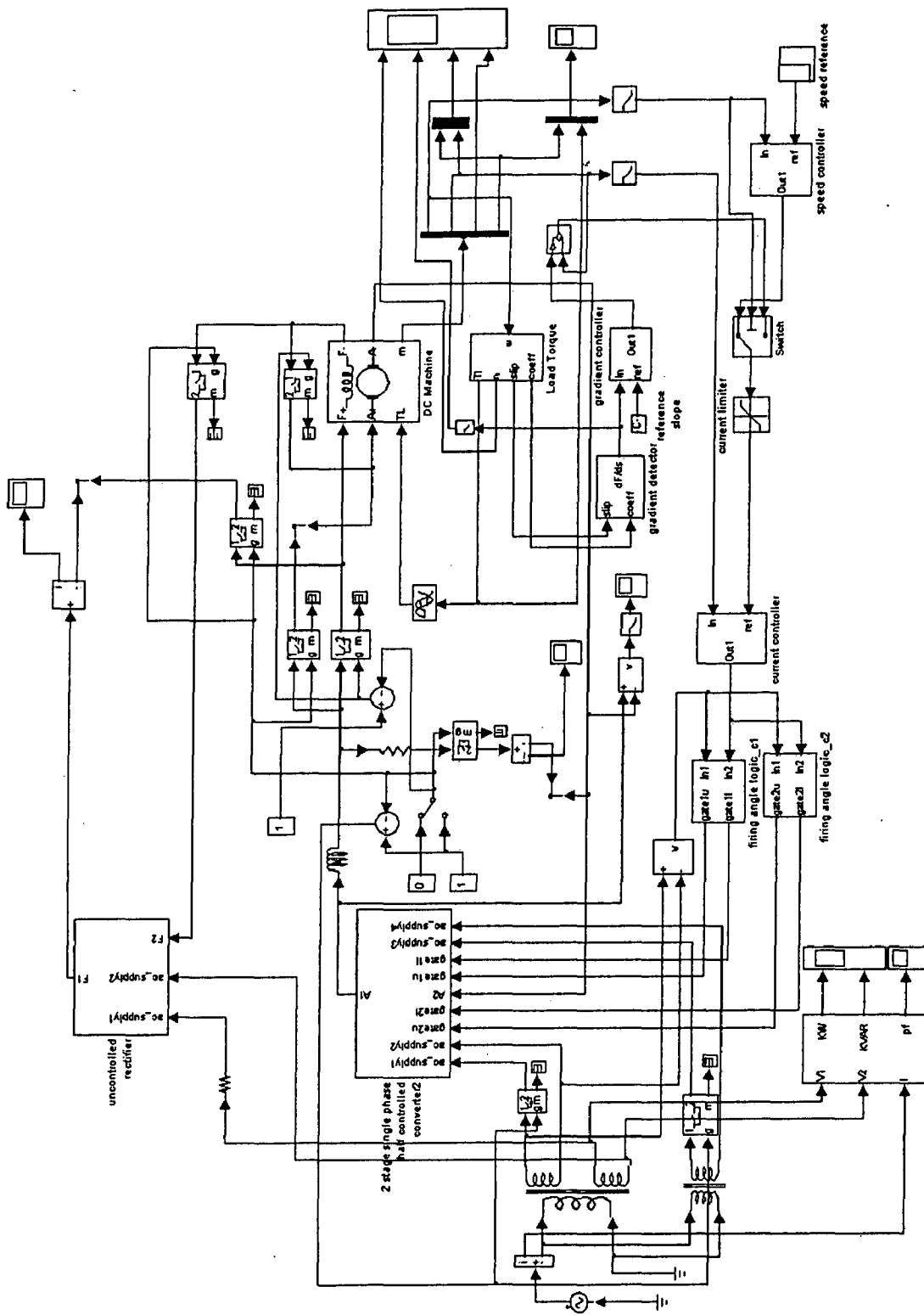
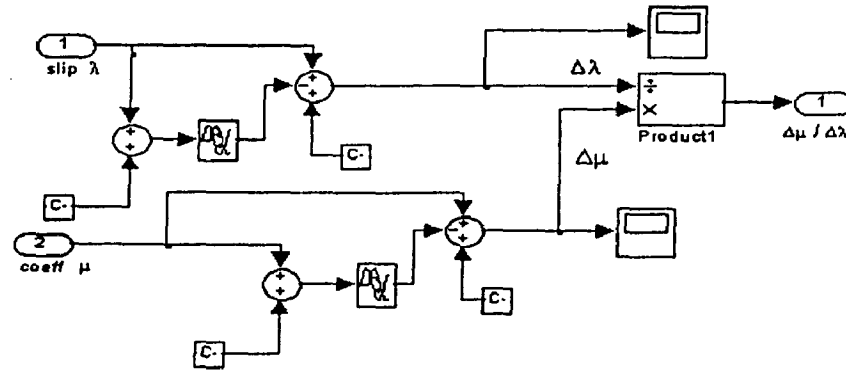


Figure 4.31 Simulink implementation. Closed loop Traction scheme employing gradient control to control the slip.



**Figure 4.32** SIMULINK implementation of gradient detector

### 4.3.3 Results

The simulation was carried out for a track whose  $\mu$ - $\lambda$  characteristic is simulated below.

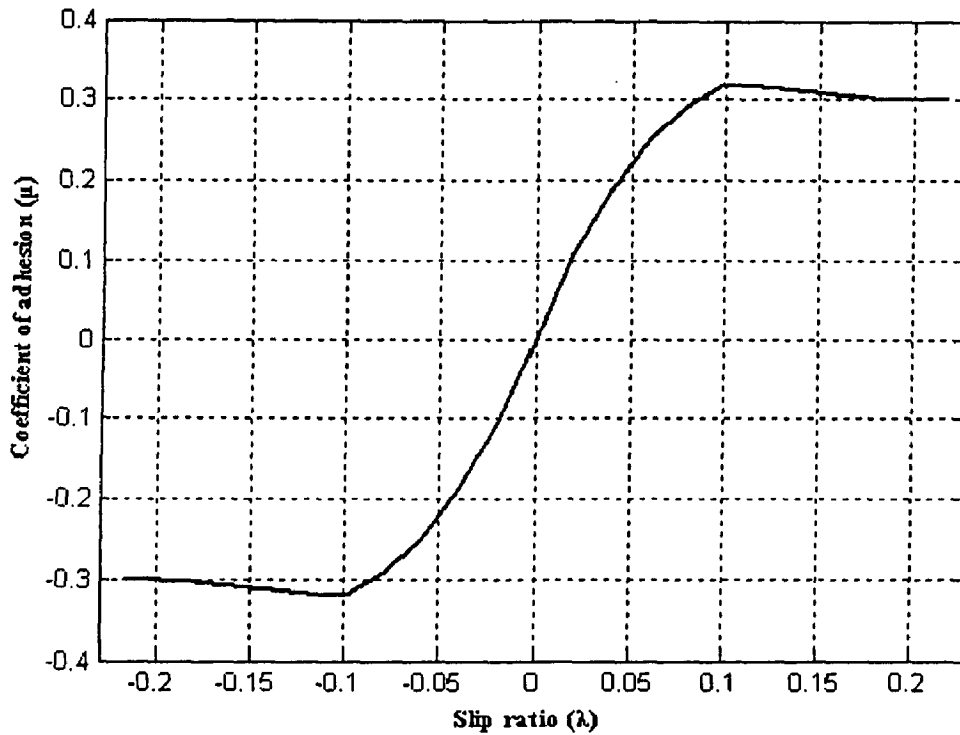


**Figure 4.33**  $\mu$ - $\lambda$  characteristic for the track.

As in the earlier case, this characteristic has been stored in form of a look up table. The simulation has been carried out for the flat track, inclined track (up the hill) and variable track conditions.



### Simulation for the flat track

Parameter specifications

Reference gradient = 2.

Desired speed = 70 Km/hr.

Nature of track= flat track.

The response of the system is given below.

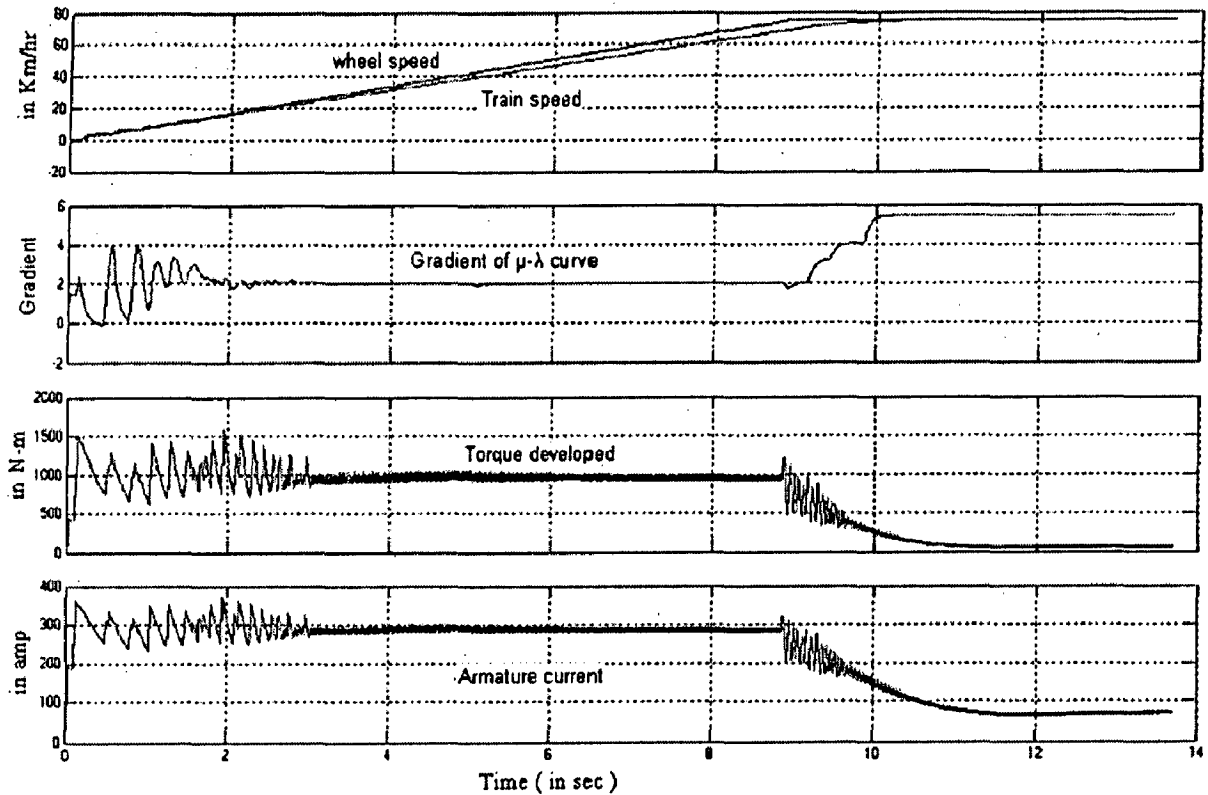


**Figure 4.34** The response of the system showing corresponding armature current and Torque developed by the motor as the slip ratio is being controlled through gradient control while the train builds up to the desired value of speed on a flat track.

Figure 4.34 clearly shows that the motor torque is controlled such that the gradient of the  $\mu$ - $\lambda$  curve is equal to the commanded value at the operating point. Some other important response for the system is shown in the figures 4.35 to 4.41.

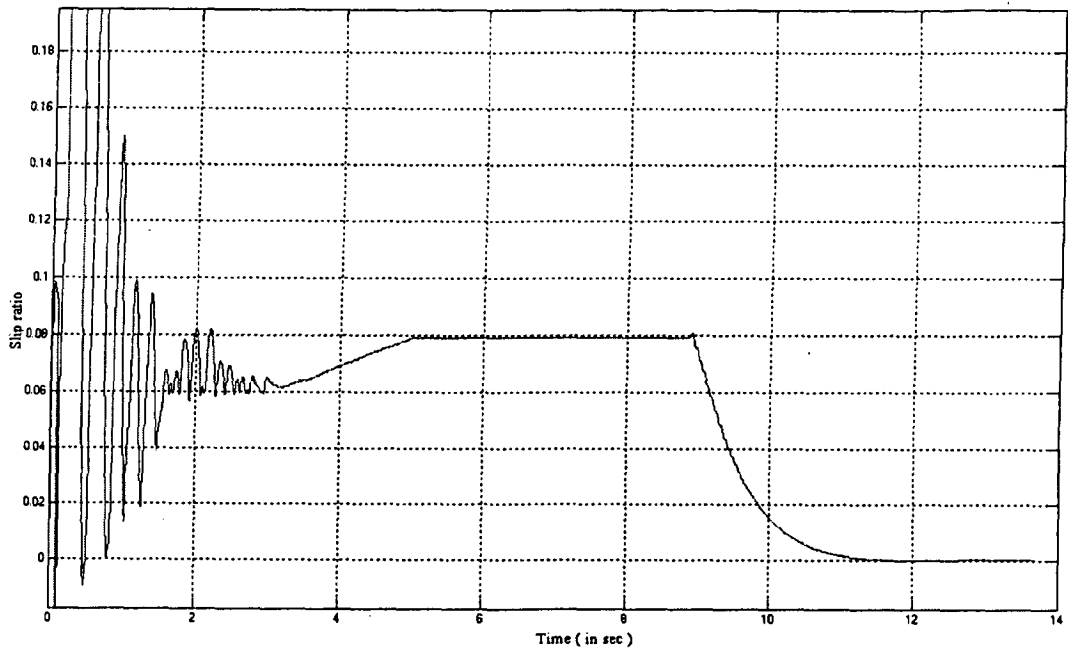


**Figure 4.35** Variation of slip ratio with time.

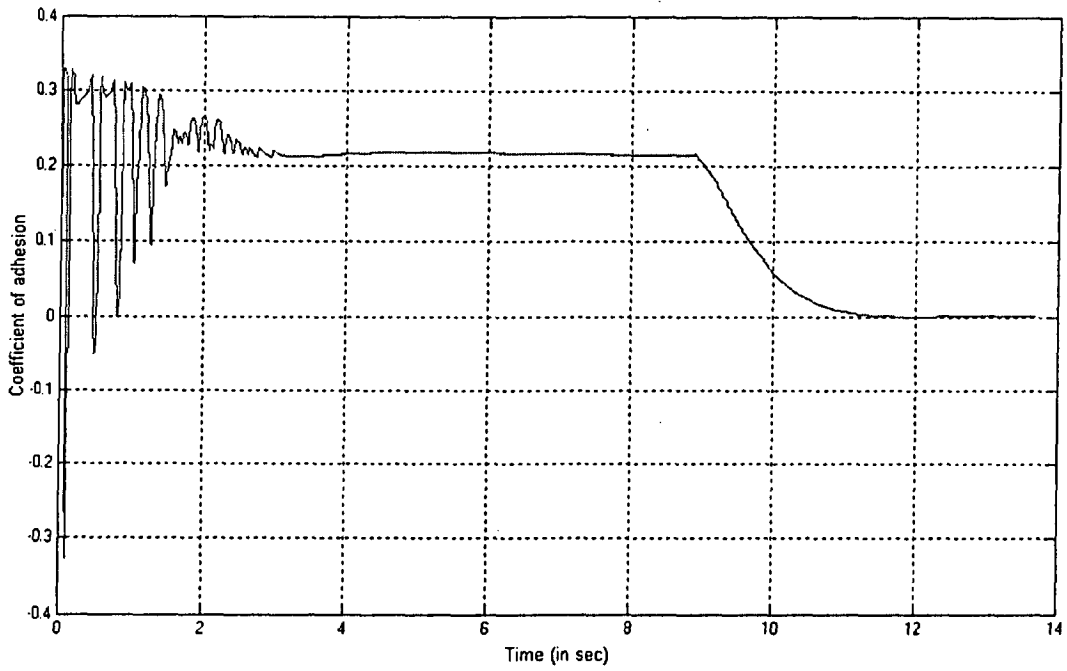


**Figure 4.36** Variation of coefficient of adhesion with time.

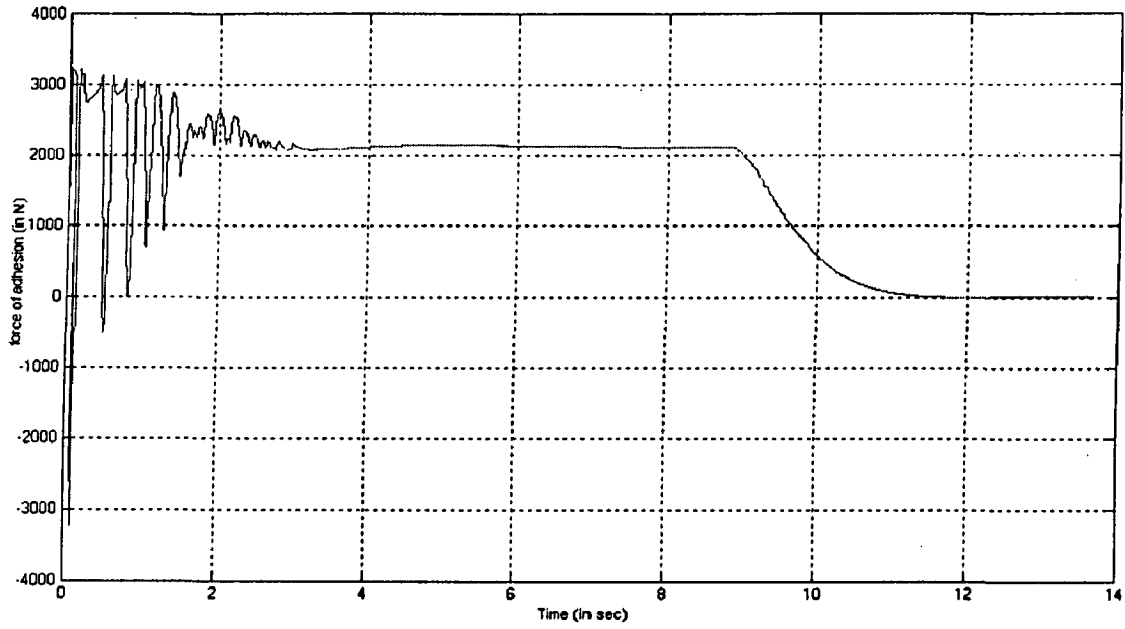


**Figure 4.37** Variation of force of adhesion with time.

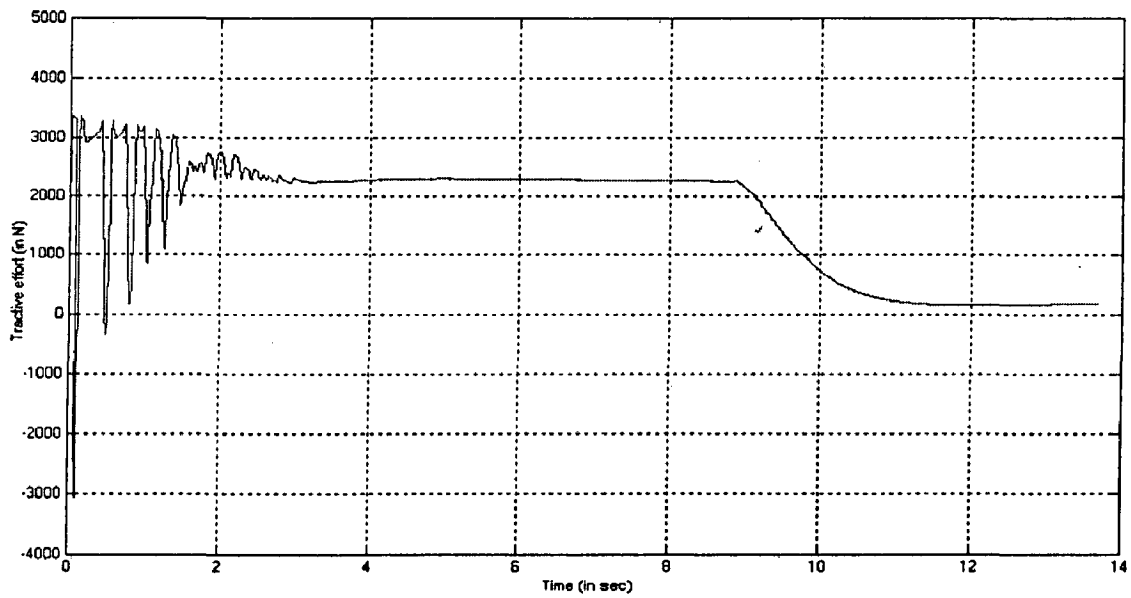


**Figure 4.38** Variation of Tractive effort with time.

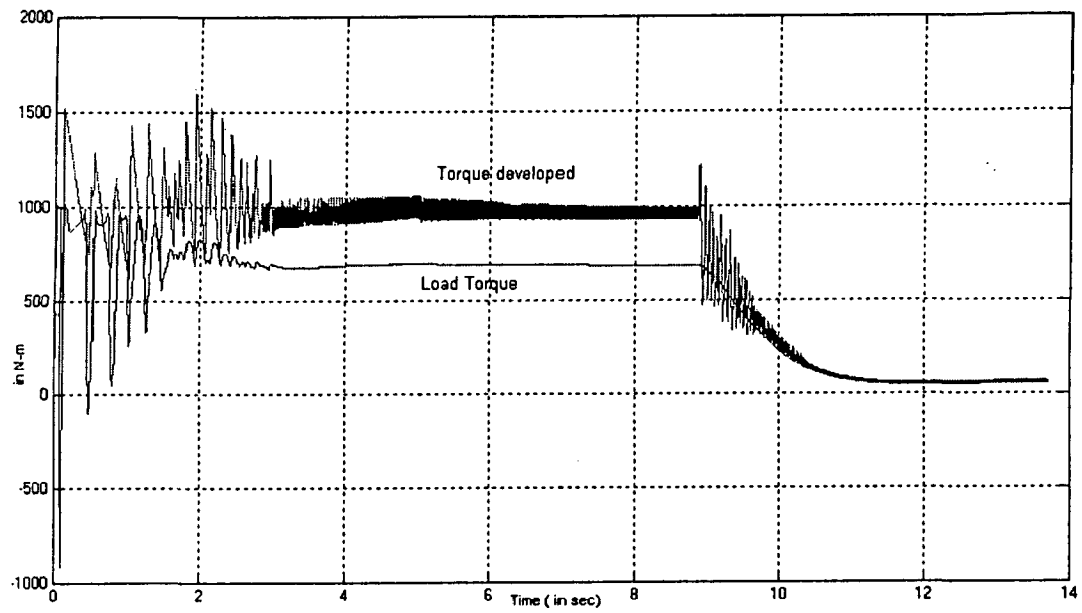


**Figure 4.39** The figure shows the torque developed by the motor and load torque on the drive on the same scale. The difference between the two curves during acceleration may be attributed to large value of  $J \frac{d\omega}{dt}$ .

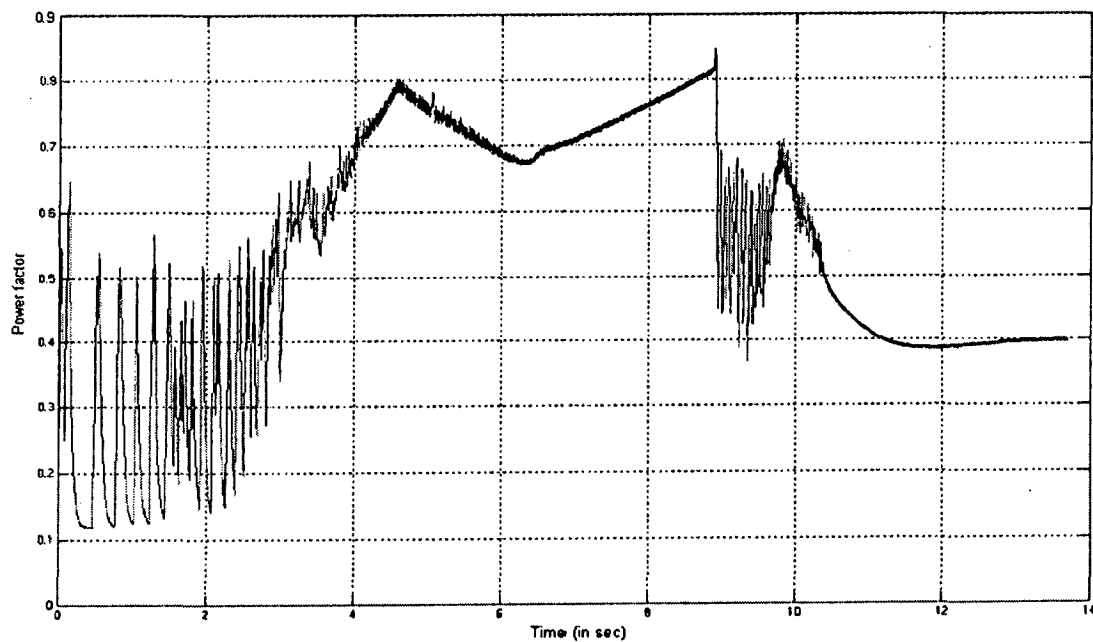


**Figure 4.40** Variation of Power factor on the source side.

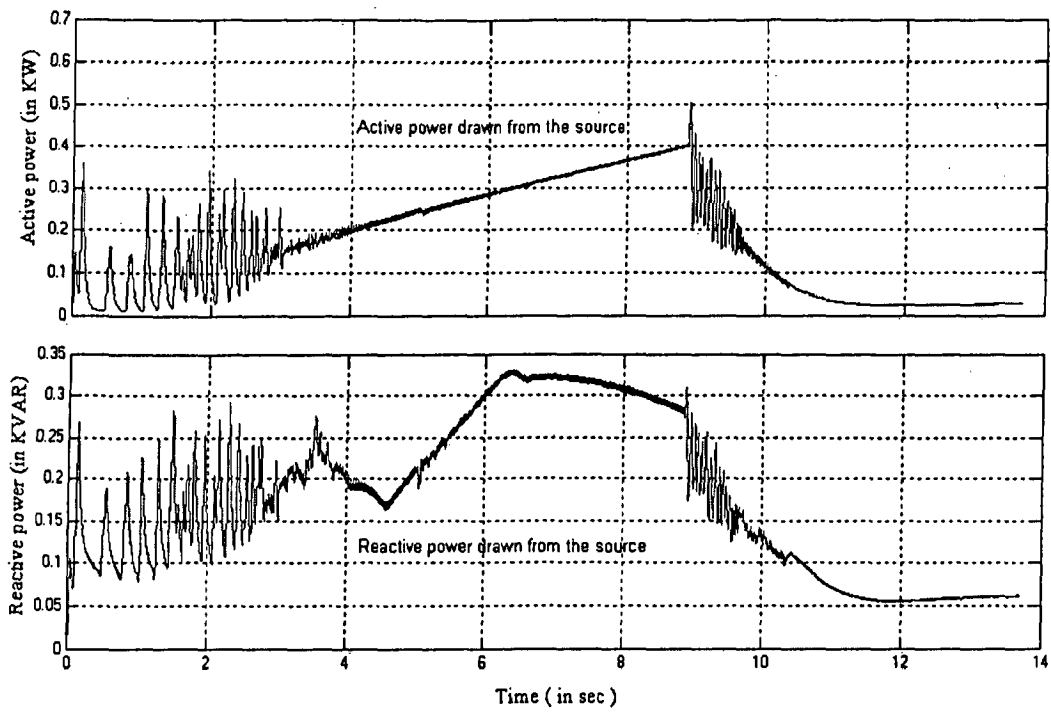


**Figure 4.41** Active and Reactive Power drawn by the motor from the supply.

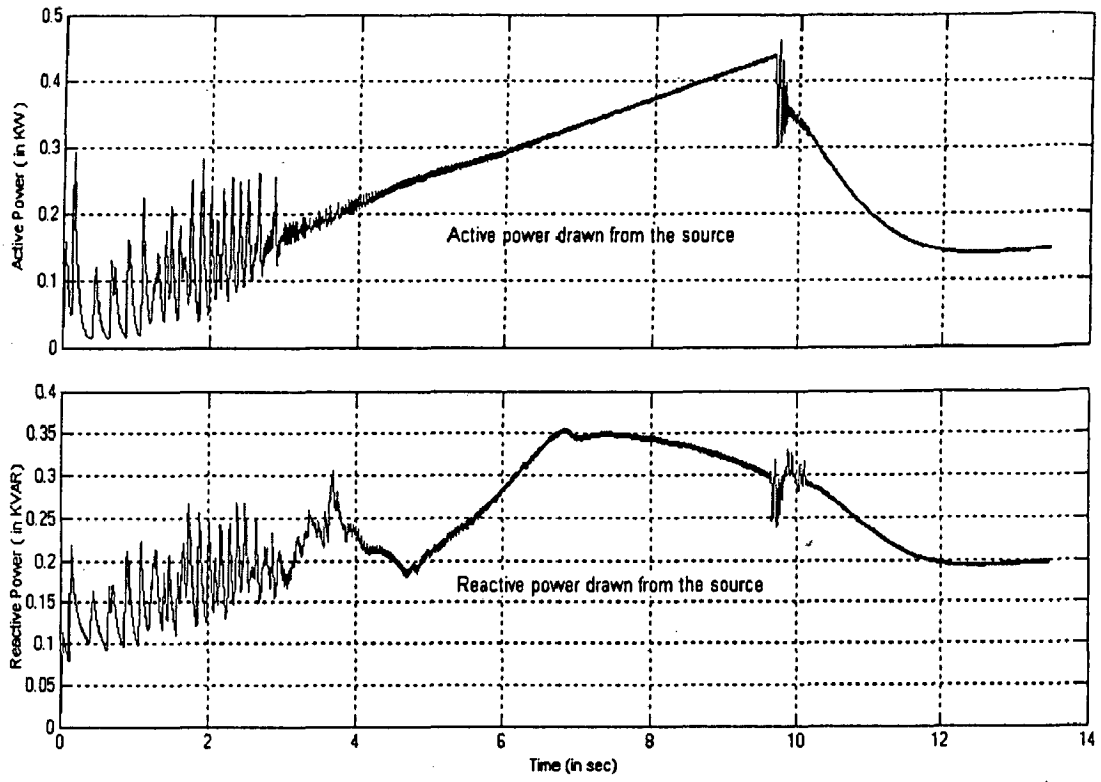


**Figure 4.49** Active and Reactive Power drawn by the motor from the supply.

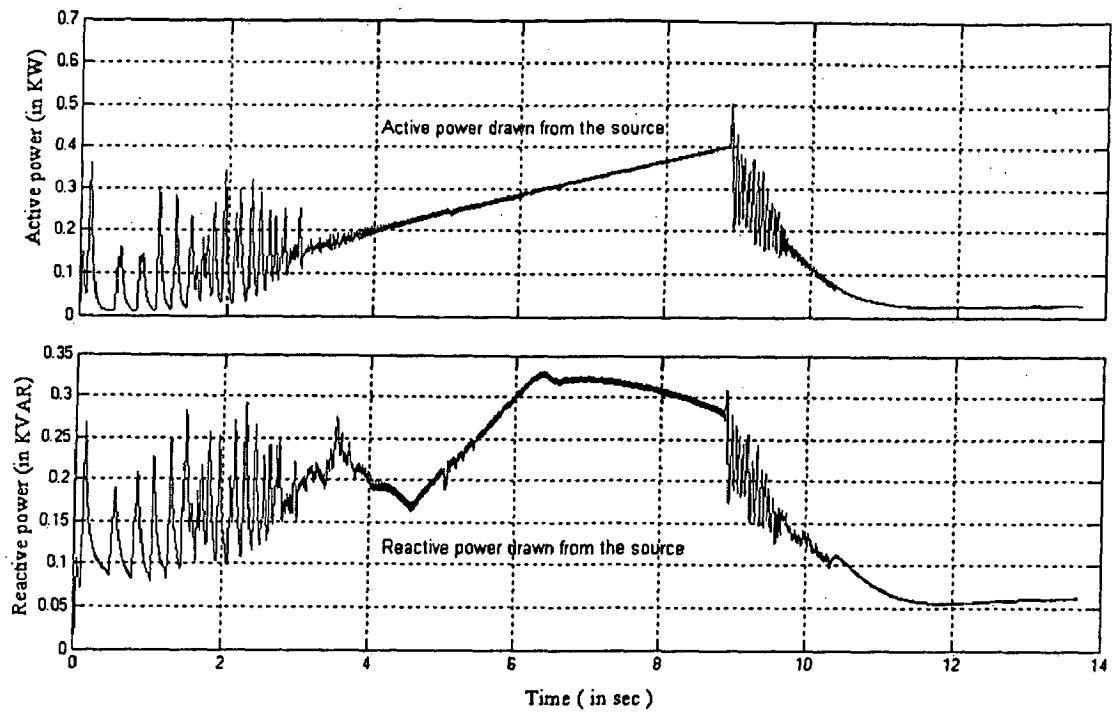


**Figure 4.41** Active and Reactive Power drawn by the motor from the supply.

### Simulation for the inclined track

Parameter specifications

Reference gradient = 2.

Desired speed = 70 Km/hr.

Nature of track =  $2^\circ$  incline (up the hill).

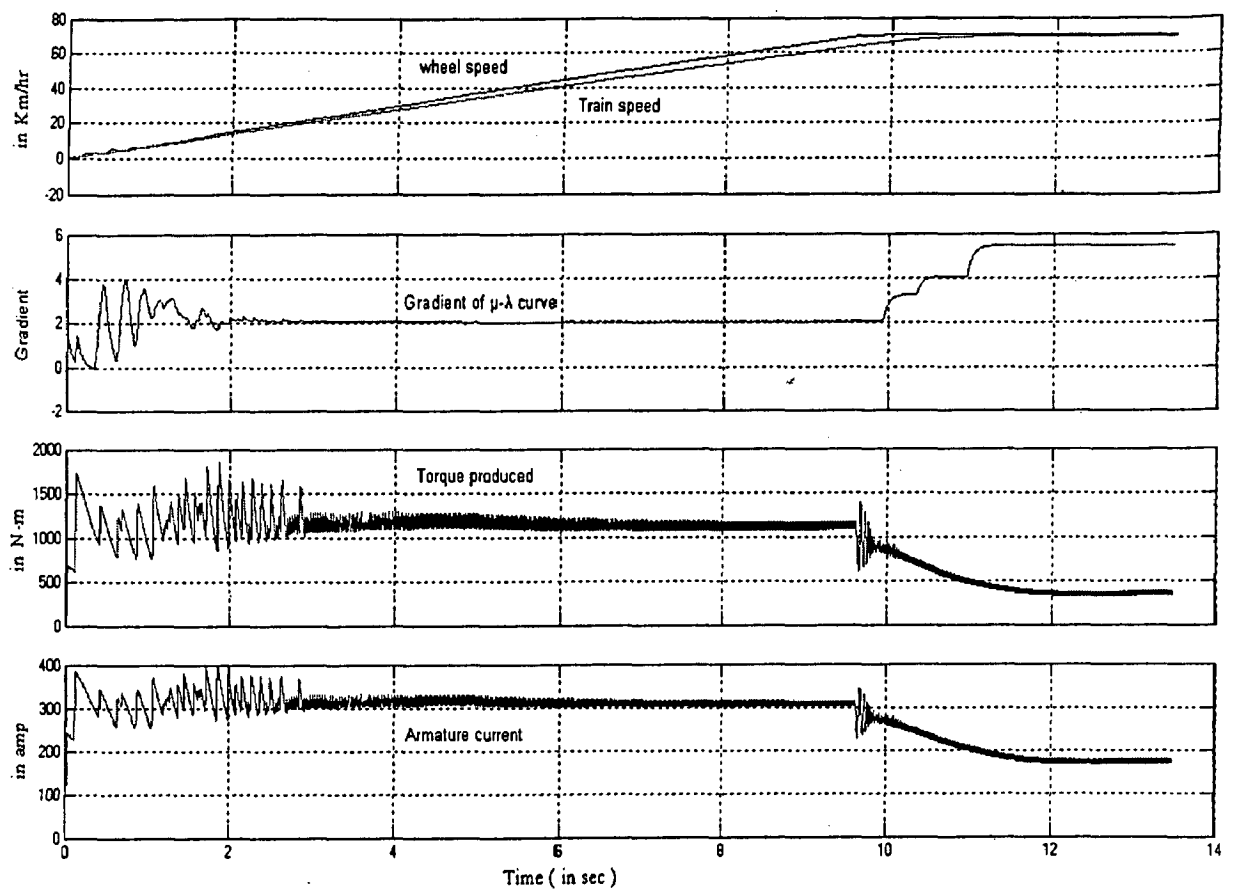


**Figure 4.42** The response of the system showing corresponding armature current and Torque developed by the motor as the slip ratio is being controlled through gradient control while the train builds up to the desired value of speed on an inclined track.



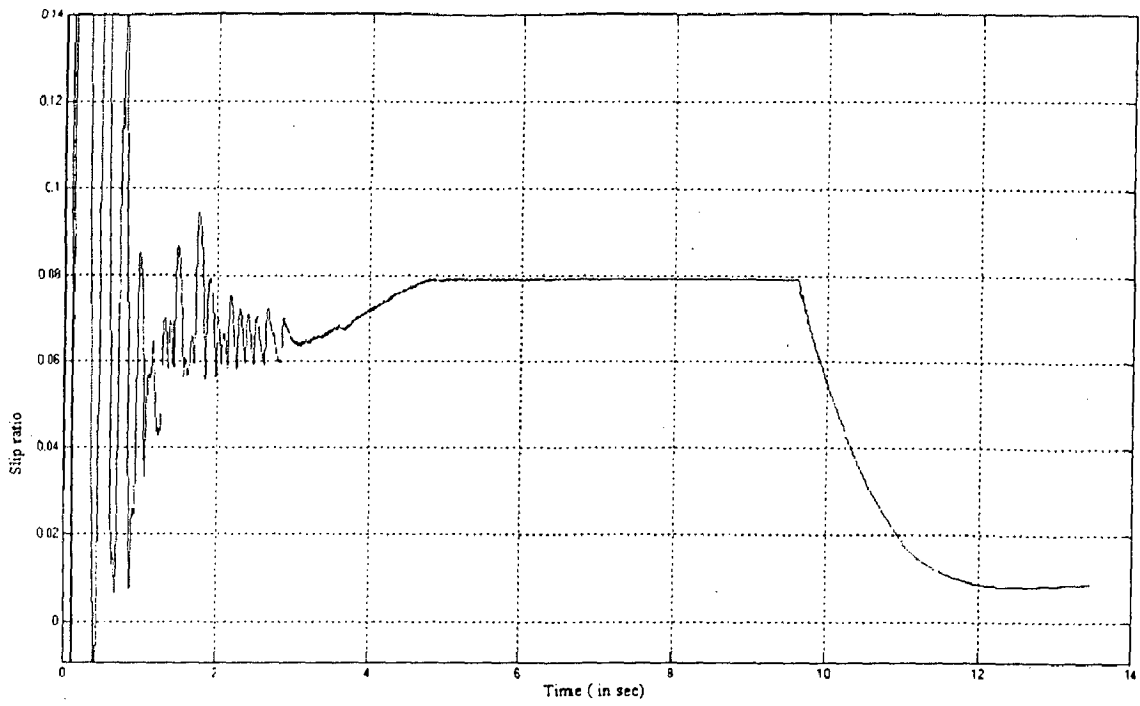


**Figure 4.43** Variation of slip ratio with time.

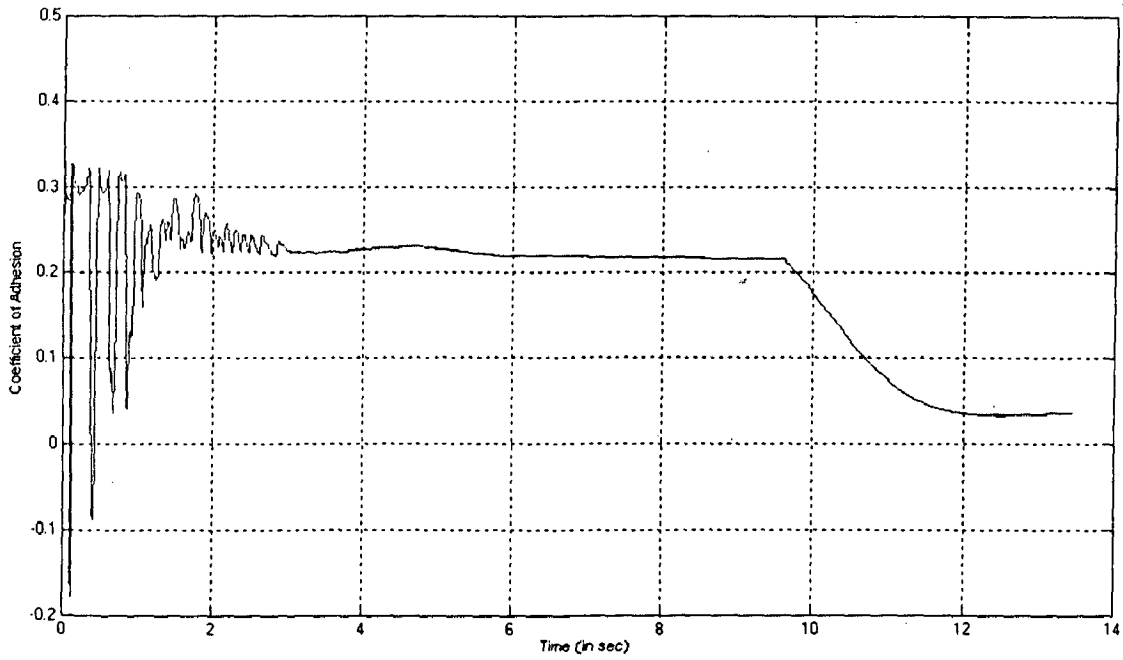


**Figure 4.44** Variation of coefficient of adhesion with time.

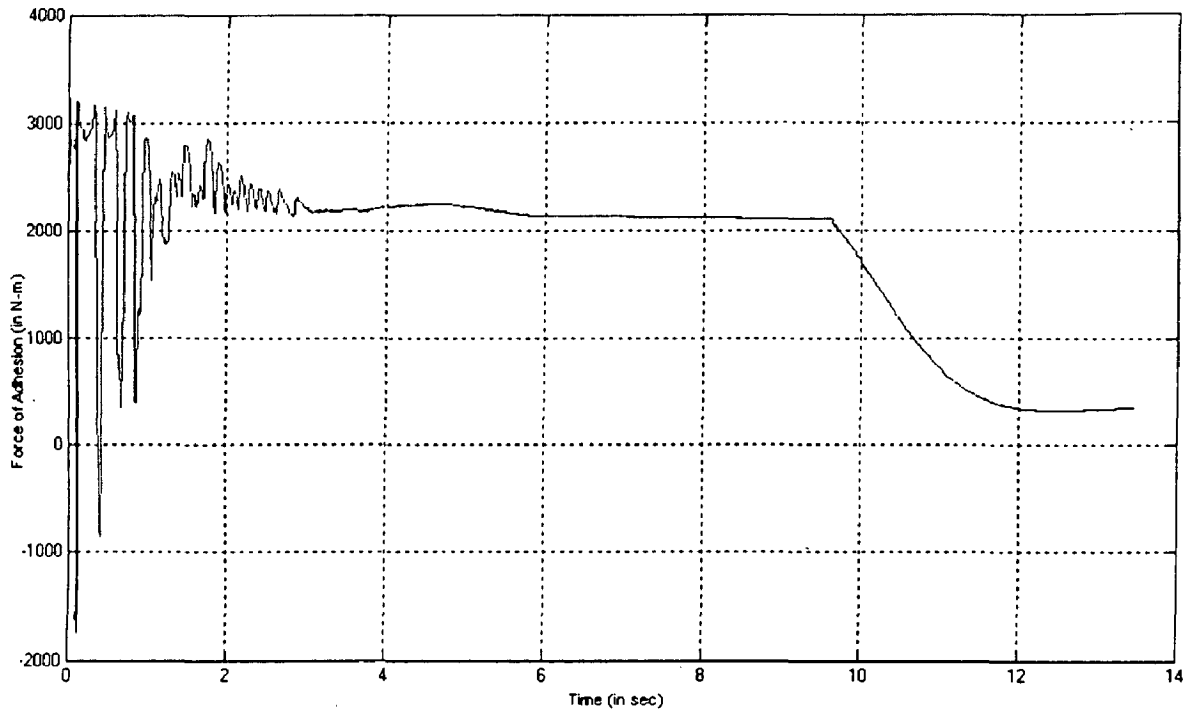


Figure 4.45 Variation of force of adhesion with time.

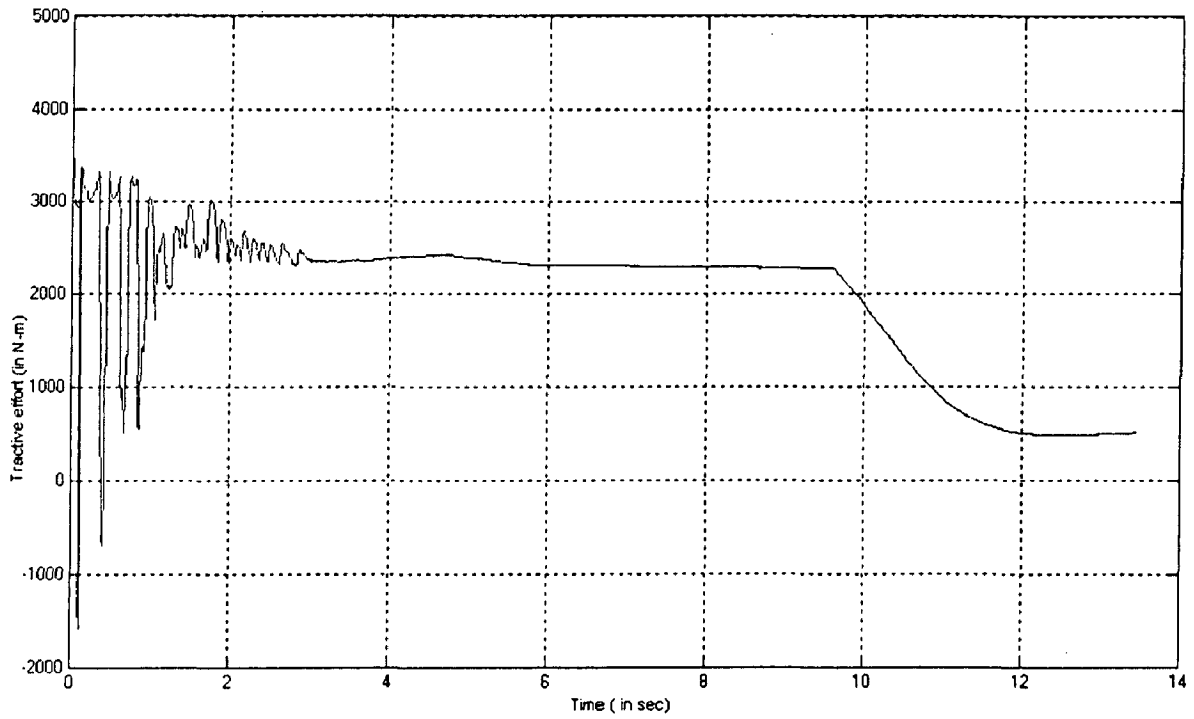
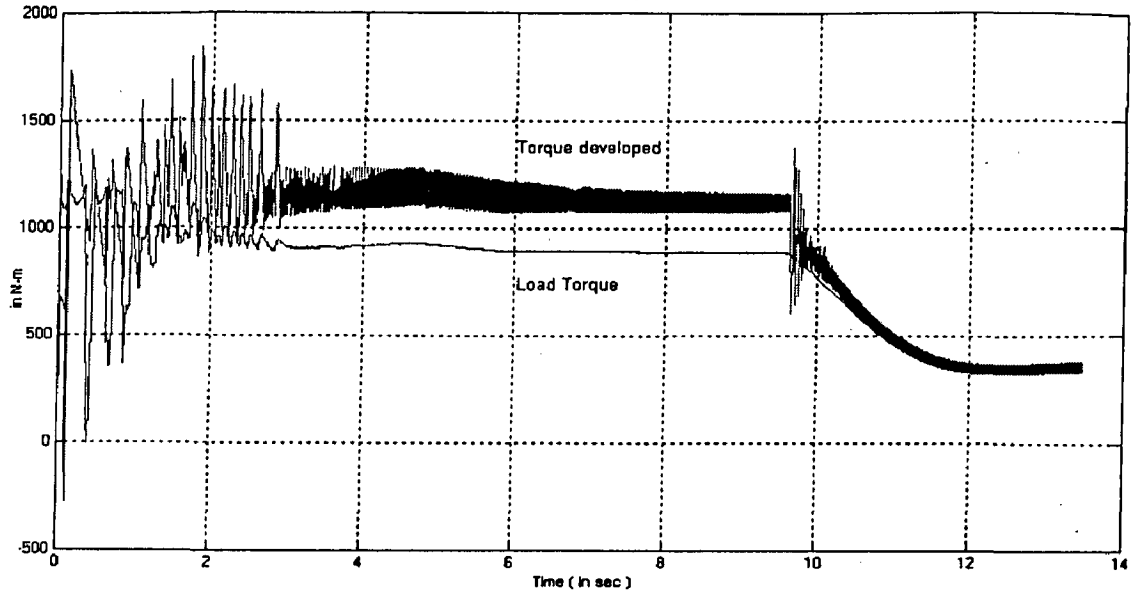
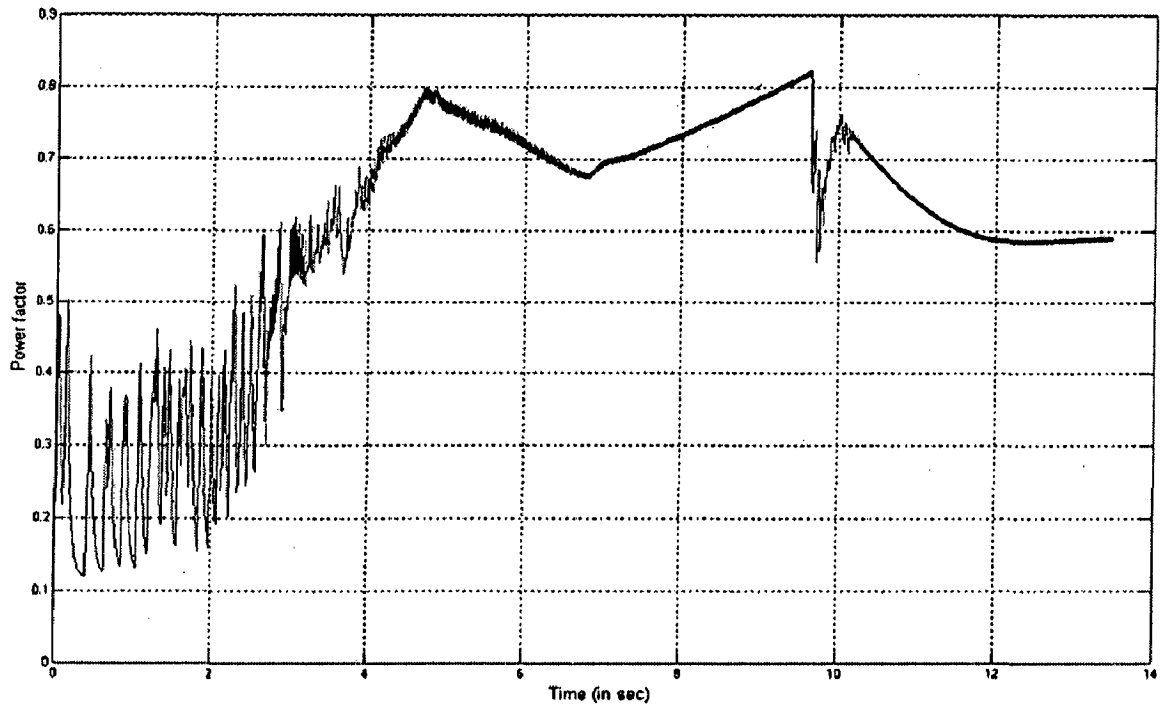


Figure 4.46 Variation of Tractive effort with time.



**Figure 4.47** The figure shows the torque developed by the motor and load torque on the drive on the same scale. The difference between the two curves during acceleration may be attributed to large value of  $J \frac{d\omega}{dt}$ .



**Figure 4.48** Variation of Power factor on the source side.

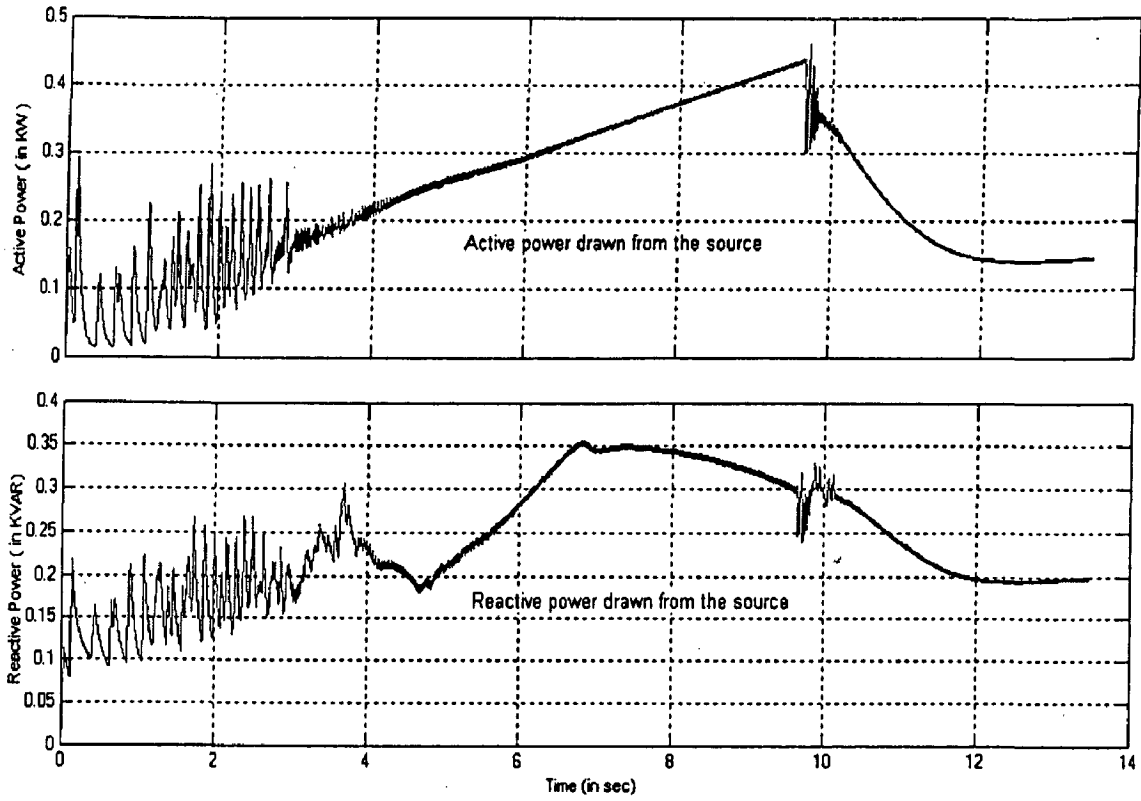


**Figure 4.49** Active and Reactive Power drawn by the motor from the supply.

**Simulation for the variable track**

Parameter specifications:

Reference gradient =  $2^\circ$ .

Desired speed = 80 Km/hr.

Nature of track = changing track.

The traction drive has been simulated to demonstrate how it re-adjusts itself to follow the reference slip when there is a change in track condition. The drive has been simulated for two track conditions shown in the figure 4.18

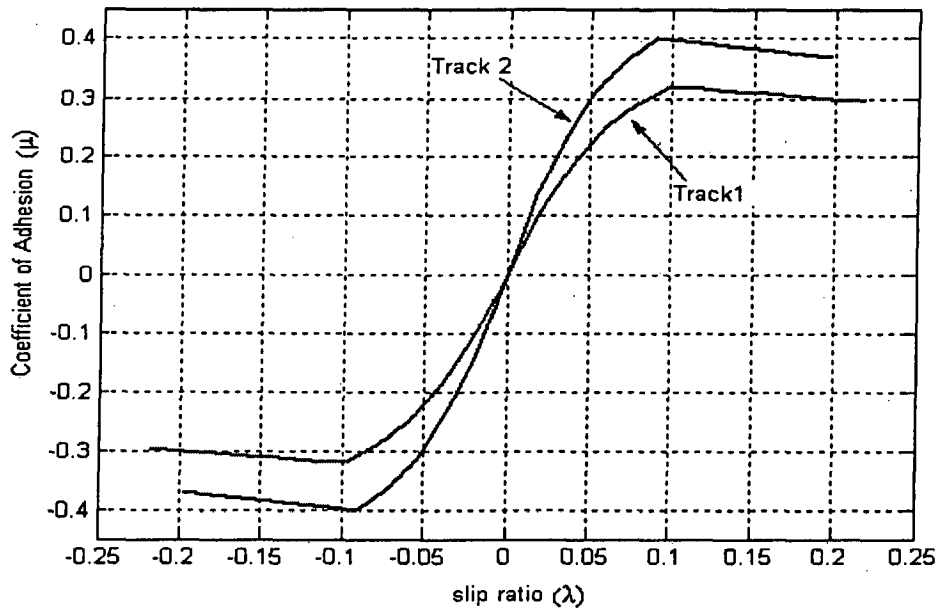


**Figure 4.50** The  $\mu$ - $\lambda$  curves for two tracks used in the simulation.

The train moves first 35 m on track 1. The track condition changes immediately at this point and the train moves on track 2 for next 45 m. It again shifts to track 1 after this. This is shown in figure 4.19.

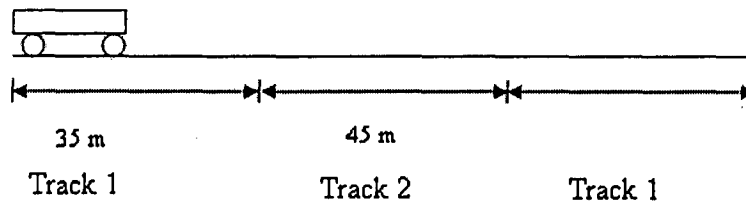


**Figure 4.51** Movement of train on the tracks.

The response of the system is shown below.

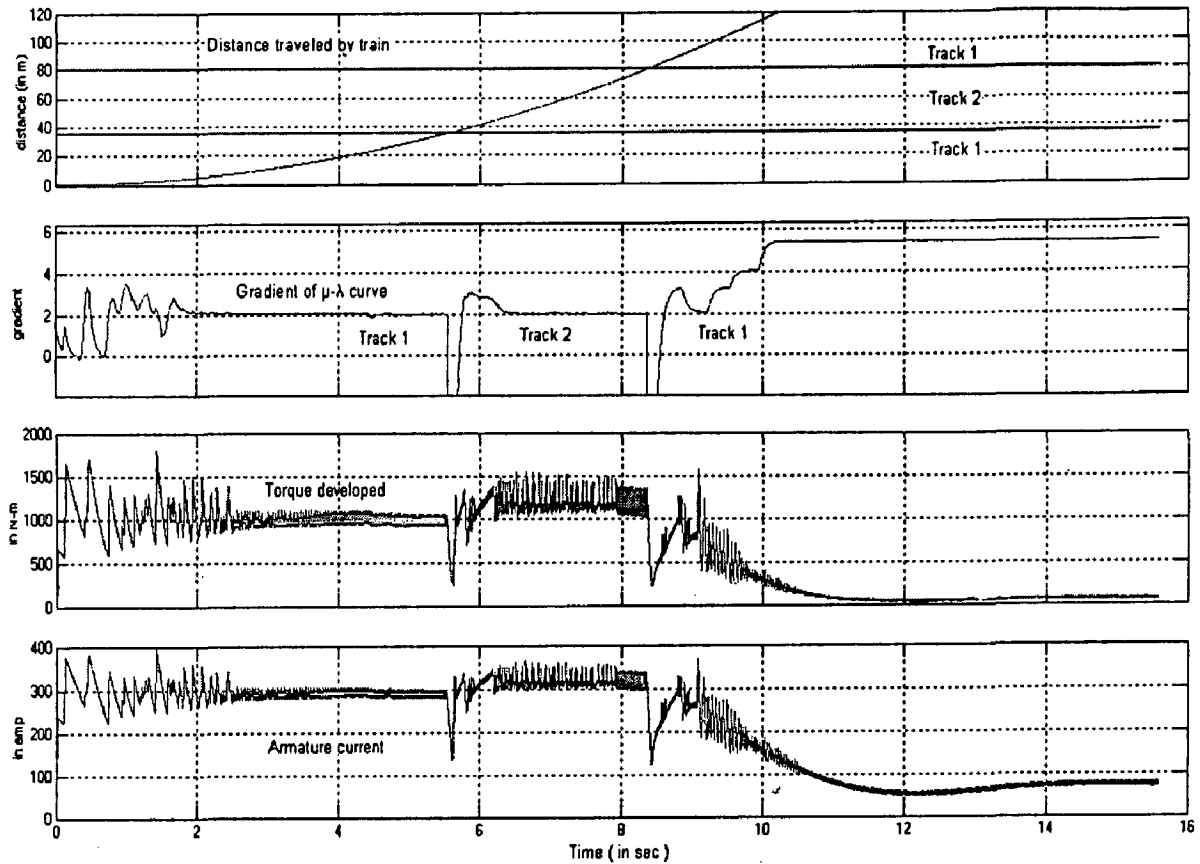


**Figure 4.52** The response of the system showing corresponding armature current and Torque developed by the motor as the slip ratio is being controlled through gradient control to the commanded value while the train builds up to the desired value of speed on a variable track.

It is evident from figure 4.52 that the motor torque has been controlled such that the gradient of  $\mu\text{-}\lambda$  curve is commanded to the reference value even when the track condition is changed. Figure 4.53 shows the locus of the  $\mu\text{-}\lambda$  curve followed by the train.

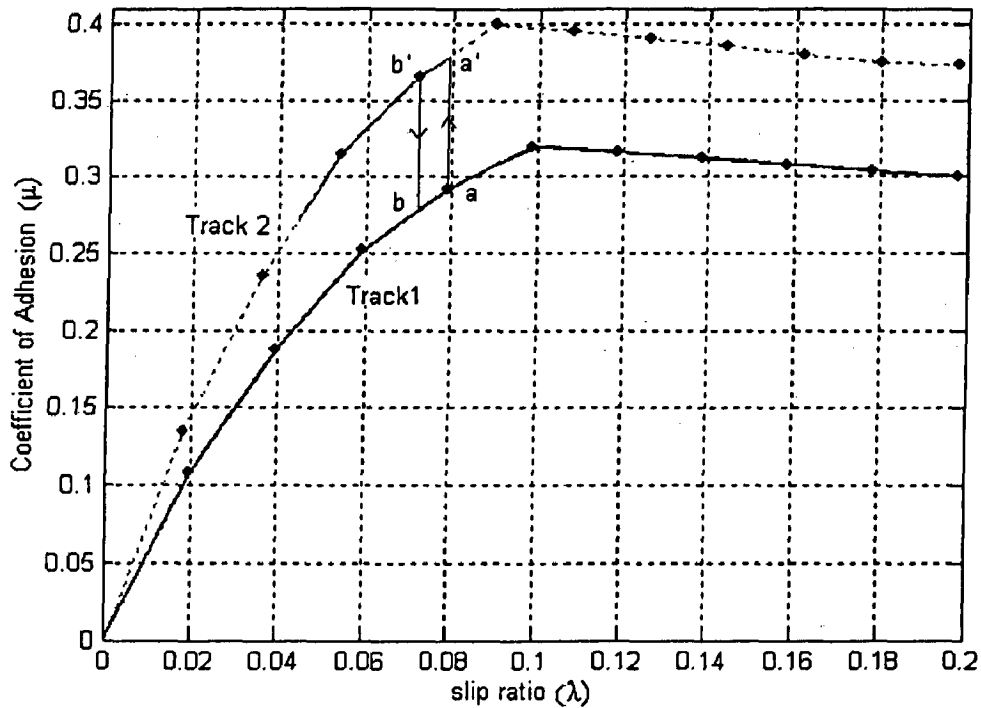


**Figure 4.53** Locus of the  $\mu$ - $\lambda$  curve followed by the train.

The locus of the  $\mu$ - $\lambda$  curve shown by figure 4.53 reveals that the train repeatedly moved from stable to unstable zone. This was the result of the oscillation during the transient period. However, soon after, the train settled at an optimum slip governed by the reference value of gradient. This is given by point 'a' in figure 4.53.

When the track condition changed the point of operation immediately shifted from a to a'. Then, after a small transient, the train settled at optimum slip for 'Track 2'. This is shown by point b'. Now when the track condition is changed back to the 'Track 1', operating point of the train drops back to point 'b' and starts building up towards the optimum slip for 'Track 1'.

A confirmation of point 'a' and point b' being the optimal points was made by zooming into figure 4.53. As said earlier, the  $\mu$ - $\lambda$  curves for the two tracks have been stored as a look-up table in MATLAB. Thus the characteristic is made up of small linear sections. These sections have different slopes and therefore the gradient controller tries to find the best suited slip condition for the commanded value. This is shown in figure 4.54

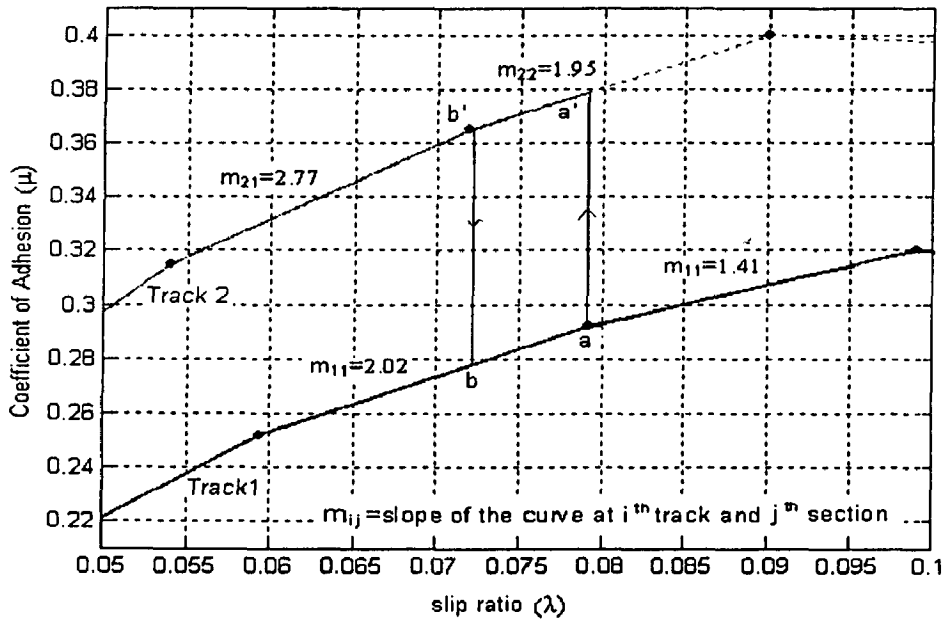


**Figure 4.54** Magnified view of  $\mu$ - $\lambda$  locus followed by the train

It may be seen from figure 4.54 that the point 'a' and 'b' are the optimal point of operation for track 1 and track 2 when the reference value of gradient was set at 2.

Other responses of interest are shown in figures 4.55 to 4.62.

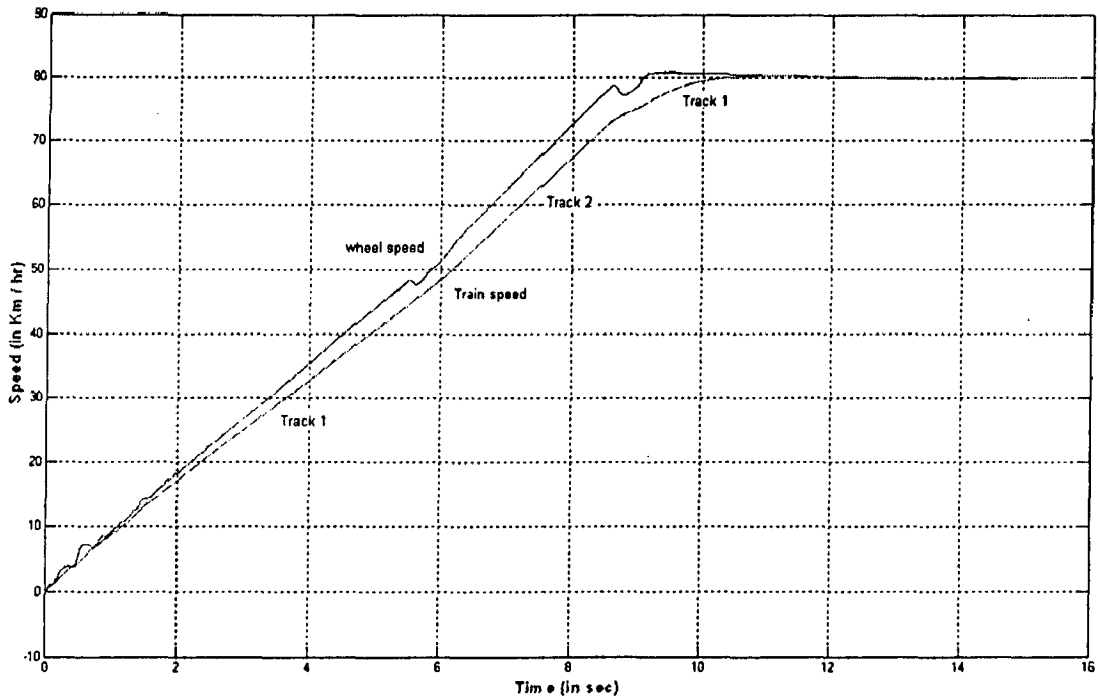


**Figure 4.55** Variation of wheel speed and train speed with time.



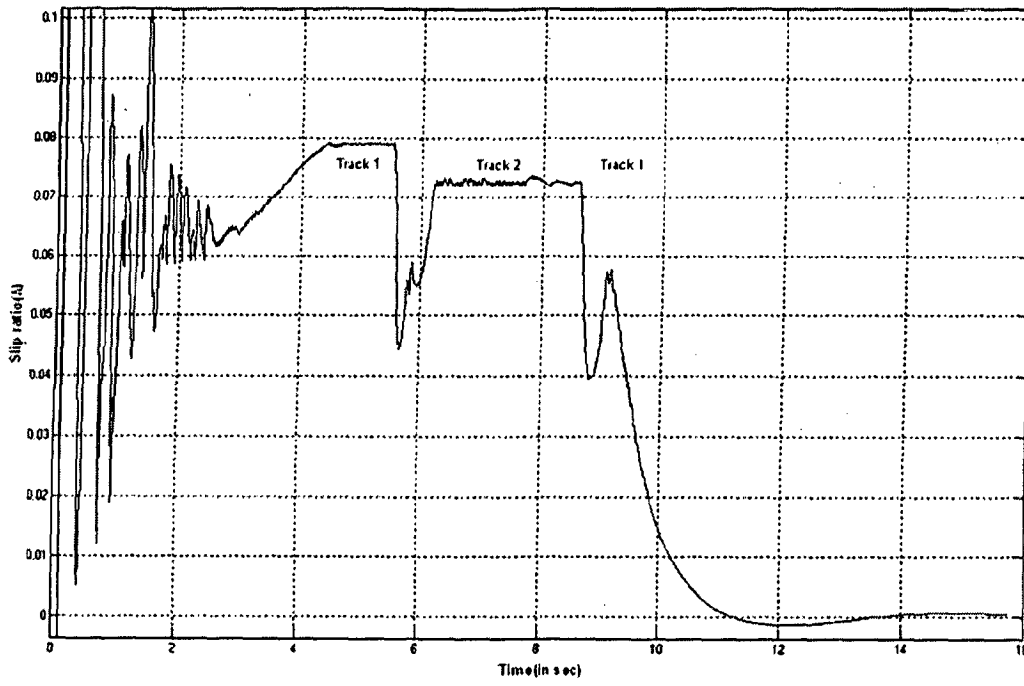


Figure 4.56 Variation of slip ratio with time.

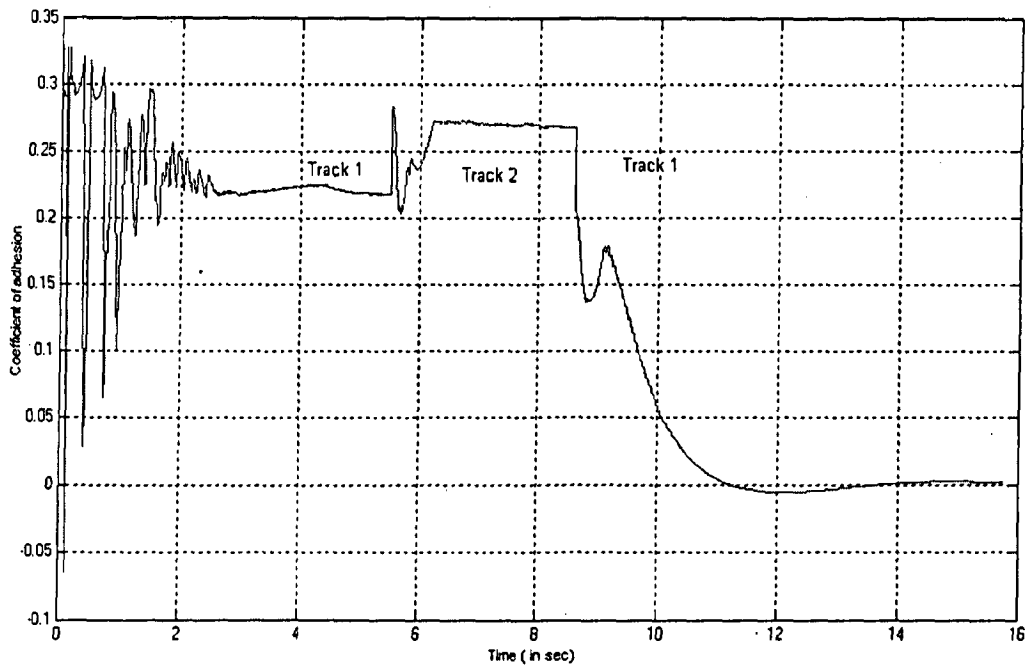
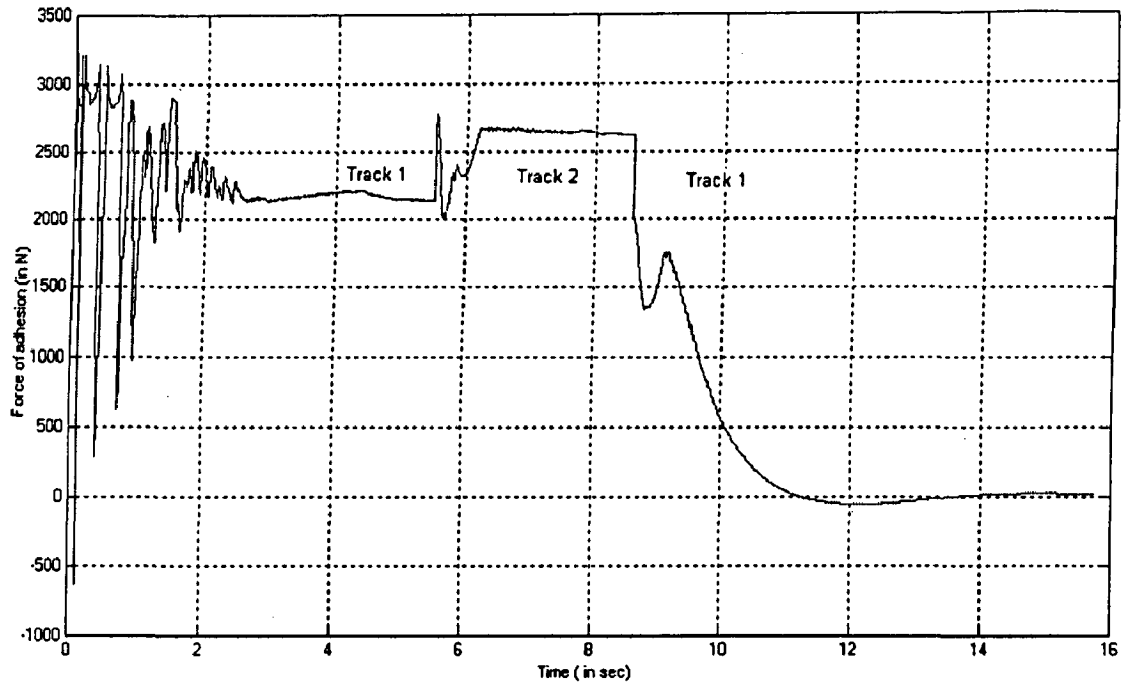
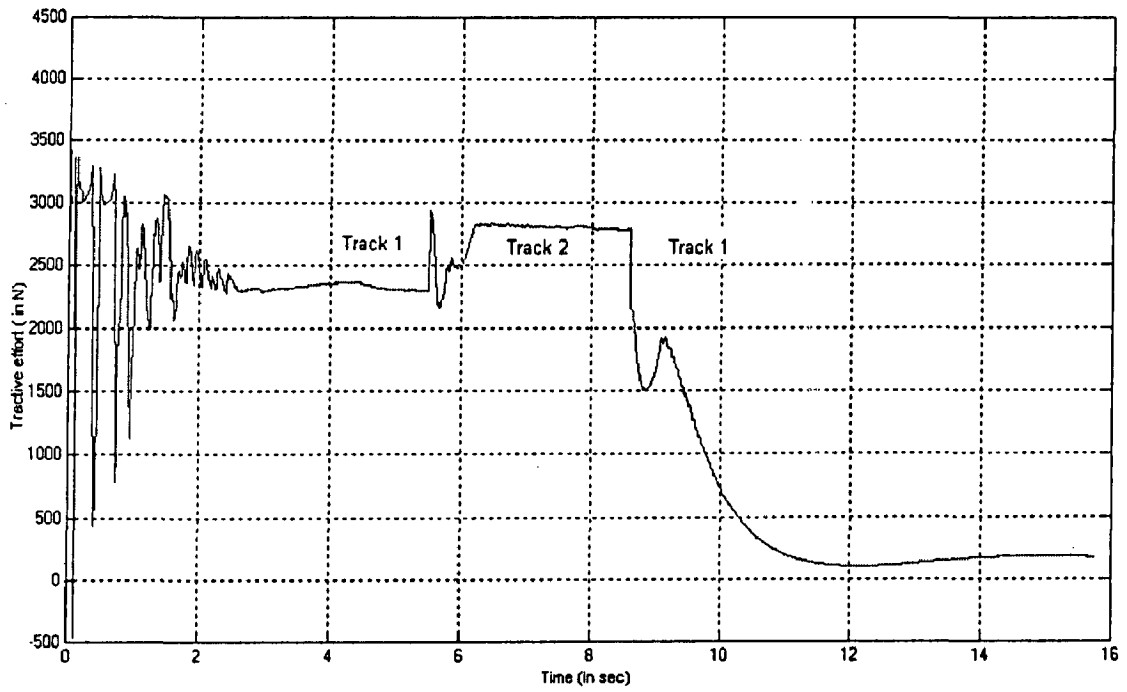


Figure 4.57 Variation of coefficient of adhesion with time.



**Figure 4.58** Variation of force of adhesion with time.



**Figure 4.59** Variation of Tractive effort with time.

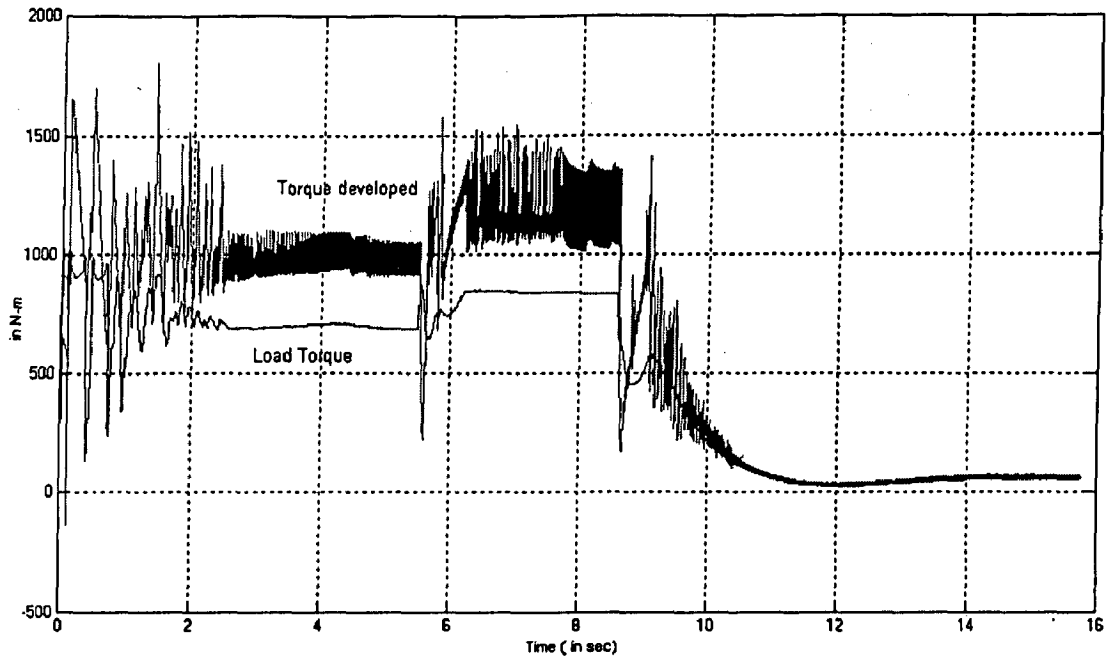


**Figure 4.60** The figure shows the torque developed by the motor and load torque on the drive on the same scale. The difference between the two curves during acceleration may be attributed to large value of  $J \frac{d\omega}{dt}$ .

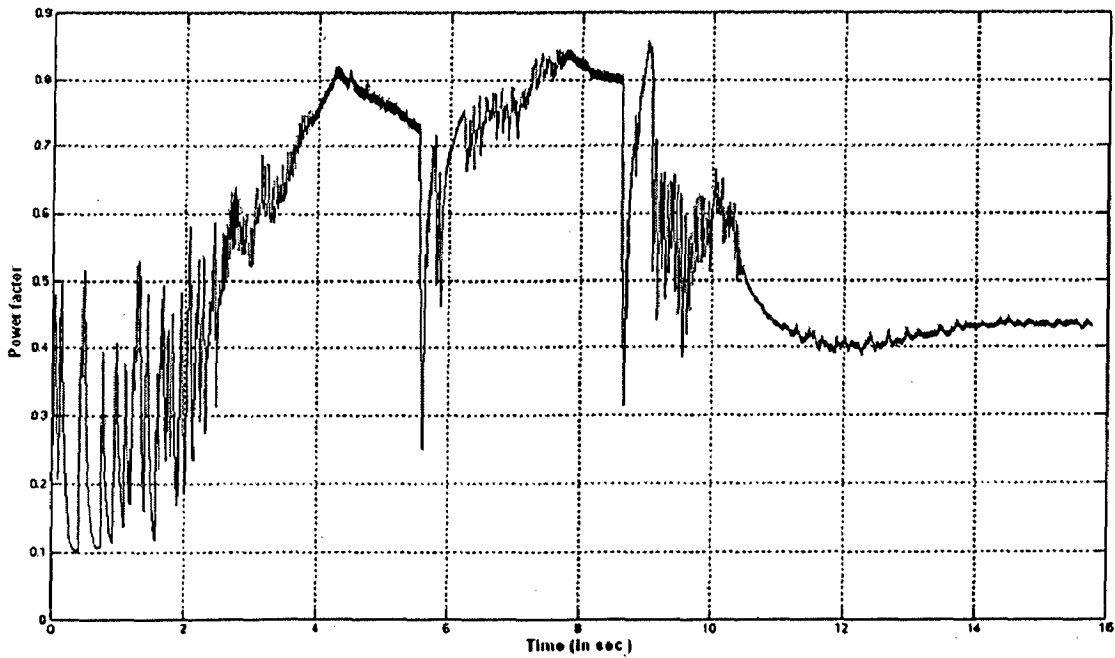


**Figure 4.61** Variation of Power factor on the source side.

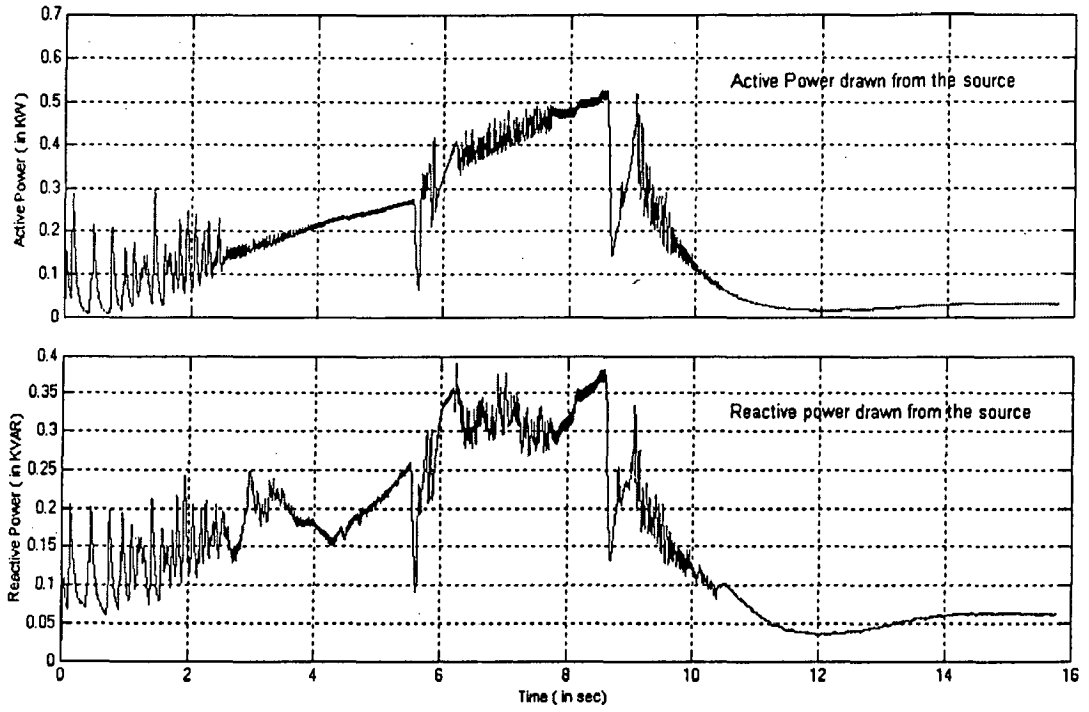


**Figure 4.62** Active and Reactive Power drawn by the motor from the supply.

## Conclusions and Scope for Further work

---

The purpose of this chapter is to summarize the work presented in this report along with brief discussions of some relevant results. This chapter ends with some recommendations for improvement of the existing model and for further work in this field.

### 5.1 Summary

This study has provided an important insight into the electrical and mechanical system which forms two units of an electric traction drive. The performance evaluation of DC motor drive operating with inner current and outer speed loop was made. Further an improvement of in power factor and reduction in current and torque ripples were observed when the drive was fed with two-stage half controlled converters rather than a single stage half controlled converter. Another important study made in this work was the modeling of traction load and its heavy dependence on wheel-rail interaction. The electric drive was integrated with the traction load model which provided us with extremely useful insight into the nature of traction load and pattern of tractive effort demand which forms the basis of the requirements from an electric traction drive. The simulation results clearly indicate the traction drive perceives a very heavy load torque during the acceleration which reduces to a small value once the acceleration period is over and the train has resumed pure rolling motion. The traction drive was modeled with wheel slip control strategies which demonstrate how the wheel slip ratio can be controlled to make optimal use of force of adhesion between train wheel and the track so as to allow maximum acceleration. The study also provides useful insight into the concept of gradient control and also how it maintains the operation of drive under stable region of  $\mu$ - $\lambda$  curve even when the track condition is changed. A simulation study of electric traction drive performance employing wheel slip control was conducted under various conditions such as motion of the train on a flat track, motion on an inclined track and motion of the train on a changing track

## 5.2 Recommendations for further work.

There lies an immense opportunity to carry out further research in this field. As said earlier, traction drive is a very complex function of wheel-rail dynamics and electric drive. What has been presented here is a simplified mechanical load model. This can be extended to include more sophistication of two or more wheel model and varying aerodynamic drag (with speed) [9]. In the current work only longitudinal motion of the train has been considered while modeling the traction load. The lateral effect displacement of the train on curved tracks called “yaw motion” has been neglected. The mechanical load model can be simulated to account for “yaw motion”. Further, the acceleration of an electric train depend upon various factors, the most important being passenger comfort [7]. Thus, the electric traction drive can be simulated to provide the acceleration control loop which controls the maximum acceleration of the train. Besides, a lot of work can be done to provide effective wheel slip control. Some of the improvements suggested for the current work are improvement in gradient detector design and using better approximations of  $\mu$ - $\lambda$  curve. The gradient control wheel slip control strategy simulated in this work uses a rather crude of way of detecting current gradient of a  $\mu$ - $\lambda$  curve. It calculates  $\Delta\mu$  and  $\Delta\lambda$  for the track by sampling  $\mu$  and  $\lambda$  in every one  $\mu$ -sec. This, however, have an advantage of avoiding divide by zero error while simulation and gives very good values, but a better way could still be found. Apart from this, a multi-motor drive with wheel-slip control can be simulated. The conventional PI controllers can be replaced by fuzzy controllers. Further, a performance estimation DC traction motor can also be made by developing a finite element model of the motor to study the effect of torque ripples on the motor. An analysis of behavior of DC traction drive under fault condition can also form an important subject of study. In this study it was observed that because of the nature of traction load, the power factor on the source side is poor. Therefore, power factor improvement techniques would also form an important topic of study.

## References

1. G.K Dubey, "*Power Semiconductor Controlled Drives*", Prentice Hall Publication, 1989.
2. G.K Dubey, "*Fundamental of Electrical Drives*" (2<sup>nd</sup> edition), Narosa Publishing House, 2001.
3. G.K Dubey, S R Doradla, A Joshi, R M K Sinha, "*Thyristorized Power Controllers*", New Age International (P) Ltd, Publishers, 2003.
4. A.T Dover, "*Electric Traction*" (4<sup>th</sup> edition), Sir Issac Pitman & Sons Ltd, 1963.
5. Sergey E. Lyshveski, "*Electromechanical Systems, Electric Machines and Applied Mechatronics*", CRC Press, 2000.
6. R. Krishnan, "*Electric Motor Drives*", Prentice Hall of India, 2003.
7. H Partab, "*Modern Electric Traction*", Dhanpat Rai & Co, 2003.
8. Dino Zorbas, "*Electric Machines, Principles, Applications and Control Schematics*", West Publishing Company, 1989.
9. R. Mathew, F. Finders and W. Oghanna, "*Locomotive "Total Systems" Simulation using SIMULINK*", Conference Publication No.405, IEE, 1995, pp 202-206.
10. S.Senini, F.Flinders, W. Oghanna, "*Dynamic Simulation of wheel rail interaction for locomotive traction studies*", IEEE/ASME Joint Railroad Conference, Pittsburgh, April 6-8, 1993, pp 27-34.
11. R.J Hill, "*Electric Railway Traction, Part1, Electric Traction and DC traction motor drives*", Power Engineering Journal, IEE, 1994, pp 47-56.
12. Yoichi Hori, Yayushi Toyoda and Yoshimasa Tsusruoka, "*Traction control of Electric Vehicles: Basic Experimental Results using the Test EV "UOT Electric March"*", IEEE Transaction on Industry Application, 1998, 1131-1138.
13. S.Burdett, J Allan, B.Mellitt, J.A Taufiq, "*A study of power factor correction for high power AC Locomotives*", Mainline Railway Electrification, International Conference, IEEE, 1989.

14. Parviz Famaouri, "Design of DC Traction motor drives for high efficiency under accelerating Conditions", IEEE Transaction on Industry Applications, Aug 1994 pp 1134-1138.
15. M.W. Winterling, E. Tuinman, W.Deleroi, "Fault analysis of Electromechanical Traction Drives", Conference Publication No.444, IEE, 1997.pp 248-252.
16. J.Chang, R. Mathew, F.Flinders, W Oghanna, "Simulation in DC Traction motors including both main pole and interpole saturation", IEE Proceedings on Electric Power Applications,1998, pp377-382.
17. S.L Ho, A.N.K Tam, C.T. Tse, T.K Ho, "Thermal analysis of DC Traction motors", International Conference on Developments in Mass Transit Systems, Conference Publication No.543, IEE, 1998.pp 161-166.
18. G.Reyne, J.C.Sabonnadiere, J.F.Imhoff, "Finite Element modeling of Electromagnetic Force Densities in DC Machines", IEEE Transactions on Magnetics,1988.pp 3171-3173.
19. Kiyoshi ohishi, yasuaki Ogawa, Ichiro Miyashita, Shinobu Yasukawa, "Anti-Slip Re-adhesion control of Electric Motor Coach Based on Force Control Using Disturbance Observer", Industry Applications Conference, IEEE, 2000,pp 1001-1007.
20. Yoshiki Ishikawa, Atsuo, Kawamura, "Maximum Adhesive Force Control in Super High Speed Train", Power Conversion Conference-Nagaoka, IEEE,1997,pp 951-954.
21. MathWorks. (2001). *What is SIMULINK*. The MathWorks, Inc. Available: <http://www.mathworks.com/access/helpdesk/help/toolbox/SIMULINK/ug/ug.shtml>.
22. IRFCA. "History of electrification. What's the history of electric traction in India?", Available: <http://www.irfca.org/IndianRailways/FAQ/ElectricTraction-I.html>.
22. Davidson, "Rolling friction", Available <http://webphysics.davidson.edu/faculty/dmb/py430/Friction/rolling.html>.



## Appendix A

### Specification of DC Motor:

Type of motor: DC Series motor.

Rated armature voltage = 535 V.

Rated armature current = 340 A.

Output Power = 167 KW.

Rated speed = 1260 rpm.

No. of poles = 6.

Armature Resistance,  $R_a = 0.0096 \Omega$ .

Armature Inductance,  $L_a = 1.71 \text{ mH}$ .

Field Resistance,  $R_f = 0.0052 \Omega$ .

Field Inductance,  $L_f = 0.99 \text{ mH}$ .

Armature-Field mutual Inductance,  $L_{af} = 3.9 \text{ mH}$ .

Moment of Inertia,  $J = 27.5 \text{ Kg- m}^2$ .

## Appendix B

### Program file: Initialize.m

```
% Name of the program: Initialize.m
% This program is used to initialize various parameters required to simulate the traction
% drive. Some of the important specifications made by the program are as follows.
% Parameters for electrical motor.
% Parameters for Locomotive.
% Reference speed.
% Total inertia of the system.
% Track specification.

clear all;
clear all;
% Motor specification.
Ra=0.0096;
La=0.00171;
Rf=0.0052;
Lf=0.99;
Laf=0.0109;
jm=27.5;
Bm=0.12;
Vao=535;
f=50;
Vcm=10;
If=340;
% Locomotive specification
Mw=100; %mass of wheel
Mt=900; % mass of locomotive (in Kg)
r=0.3; % radius of locomotive (in m)
Fr=25; % air resistance(in N).
```

```

% Assuming gear ratio to be unity
a=1;
Jw=jm/(a^2);

% Track specification
theta=0; % gradient angle of the track(in degree)
th=theta*pi/180;
g=9.81; % acceleration due to gravity
M=Mt+Mw;
G=(M)*g*sin(th);
N=(M)*g*cos(th);
% Set train speed,v Km/hr
v=80;
vt=(5/18)*v;
W=vt/r;
% Total moment of inertia of the system
J=Jw+Mw*r^2;
Tr=J*accn/r;

```

**Program file: Locus.m**

```
% Name of the program: Locus.m
% This program plots the locus of train on the  $\mu$ - $\lambda$  curve as it toggles between the two
% tracks simulated in the scheme.
% To show this in an effective manner, the two tracks are simulated along with the
% running values of slip ratio and coefficient of adhesion. These values are stored in the
% MATLAB workspace as in form of a structure (in variables 'slip' and 'coeff') and the
% actual values are then retrieved by decoding the data structure. All three curves viz. the
% two tracks and the running values are plotted in the same curve to shoe the locus of
% train on a  $\mu$ - $\lambda$  curve.
% Track 1.
slip1 = [-0.198:0.018: 0.198];
mu1 = ([-0.373 -0.375 -0.38 -0.385 -0.39 -0.395 -0.4 -0.365 -0.315 -0.235 -0.135 0.0
        0.135 0.235 0.315 0.365 0.4 0.395 0.39 0.385 0.38 0.375 0.373]);

% Track 2
slip2= [-0.2178 :0.0198:0.2178];
mu2=( [-0.2984 -0.3000 -0.3040 -0.3080 -0.3120 -0.3160 -0.3200 -0.2920 -0.2520
        -0.1880 -0.1080 0 0.1080 0.1880 0.2520 0.2920 0.3200 0.3160 0.3120 0.3080
        0.3040 0.3000 0.2984]);
plot (slip1, mu1, 'r -');
hold on;
plot (slip2, mu2, 'b -');
hold on;
plot (slip.signals.values, coeff.signals.values, 'm -');
axis ([0.0 0.1 0. 0.41]);
```